

D420095  
N 7 5 - 21 2 6 7

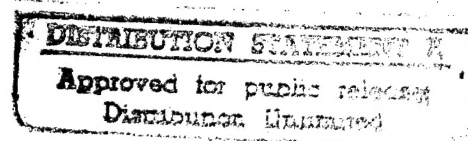
NASA CR-132611  
ARDE J/N 41004



FINAL REPORT  
FABRICATION AND TESTING OF  
PRESTRESSED COMPOSITE ROTOR BLADE  
SPAR SPECIMENS

Oct. 1974

19960206 142



by  
D. Gleich

Prepared Under Contract No. NAS1-11594

Submitted by:

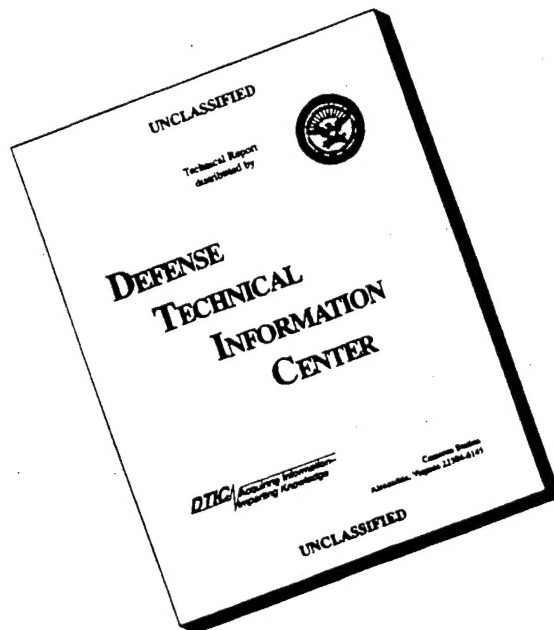
ARDE, INC.  
19 Industrial Avenue  
Mahwah, New Jersey 07430

for  
National Aeronautics & Space Administration

DTIC QUALITY INSPECTED 1

PLASTIC 22550

# DISCLAIMER NOTICE



**THIS DOCUMENT IS BEST  
QUALITY AVAILABLE. THE  
COPY FURNISHED TO DTIC  
CONTAINED A SIGNIFICANT  
NUMBER OF PAGES WHICH DO  
NOT REPRODUCE LEGIBLY.**

-- 1 OF 3


\*\*\*DTIC DOES NOT HAVE THIS ITEM\*\*\*

-- 1 - AD NUMBER: D420095  
-- 3 - ENTRY CLASSIFICATION: UNCLASSIFIED  
-- 5 - CORPORATE AUTHOR: ARDE INC MAHWAH N J  
-- 6 - UNCLASSIFIED TITLE: FABRICATION AND TESTING OF PRESTRESSED  
COMPOSITE ROTOR BLADE SPAR SPECIMENS.  
-- 8 - TITLE CLASSIFICATION: UNCLASSIFIED  
-- 9 - DESCRIPTIVE NOTE: FINAL REPT., JUN 72-OCT 74,  
--10 - PERSONAL AUTHORS: GLEICH,D. ;  
--11 - REPORT DATE: OCT , 1974  
--12 - PAGINATION: 115P  
--14 - REPORT NUMBER: ARDE-J/N-41004  
--15 - CONTRACT NUMBER: NAS1-11594  
--18 - MONITOR ACRONYM: NASA  
--19 - MONITOR SERIES: CR-132611  
--20 - REPORT CLASSIFICATION: UNCLASSIFIED  
--22 - LIMITATIONS (ALPHA): APPROVED FOR PUBLIC RELEASE; DISTRIBUTION  
UNLIMITED. AVAILABILITY: NATIONAL TECHNICAL INFORMATION SERVICE,  
SPRINGFIELD, VA 22161.  
--27 - ABSTRACT: PRESTRESSED COMPOSITE SPAR SPECIMENS WERE FABRICATED

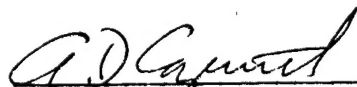
# FOREWORD

This report is submitted by ARDE, INC. in fulfillment of contract NAS1-11594 and covers the period from June 1972 to October 1974. The principal investigator was Mr. David Gleich. The contract research effort which led to the results in this report was financially supported by USAAMRDL (Langley Directorate).

Prepared by:

  
\_\_\_\_\_  
David Gleich

Approved by:

  
\_\_\_\_\_  
A. D. Cozewith



FABRICATION AND TESTING OF  
PRESTRESSED COMPOSITE ROTOR BLADE  
SPAR SPECIMENS

by

D. Gleich

ABSTRACT

Prestressed composite spar specimens were fabricated and evaluated by crack propagation and ballistic penetration tests. The crack propagation tests on flawed specimens showed that the prestressed composite spar construction significantly suppresses crack growth. This provides a "fail-safe" feature leading to increased safe operational life and improved survivability. Damage from three (3) high velocity 30 caliber projectile hits was confined to three small holes in the ballistic test specimen. No fragmentation or crack propagation was observed indicating good ballistic damage resistance. Rotor attachment approaches and improved structural performance configurations were identified. Design theory was verified by tests. The prestressed composite spar configuration consisted of a compressively prestressed high strength ARDEFORM 301 stainless steel liner overwrapped with pretensioned S-994 fiberglass. The prestresses, imparted during cryogenic stretchforming fabrication, are chosen to maintain compression in the metal liner under operating loads. This prestressed composite material construction presents considerable crack propagation and fatigue property improvements leading to increased structural performance.

## CONTENTS

	<u>Page</u>
SUMMARY . . . . .	viii
1.0 INTRODUCTION . . . . .	1
2.0 DESCRIPTION OF THE PRESTRESSED COMPOSITE SPAR. . . . .	3
3.0 TECHNICAL DISCUSSION . . . . .	6
3.1 Review of Composite Spar Structural Design Considerations & Fabrication Methods. . . . .	6
3.2 Composite Spar Testing. . . . .	12
3.2.1 Test Program Description . . . . .	12
3.2.2 Test Adapter & Composite Spar Specimen Design . . . . .	26
3.2.3 Test Adapter & Composite Spar Specimen Fabrication. . . . .	28
3.2.4 Description of Test Set-Up & Procedures. .	31
3.2.5 Test Results . . . . .	37
3.2.6 Improved Structural Performance Options. .	60
4.0 CONCLUSIONS AND RECOMMENDATIONS. . . . .	65
4.1 Conclusions . . . . .	65
4.2 Recommendations . . . . .	65
5.0 REFERENCES . . . . .	66
6.0 APPENDICES . . . . .	67
6.1 Appendix 1 - Test Vendor Report . . . . .	67
6.2 Appendix 2 - Calculations . . . . .	95
7.0 DISTRIBUTION LIST. . . . .	104

# LIST OF FIGURES

<u>Figure No.</u>	<u>Description</u>	<u>Page</u>
1	Prestressed Composite Spar Configuration. . .	4
2	Fiber Wrap Angle Vs. Prestress. . . . .	7
3	Constrictive-Wrap Buckling Stengths for Cylindrical Tubes . . . . .	9
4	Constrictive Overwrapped Cylinder - Typical Buckling Mode Shape . . . . .	10
5	Prestressed Composite Spar Major Fabrication Steps . . . . .	11
6	Liner Preform Components. . . . .	13
7	Boss to Head Weld . . . . .	14
8	Completed Composite Spar Preform Weldment Assembly. . . . .	15
9	Annealing Fixture . . . . .	16
10	Hydrostretch Die. . . . .	17
11	Start of Fiber Wrapping of Composite Spar Metal Liner Preform . . . . .	18
12	Beginning Stage - Fiber Wrapping of Composite Spar Metal Liner Preform. . . . .	19
13	Final Stage - Fiber Wrapping Composite Spar Metal Liner Preform . . . . .	20
14	Completed Fiber Wrapped Composite Spar Preform Assembly. . . . .	21
15	Cryogenic Stretch Die Components. . . . .	22
16	Stretch Facility. . . . .	23
17	Composite Spar Cryogenic Stretch In Die . . .	24
18	Composite Spar Preform and Portform Assemblies	25
19	E 3866-D, Composite Spar-Crack Propagation Test Specimen Assembly. . . . .	27
20	C 104678, Tube-Adapter Specimen . . . . .	29
21	Composite Spar Crack Propagation Test Oval Tube Forming. . . . .	30
22	Composite Spar Crack Propagation Test Assembly P/N E 3866-D S/N 6 & 10. . . . .	32

# LIST OF FIGURES

<u>Figure No.</u>	<u>Description</u>	<u>Page</u>
23	Composite Spar Crack Propagation Test Assembly P/N E 3866-D S/N 1 . . . . .	33
24	Composite Spar Crack Propagation Test Assembly P/N E 3866-D S/N 1 Axial Load Proof Test Set-Up . . . . .	34
25	Crack Propagation Test Set-Up Schematic . . .	36
26	Specimen No. 1 (S/N 10) Strain Gage Locations	38
27	Specimen No. 1 (S/N 10) Static Bending Moment Vs. Test Stations . . . . .	39
28	Specimen No. 1 (S/N 10) Bond Failure after 7000 lb. Overnight Axial Tension Load application . . . . .	40
29	Schematic - Modified Crack Propagation Test Specimen Assembly . . . . .	42
30	Crack Propagation Test Specimen Assembly Installed in Test Fixture . . . . .	43
31	Specimen No. 1 (S/N 10) Crack Growth Vs. Cycles. . . . .	44
32	Specimen No. 2 (S/N 6) Static Bending Moment Vs. Test Stations . . . . .	46
33	Specimen No. 2 (S/N 6) Crack Growth at $\pm$ 30 ksi Alternating Stress. . . . .	48
34	Specimen No. 2 (S/N 6) In Crack Propagation Test. . . . .	49
35	Specimen No. 2 (S/N 6) after Crack Propagation Test. . . . .	50
36	Specimen No. 3 (S/N 1) Static Bending Moment Vs. Test Stations . . . . .	52
37	Specimen No. 3 (S/N 1) During Crack Propagation Test. . . . .	53
38	Specimen No. 3 (S/N 1) Crack Propagation with Fiberglass Removed. . . . .	54
39	Unprestressed Specimen No. 3 (S/N 1) after Crack Propagation Test. . . . .	55

## LIST OF FIGURES

<u>Figure No.</u>	<u>Description</u>	<u>Page</u>
40	Ballistic Specimen (S/N 3) Entrance Damage. . . . .	57
41	Ballistic Specimen (S/N 3) Exit Damage. . . .	58
42	Fatigue Test of Prestressed Composite Metallic Fiberglass Spars . . . . .	59
43	Prestressed Composite Spar - "Tuned" Rigidity"	62
1 through 27	(Boeing Test Report). . . . .	68
A-1	Sketch of Prestressed Composite Spar Cross- Section . . . . .	96

LIST OF TABLES

<u>Table No.</u>	<u>Description</u>	<u>Page</u>
1	Specimen No. 2 (S/N 6) Bending Stress Levels Versus Cycles. . . . .	47
2	Ballistic Test-Projectile Type and Velocity .	51
3	Weight and Stiffness Comparison - Prestressed Composite Versus Homogeneous Material Spars .	63

FABRICATION AND TESTING OF  
PRESTRESSED COMPOSITE ROTOR BLADE  
SPAR SPECIMENS

by

D. Gleich

SUMMARY

Feasibility of applying prestressed composite material design and construction methods to helicopter blade spars was successfully demonstrated on a prior program (Contract NAS1-10028). This current fabrication and test program under Contract NAS1-11594 was performed to demonstrate the theoretically predicated superior crack propagation and fatigue life properties of the prestressed composite spar construction and to further verify design theory. The composite spar construction utilized consists of a high strength and tough ARDEFORM 301 stainless steel liner overwrapped with S-994 fiberglass. The metal liner is prestressed in compression and the fibers are pretensioned. The prestresses are selected to maintain compression in the metal liner under operating service loads. This precompression, coupled with the fiber tensioning, suppresses crack growth and provides considerable improvement in fatigue life properties as verified by the test results reported herein.

The current program included the design of a test specimen and test apparatus, fabrication of the test specimens and crack propagation and ballistic tests. Six (6) prestressed composite spars were fabricated using existing tooling. The prestressed composite spar configuration had been designed and verified on a prior program. Appropriate test adapters, needed to mate the spar test specimens with the test vendor's existing testing machine, were designed and fabricated. Four (4) prestressed composite spar test specimen assemblies (spar plus adapters) were built and tested; three (3) in crack propagation tests and one (1) in a ballistic test.

The superior crack propagation and fatigue life properties of the prestressed composite spar construction (compared to current metal spar configurations) were experimentally verified. Test results equivalent to about 1500 continuous hours of flight in the damaged condition at much higher operating stresses than current spars, were

obtained. Propagation of artificially introduced fatigue cracks did not occur until alternating bending stress levels of  $\pm 30$  ksi were applied (compared to  $\pm 10$  ksi for current metal spars). Structural design theory was confirmed by agreement between measured and predicted strains. The design technology for the composite prestressed spar construction was thus confirmed by these experimental results.

Damage from three (3) 30 caliber projectile hits on a prestressed composite spar specimen consisted solely of three small holes due to the projectile penetrations. No fragmentation or crack propagation occurred, implying high ballistic resistance. Rotor design approaches were identified by spar specimen constructions evolved and proven during testing. Further improved structural performance prestressed composite spar configurations utilizing higher stiffness and lower density fibers (PRD-49 and graphite) were defined.



## 1. INTRODUCTION

### 1.1 Background

There is a need for improved operational life, "fail-safe" and structurally efficient helicopter blades. Considerable work has been done on composite structures, which can be applied to meet this need. Stiffnesses can be tailored at good weight trade-offs compared to homogeneous material designs and redundant load carrying capability is inherent in this type of configuration. These composite structures<sup>(1), (2)</sup> generally consist of fiber-metal constructions in which the fibers, imbedded in a resin matrix, are attached to the metal primarily by adhesively bonded joints (shear-type connections). The operational life of this construction (measured by fatigue and crack propagation rate considerations) is a strong function of the effectiveness of these shear-ties.

Another approach to composite metal-fiber material construction, aimed at providing even more improved operational life and fail-safe helicopter blade structures, consists of a high-strength and tough compressively prestressed metal liner overwrapped with pretensioned fibers. No adhesive bonds between the fibers and metal liner or between the fibers themselves are required. The fiber resin matrix merely provides protection against fiber abrasion and moisture. By regulating the magnitude of the metal liner compressive prestress so that the liner is always in compression under operational blade loads, liner crack propagation is theoretically eliminated and significant improvements in liner fatigue life should be obtained. Fiber pretensioning also should provide substantial increases in fiber fatigue cycle life compared to zero pretensioned fibers at the same maximum service stress levels. Theoretical considerations indicate that these crack propagation and fatigue life advantages should be attained at good stiffness-weight trade-offs compared to homogeneous material and other types of composite material blades. Finally, in addition to inherent redundant load carrying capability and relatively high structural damping capacity, the option exists to provide even more enhanced torsional, bending and extensional stiffness properties at little weight penalty by winding additional fibers at selected angles subsequent to the prestressing operation.

The design principles and fabrication techniques for prestressed metal-fiber structures have been successfully verified by previous ARDE work<sup>(3), (4)</sup> for NASA with 13-1/2 inch diameter

spherical shapes used for pressure vessels and by in-house effort with cylindrical shapes. Significant improvements in structural efficiency were demonstrated compared to homogeneous material and other composite constructions (3), (5). The composite spherical vessels consisted of a high strength ARDEFORM (6) 301 stainless steel liner overwrapped with S-994 fiberglass. The high liner strength and toughness, together with the prescribed prestresses in the liner and fiberglass as well as final sizing, were imparted by means of cryogenic stretch-forming at  $LN_2$  temperature, followed by release of load and warm up to room temperature.

The feasibility of applying this prestressed composite design and construction technology (initially developed for spherical and cylindrical shapes) to the relatively long and slender helicopter blade spar shape was demonstrated on a prior program (7) under Contract NAS1-10028. Subscale oval-shaped cross-section prestressed composite spar structural models about three (3) feet long were designed and successfully fabricated. Special tooling required for prestressed composite spar fabrication was designed, built and proven. The prestressed state of these composite spars, determined and verified by means of structural theory coupled with spar inspection data, was in the desired design range. Suitable spar fiber wrap patterns, together with compatible spar metal liner head closure shapes needed to properly anchor the fibers, were determined and verified.

Following this verification of prestressed composite spar design and fabrication techniques, the primary goal of the current program under NAS1-11594 was therefore to experimentally prove the theoretically predicted structural performance advantages obtainable by virtue of the enhanced crack propagation and fatigue properties of the prestressed composite spar construction. Additional prestressed composite spar specimens were fabricated utilizing the existing three (3) foot long design configuration and tooling. These spar specimens were then evaluated by means of crack propagation and ballistic tests. This report presents a detailed summary and discussion of all work performed during the program.

## 1.2 Program Description

The primary program objective was to demonstrate by test results the superior crack propagation properties of the prestressed composite spar construction. The goals were 1, to verify the significant retardation of crack growth of the prestressed composite

spar compared to current spar configurations and to demonstrate that the compressive prestressing was responsible for the "zero" crack growth, 2, to further substantiate composite spar structural design theory, and 3, to provide an initial demonstration of the high inherent ballistic damage resistance of the prestressed composite spar.

The program consisted of a three (3) task effort comprising prestressed composite spar test specimen design and fabrication (including test adapters) spar testing and evaluation (crack propagation and ballistic tests) and documentation and reports.

Program effort culminated in successful crack propagation and ballistic tests. The superior crack propagation properties and good ballistic damage resistance of the prestressed composite spar construction were experimentally verified. Prestressed composite spar structural design theory was substantiated by test measurements. Test adapter/test specimen design and fabrication effort coupled with test verification identified plausible prestressed composite spar rotor attachment options. Improved structural performance prestressed composite spar configurations were defined. These various factors and results are described in detail in Section 3.

## 2. DESCRIPTION OF THE PRESTRESSED COMPOSITE SPAR

The prestressed composite spar model considered herein consists of a relatively long and slender inner ARDEFORM 301 stainless steel member (liner) overwrapped with S-994 fiberglass impregnated in a resin matrix, Figure 1. The fibers are wrapped at a constant helix angle,  $\alpha$ , on the spar body as shown. The head closure shape is chosen so that the fibers, under constant tensions, are anchored on the head and body by bearing forces alone. No shear stresses in the resin are needed to hold the fibers in place. Threaded bosses (loading adapters) with central holes are provided at each closure end to facilitate pressurization during spar fabrication and to permit test load application.

During fabrication, the composite spar is immersed in and pressurized internally with liquid nitrogen which plastically stretches the spar to its final configuration and material properties. The plastic straining operation is done in a closed die which controls the final spar shape. The cryogenic stretch

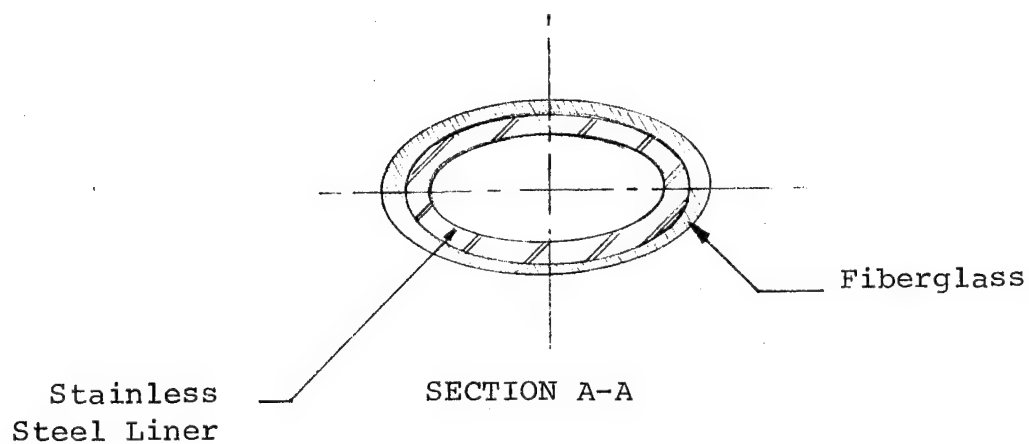
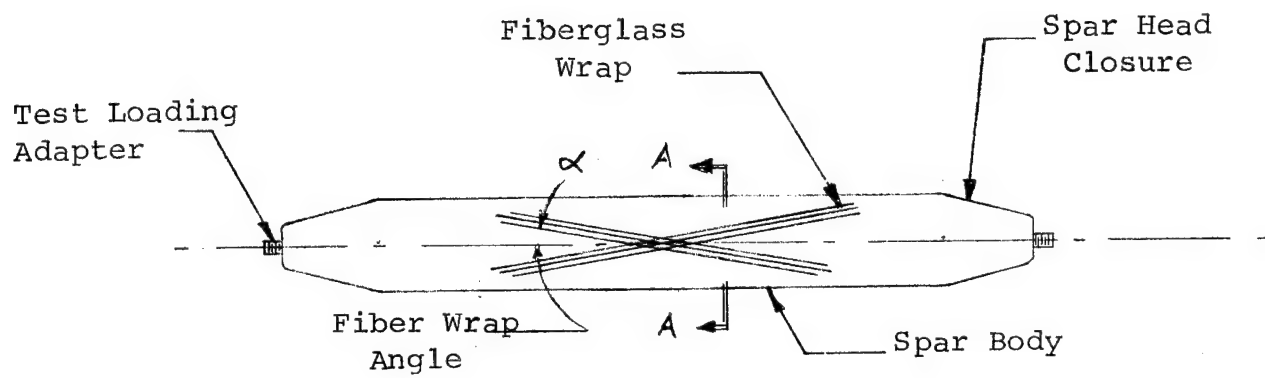


FIGURE 1

PRESTRESSED COMPOSITE SPAR CONFIGURATION

forming transforms the initially annealed ARDEFORM 301 austenitic stainless steel inner member to martensite, imparting high strength and toughness to the material. After release of the cryogenic stretch forming pressure, the stainless steel liner and the fiberglass spring back elastically to their unpressurized room temperature state with the fiberglass under initial tension and the metal under initial compression due to the prior plastic straining of the metal liner. In operation, both the fiberglass and metal resist the applied loads, with the metal member designed to always be in compression and the fiberglass always in tension.

### 3. TECHNICAL DISCUSSION

This section describes the technical effort and accomplishments, presents analytic and test data, details problem areas encountered during the program and discusses approaches taken to resolve these problems.

#### 3.1 Review of Composite Spar Structural Design Considerations and Fabrication Methods

Prestressed composite spar structural design considerations and fabrication techniques have been described in detail in a prior report<sup>(7)</sup>. They are briefly discussed in this text for sake of completeness.

##### 3.1.1 Structural Design Factors

The basic design objective of the composite metal-fiber configurations considered herein is to provide a prestressed member with the high strength and tough liner always in compression and the fibers always in tension throughout the spar storage and operating life. As demonstrated by the test data obtained in the program, this technique retards crack propagation thus providing long, safe, operational life at excellent weight/stiffness trade-off as heretofore indicated. The structural design considerations related to achievement of this basic design objective are strongly coupled with spar fabrication. The magnitude of the cryogenic strain imparted to the composite spar during fabrication not only determines the metal liner strength level, but together with fiber wrap angle, metal and fiber thickness and material properties, determines the spar prestresses and influences spar operational characteristics. Figure 2, previously derived <sup>(7)</sup>, shows the relation between spar prestresses and fiber wrapped angle and fiber to metal thickness ratio for a particular metal liner cryogenic stretch forming design point.

In addition to prescribing a metal liner operating in compressive stress, other structural criteria are utilized to select the prestressed composite spar design point. The magnitudes of the metal liner precompression and liner tensile and compressive yield and ultimate strengths as well as operating stress level are selected to prevent elastic buckling of the liner, compressive yielding of the liner followed by plastic buckling, or liner fatigue failure. Fiber pretension and operating stress are chosen to preclude fiber creep effects or fatigue failure.

# FIBER WRAP ANGLE VS. PRESTRESS

(for  $\sigma_{MH} = 250 \text{ Ksi}$  and  $\sigma_{ML} = 125 \text{ Ksi}$ )

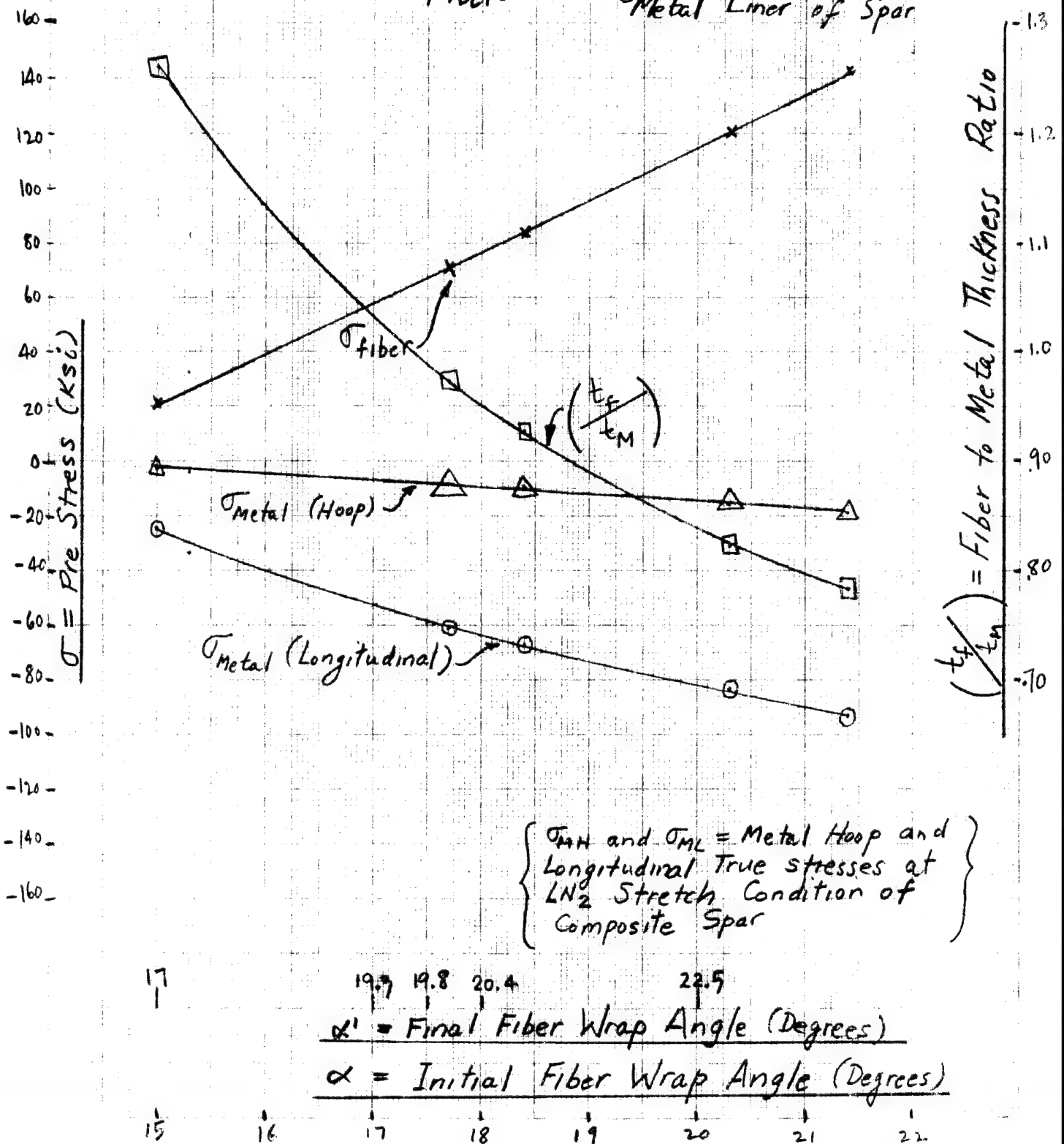
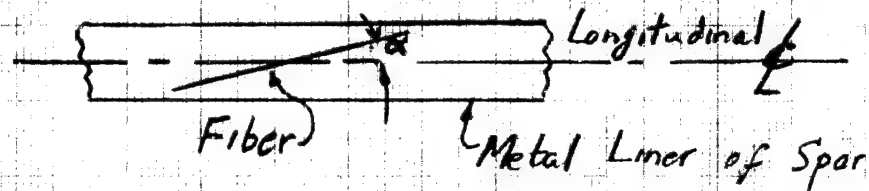


FIGURE 2-

The critical buckling loads for fiber overwrapped shells are much greater than the critical buckling loads for the same shells without the constrictive (pretensioned) fiber overwrap. Test data for hoop fiber wrapped cylindrical tubes (5) (7) (9) as well as a comparison with classical (unwrapped) cylindrical tube buckling strength, are given on figure 3. Many orders of magnitude improvement in buckling strength due to the fiber overwrap is evident. ARDE has had similar experience with fiber overwrapped spherical shells (4) wherein compressive prestresses as high as 120 ksi (72% of tensile yield point) at a diameter to thickness ratio of 650 were applied without liner buckling occurring. Some very limited data on buckling load improvement due to the constrictive fiber wrap for the prestressed composite spars fabricated and tested on this program are also available as discussed in section 3.2 and further detailed in Appendix 6.2. The physical reason for the improved buckling characteristics of the constrictively wrapped shells is that the fibers act like spring supports which resist shell displacement under the applied compressive loads and thus rule out the "classical" buckling mode shapes consisting of outward as well as inward displacements. Local inward cusp-like buckling mode shapes, as sketched on figure 4, have been observed. These buckling mode shapes correspond to much higher energy (or compressive load levels) compared to classical buckling mode shapes. Additional test data are obviously needed to properly define prestressed composite spar buckling criteria.

The prestressed composite spar test hardware fabricated was a  $17\frac{1}{2}^{\circ}$  initial fiber wrap angle configuration ( $\approx 20^{\circ}$  final fiber angle after cryostretch). Maximum liner operating bending stress was selected as  $\pm 34$  ksi. With a -50 ksi metal liner precompression, a constant axial tensile stress of 11 ksi was chosen to give a net liner compression of -5 ksi on the tension side of the spar liner "beam - column". These metal liner bending and direct axial stresses corresponded to a maximum estimated applied test bending moment of 22.5 inch kips at the crack station and a constant axial applied test load of 7 kips as detailed in Appendix 6.2.1.

### 3.1.2 Spar Fabrication Methods

The major fabrication steps utilized in building the prestressed composite spar hardware for the program are listed below and further defined by the sketches of figure 5.

- a) Metal head sub-assembly fabrication
- b) Metal body section fabrication
- c) Weld heads to body section to construct metal liner preform.
- d) Furnace anneal metal preform
- e) Hydrostatically shape metal preform in closed die



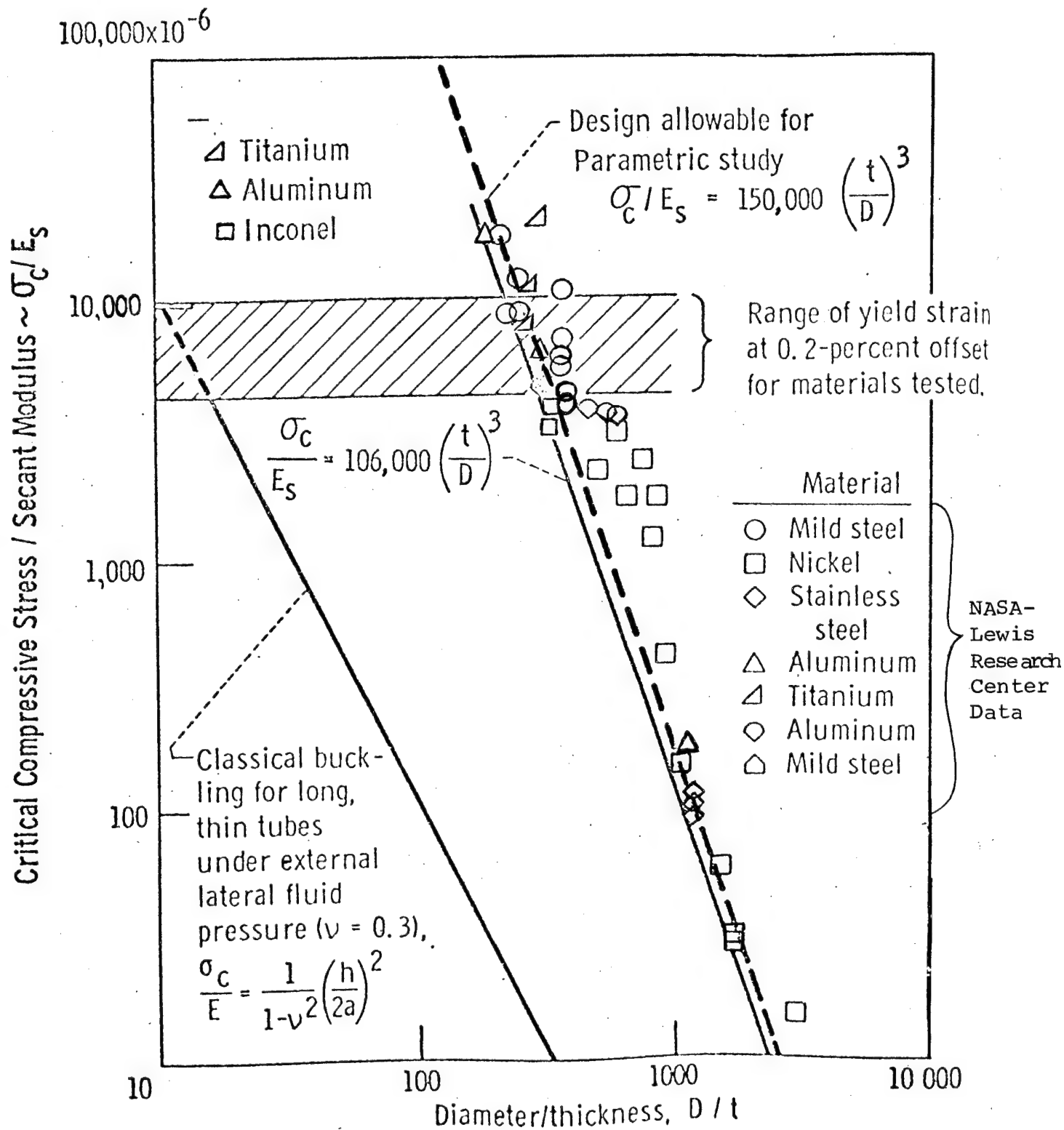
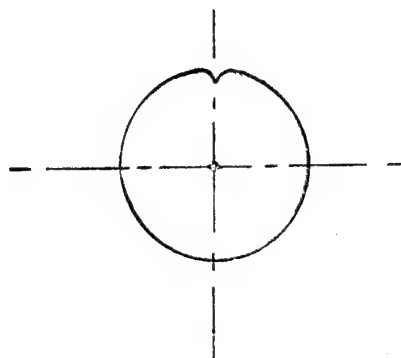
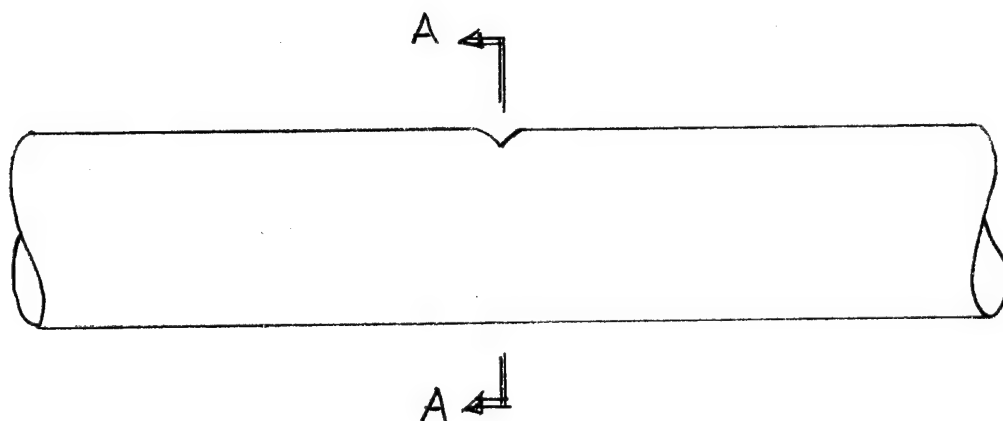


FIGURE 3

CONSTRUCTIVE-WRAP BUCKLING STRENGTHS  
FOR CYLINDRICAL TUBES

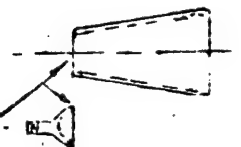


SECTION A-A

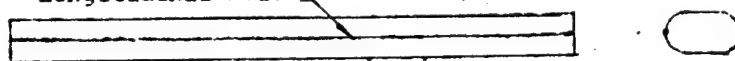
FIGURE 4  
CONSTRICTIVE OVERWRAPPED CYLINDER -  
TYPICAL BUCKLING MODE SHAPE

Head  
Subassembly  
Preform

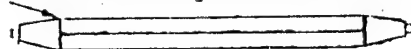
- Form metal heads from sheet (hydroform)
- Machine head bosses from bar stock
- Weld bosses to heads (TIG)



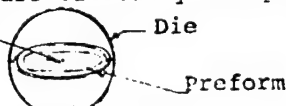
- Form metal body sections in two cross-sectional halves and weld together (simple forming tools "roll and weld" techniques)  
Longitudinal Weld



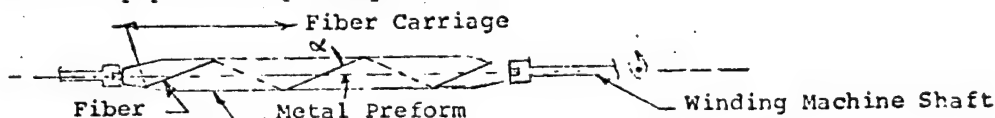
- TIG weld heads to body section(s) to construct metal preform.



- Furnace anneal
- Final shape preform hydrostatically in split, shaped, closed die  
Internal Hydrostatic Pressure (R.T. Water)



- Fiber wrap preform (primary fibers)



- Cryogenically stretchform fiberwrapped preform in split, shaped, closed die using liquid nitrogen as the coolant and pressurant.  
(Cryostrain strengthens metal liner pressure release & warm-up to ambient gives desired prestresses)



FIGURE 5

PRESTRESSED COMPOSITE SPAR MAJOR FABRICATION STEPS

- f) fiber wrap metal liner preform with primary fibers.
- g) Cryogenically stretch form fiber wrapped metal preform in closed die using liquid nitrogen as coolant and pressurant to strengthen liner and achieve the desired prestresses.

Additional descriptions of the prestressed composite spar fabrication processes are given on the photographs of figures 6 through 18. The fiber wrapping was done by Hercules, Inc., Aleghaney Ballistics Laboratory under a subcontract effort. All other spar fabrication work was performed by ARDE, INC.

### 3.2 Composite Spar Testing

#### 3.2.1 Test Program Description

A total of four (4) prestressed composite spar specimens were tested on the program, as detailed herein. Three (3) specimens were subjected to crack propagation testing and one (1) specimen was ballistically tested. The testing was performed by the Boeing Company, Vertol Division, under a subcontract from ARDE. The test vendors report is given in Appendix 1, Section 6.1.

##### 3.2.1.1 Crack Propagation Testing

Loading adapters were attached to the prestressed composite spar crack propagation test specimens to permit application of constant axial tension and variable cyclic bending moment loads by an existing testing machine. A 3/8" diameter circular hole was cut completely through the fiber wrap at the spar specimen center to facilitate application of a brittle arc burn defect to the metal liner. The constant axial load of 7 kips was applied and maintained for the duration of the tests. The crack propagation test specimen was then cycled at a high completely reversed bending stress level until a fatigue crack was formed in the brittle arc burn area of the liner. Various levels of cyclic (completely reversed) bending stresses were then applied to this precracked specimen for specific numbers of cycles and crack growth (if any) was monitored. The level of cyclic bending stresses at the constant number of cycles was increased in increments until crack growth was noted. Cyclic testing was then continued at the bending stress level that initiated growth of the artificially induced fatigue crack. Increase of crack length versus number of cycles was monitored to give the crack propagation rate data. The fibers on one (1) crack propagation specimen were intentionally cut completely through during testing to release the metal liner prestress and thus provide crack propagation baseline data on unstressed spar liners.

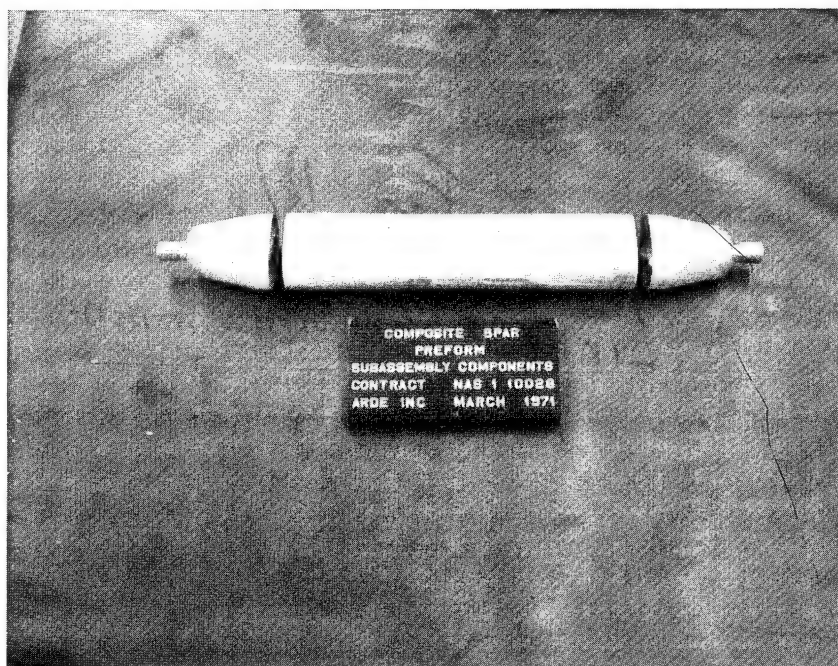


FIGURE 6  
LINER PREFORM COMPONENTS

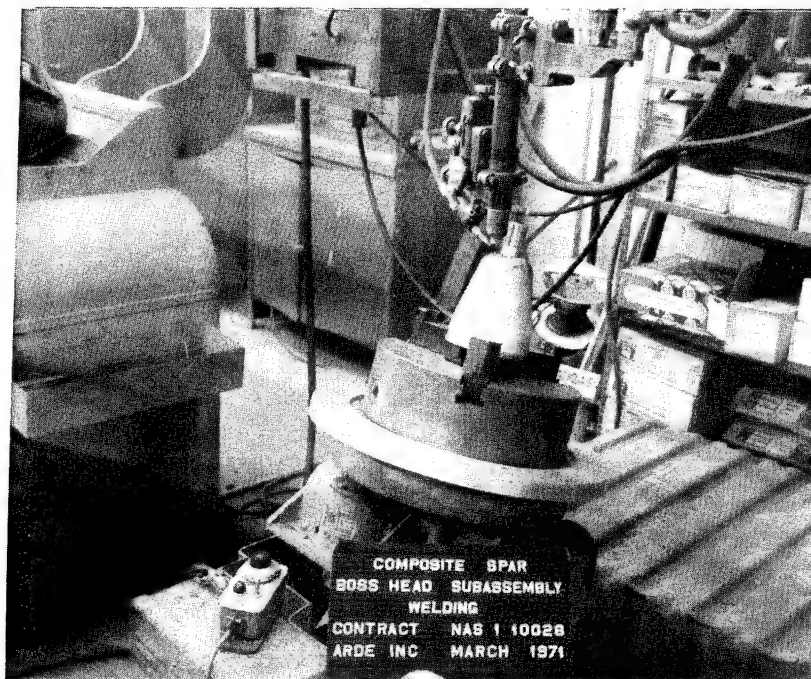


FIGURE 7

BOSS TO HEAD WELD

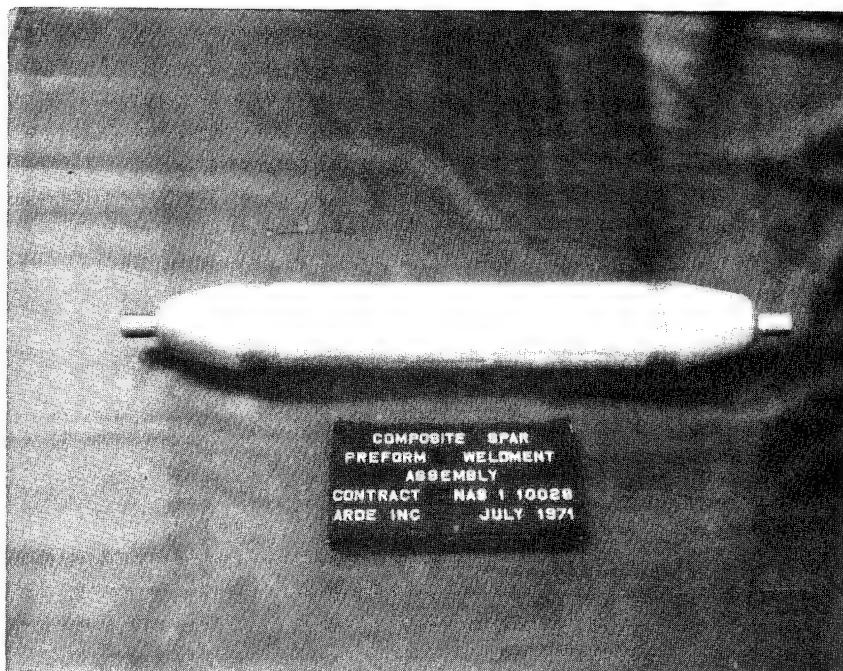


FIGURE 8

COMPLETED COMPOSITE SPAR PREFORM  
WELDMENT ASSEMBLY

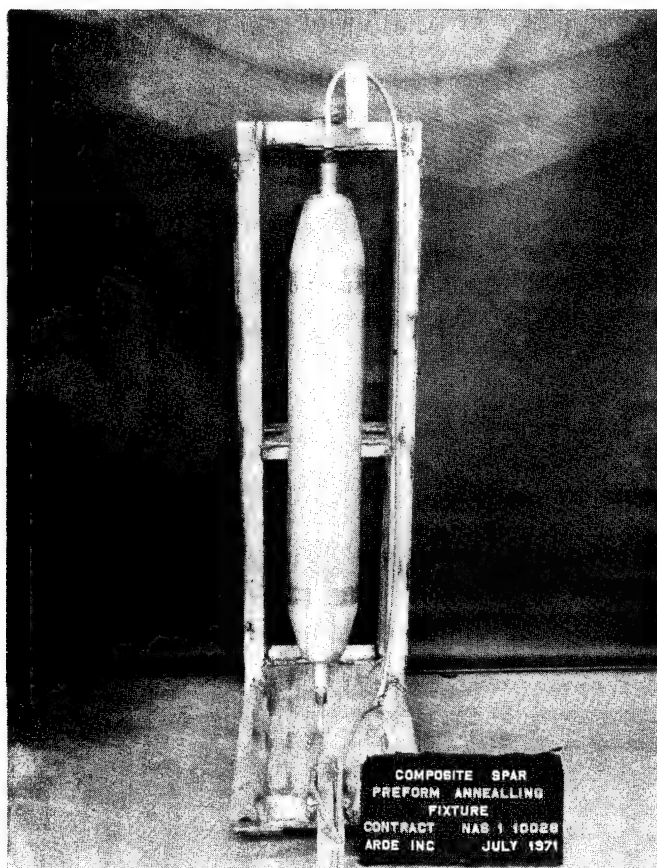


FIGURE 9  
ANNEALING FIXTURE





FIGURE 10

HYDROSTRETCH DIE

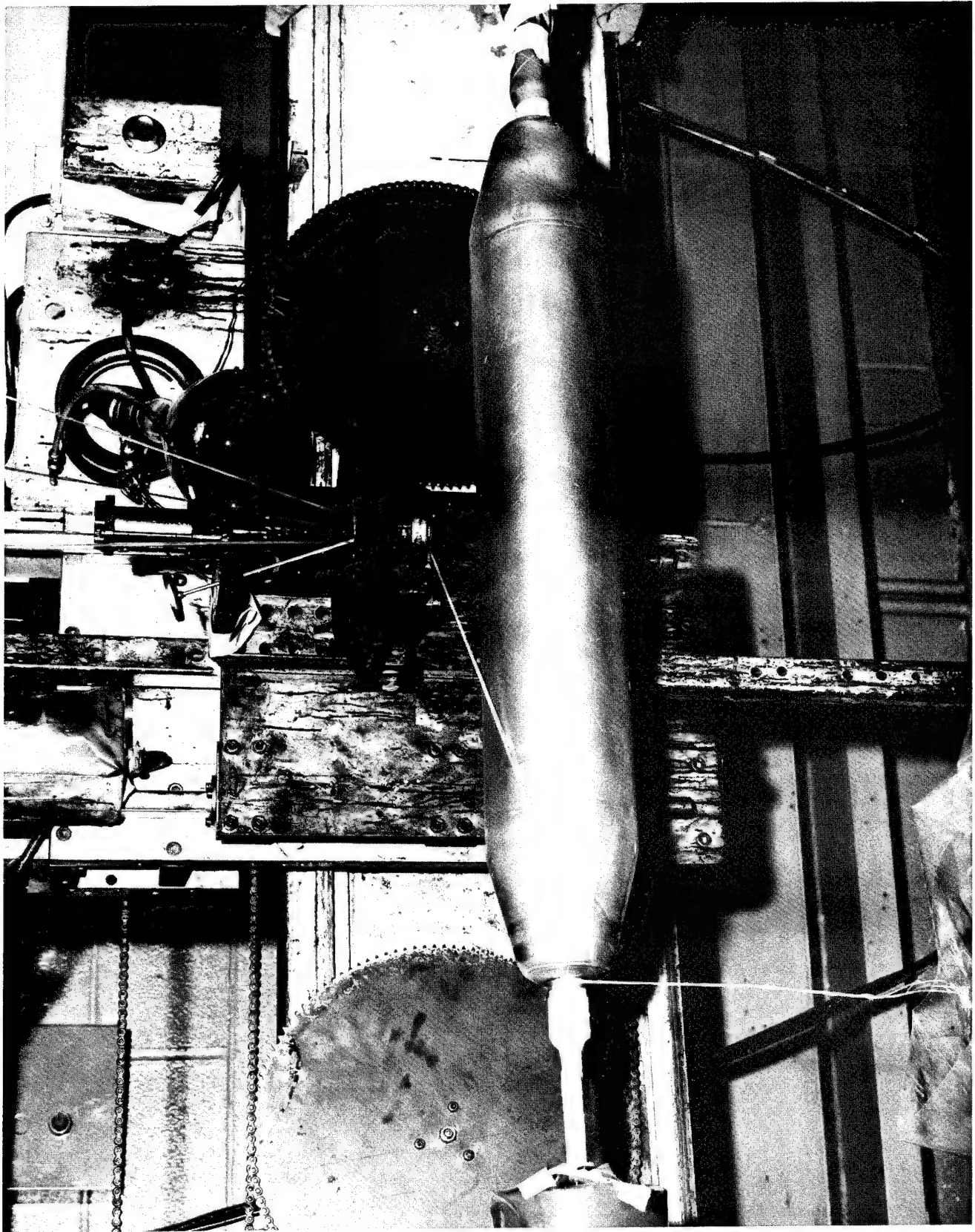


FIGURE 11  
START OF FIBER WRAPPING OF COMPOSITE  
SPAR METAL LINER PREFORM

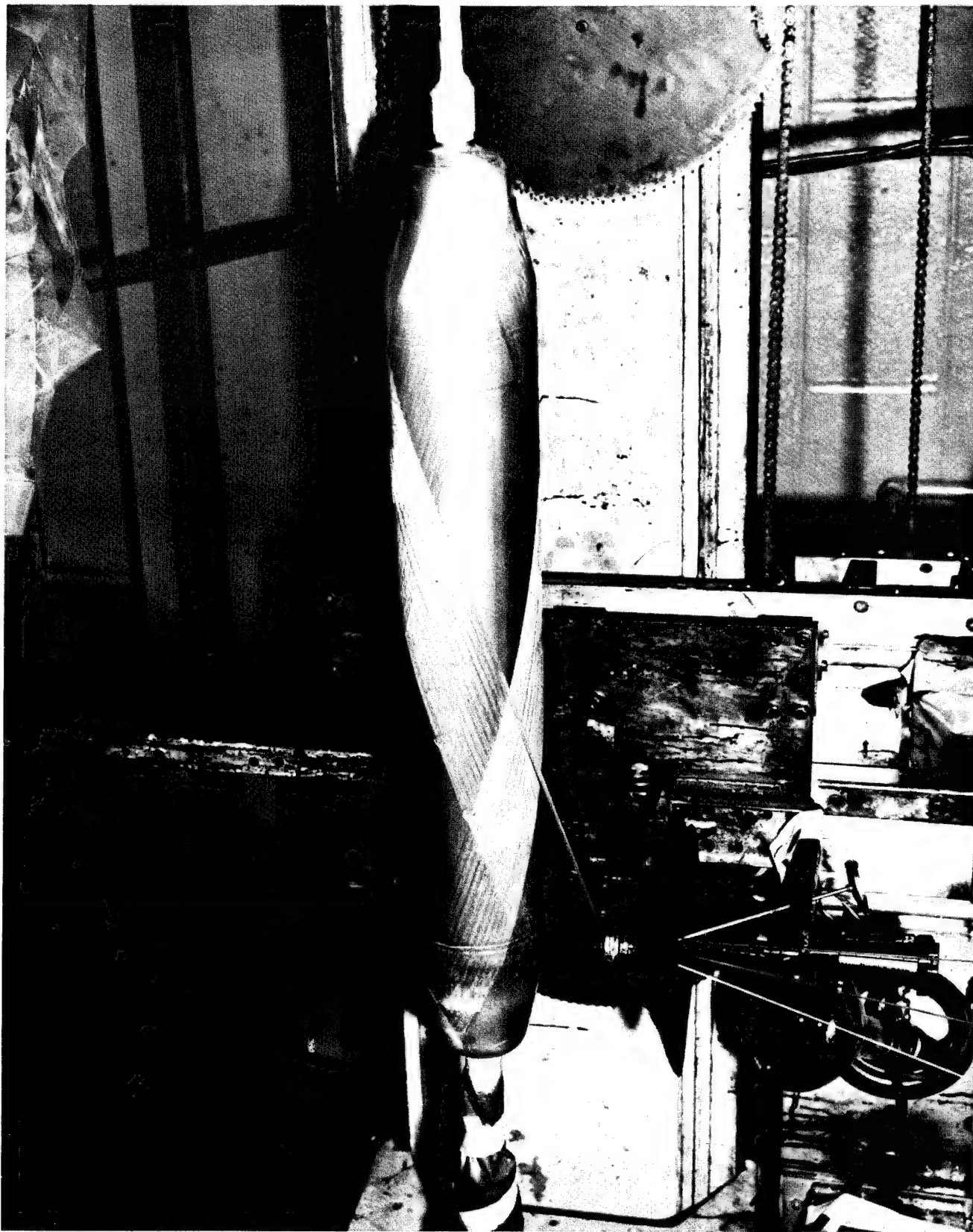


FIGURE 12  
BEGINNING STAGE - FIBER WRAPPING  
OF COMPOSITE SPAR METAL LINER PREFORM

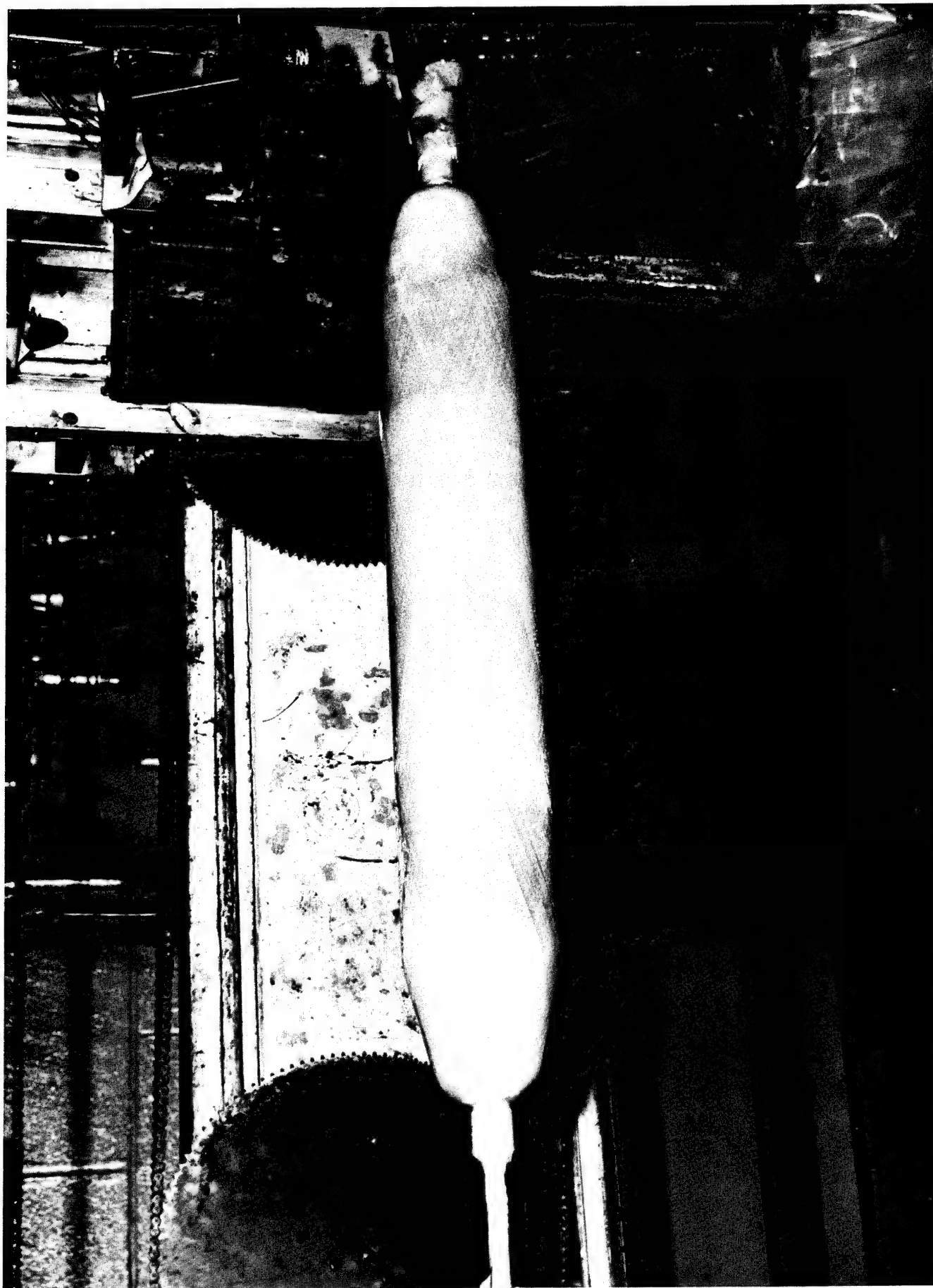


FIGURE 13  
FINAL STAGE - FIBER WRAPPING  
COMPOSITE SPAR METAL LINER PREFORM

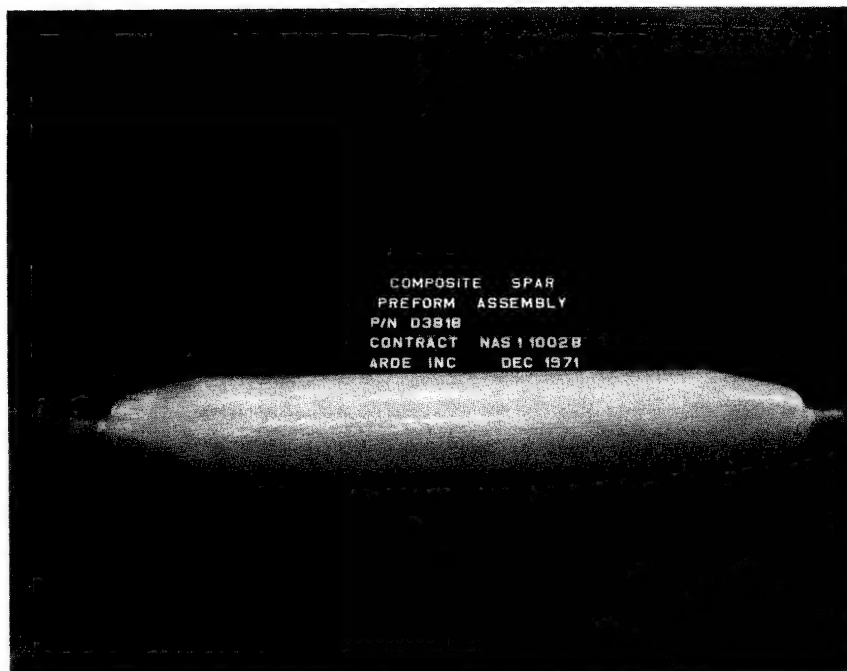


FIGURE 14

COMPLETED FIBER WRAPPED COMPOSITE SPAR  
PREFORM ASSEMBLY

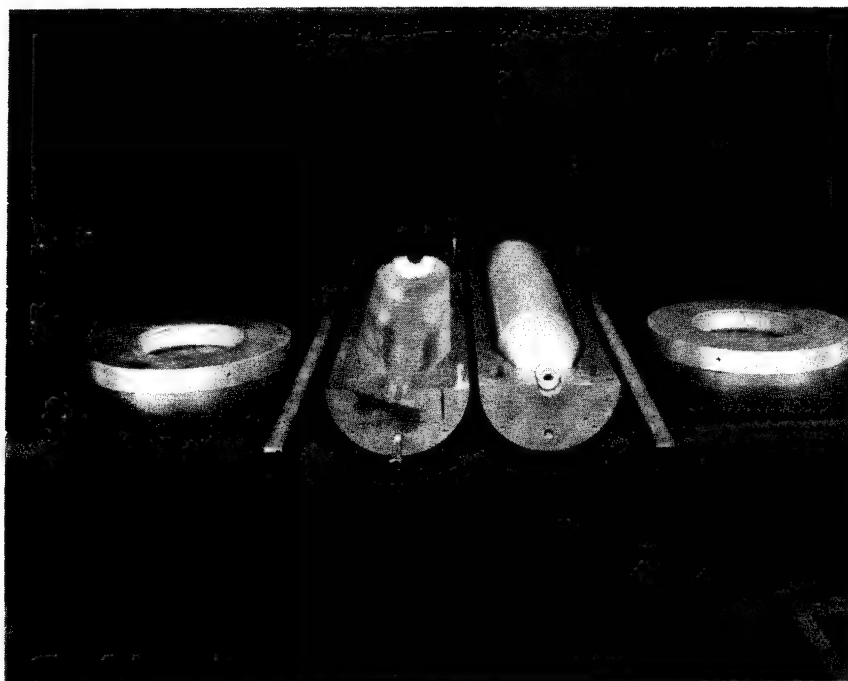


FIGURE 15

CRYOGENIC STRETCH DIE COMPONENTS



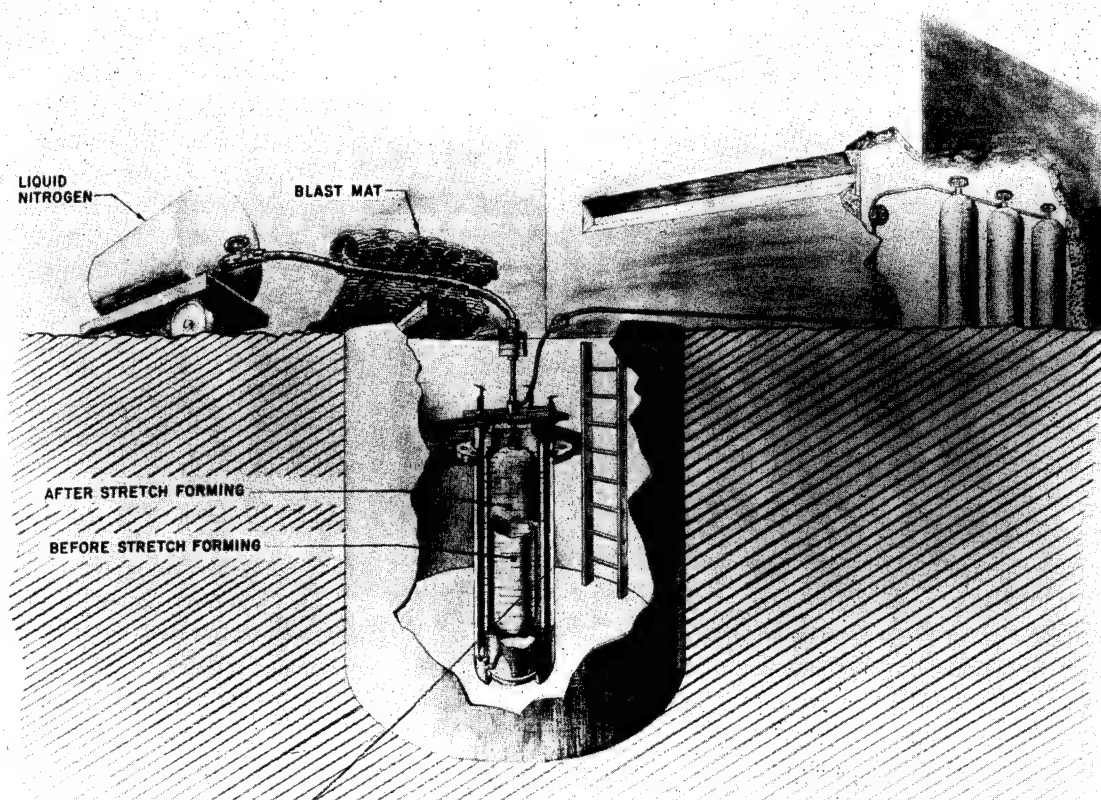


FIGURE 16

SCHEMATIC-CRYOGENIC  
STRETCH FACILITY



FIGURE 17

COMPOSITE SPAR CRYOGENIC STRETCH IN DIE



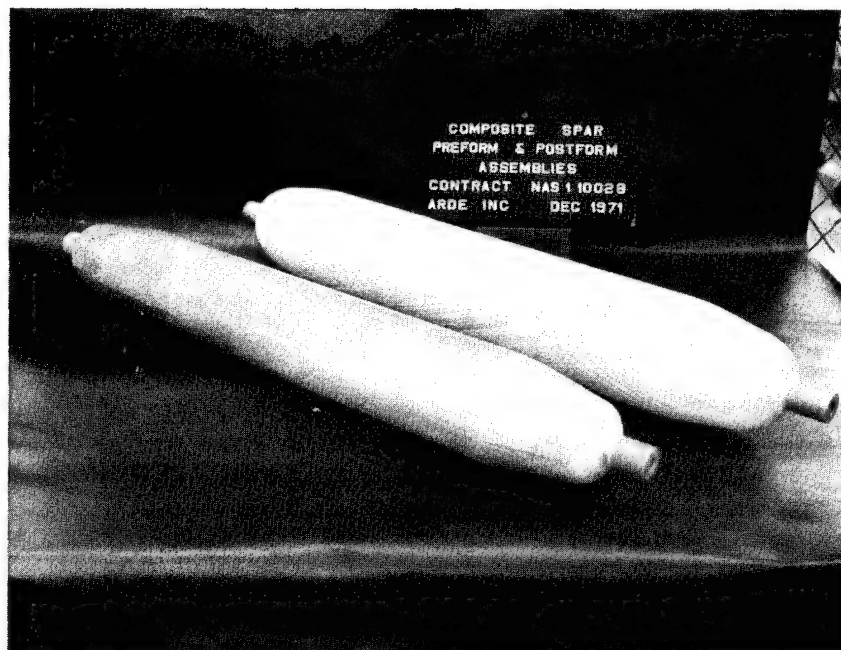


FIGURE 18

COMPOSITE SPAR PREFORM AND POSTFORM ASSEMBLIES

#### 3.2.1.2 Ballistic Testing

Three (3) ballistic hits with high velocity 30 caliber projectiles were made on a prestressed composite spar specimen. The condition of the specimen and the character of the ballistic damage was noted.

#### 3.2.2 Test Adapter and Composite Spar Specimen Design

The prestressed composite spar specimens fabricated were approximately 33 inches long. The minimum length specimen the existing testing machine could accomodate was 57 inches. Loading adapters were therefore needed at each end of the specimen to connect it to the testing machine so that the required constant axial tension and alternating bending moment loads could be applied to the prestressed composite spar test specimen. The spar specimen heads had been configured to facilitate axial loading through the metal threaded bosses at each end and bending load application by transverse bearing forces. This desireable specimen loading configuration could not be achieved without modification to the existing testing machine. Instead, a high risk, less desirable loading system had to be used. Axial loads had to be applied to the spar specimen by shear and bending loads applied by combined shear-bearing action.

The use of this existing testing machine therefore produced problems in load application during crack propagation testing of the first prestressed composite spar specimen (S/N 10). Test machine modifications and accompanying spar specimen assembly changes were subsequently made to permit load application by the originally conceived more structurally desireable method. These factors are discussed in detail in section 3.2.5. Solution of this load application problem has led to identification of rotor attachment concepts(s).

The original design of the crack propagation specimen is shown on ARDE drawing E 3866D (figure 19). The solid aluminum pillow blocks (E 3866-1) and overall specimen length are configured to mate with the existing testing machine. The aluminum tubular adapters (E 3866-2) connect the spar specimen to the testing machine via the solid pillow block. The tubular adapters are round at the pillow block interface region and oval shaped at the other end region to mate with the spar oval cross-section as shown on the drawing. The pillow blocks and tubular adapters are connected by shoulder bolts and adhesive. The prestressed composite spar



specimen is adhesively bonded to the tubular adapters. Fiber glass hoop overwrap is used to reduce "prying action" due to shear and bending load transfer from the tubular adapter to the spar specimen. A bi-directional fiber glass cloth doubler is bonded to the fiber wrap at the center of the spar specimen as detailed on figure 19. A 3/8" diameter hole is subsequently machined completely through the fiberglass to expose the metal liner for application of the brittle arc burn defect and start a fatigue crack in the metal for crack propagation testing.

### 3.2.3 Test Adapter and Composite Spar Specimen Fabrication

The major fabrication steps for the composite spar crack propagation test specimen assembly E 3866 (Fig. 19) are outlined below. Prestressed composite spar specimen fabrication methods have been previously described in section 3.1.2.

#### 3.2.3.1 E 3866-1 Adapter - Pillow Block

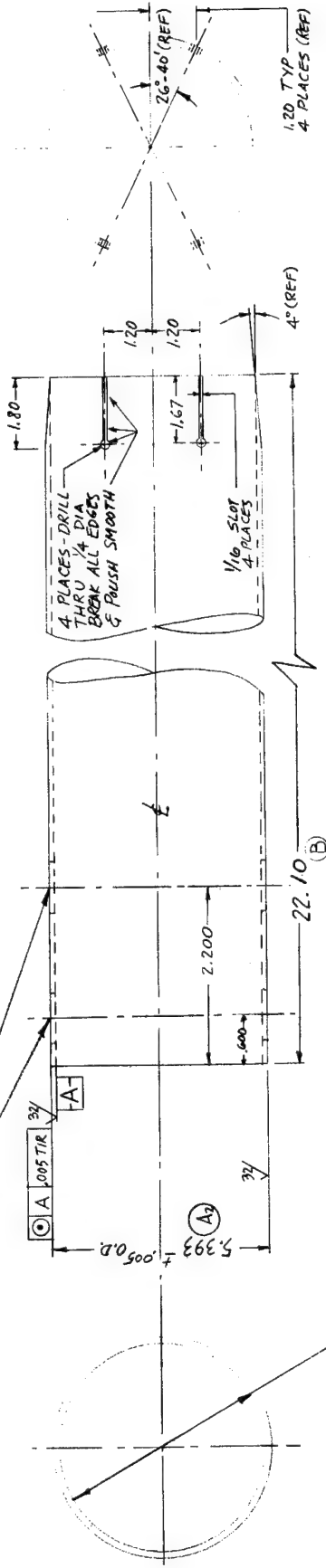
This pillow block adapter was machined as detailed on figure 19 from 7075-T6 aluminum cylindrical rod stock 6" in diameter and the required heli-coil inserts and headless steel bushings were then installed.

#### 3.2.3.2 E 3866-2 Adapter - Specimen

a) The tubular adapter was fabricated starting with 5½ O. D. x ½" wall 6061T6 aluminum tube stock machined as detailed on drawing C104678 (figure 20). The inside diameter of the machined tube was selected to give a circular cross-section perimeter equal to the outer perimeter of the oval shaped composite spar body section plus gluing clearance allowance. A close fit with the E 3866-1 adapter - pillow block mating cylindrical surface was also provided.

b) The machined tube-adapter specimen (figure 20) was then formed by pushing an oval shaped solid plug tool into the tube. A solid lubricant was used on the plug-tube interface. The E 3866-1 adapter - pillow block was assembled to the C104678 tube during this forming operation to keep the other end of the tube round as required. A 60,000 pound capacity Tinius Olsen tensile testing machine was used to supply the force required for forming and removal of the oval shaped forming tool. Figure 21 shows the tube forming set up with the oval shaped forming tool being inserted at the tube top. This forming technique developed for forming the required circular to oval cross-section tubular

SIX (6) HOLES EQUALLY SPACED TWO PLACES AS SHOWN (12 HOLES TOTAL)  
 39/64 DRILL THRU & REAM .005 DIA THRU  
 INSTALL E3866 DETAIL ⑧ BUSHING & DETAIL ⑩ WASHER



5.133 ± .003 I.D. (A)

NOTES:

MAKE FROM COMMERCIAL TUBE  
 5 1/2 O.D. x 1/2 WALL  
 6061 T6 ALUMINUM

C104678

E.O. NO.		SYMBOL		REVISIONS		DATE		APPROVED	
				DESCRIPTION					
		A		1) 5.133 ± .003 I.D. WAS 5.102 I.D.		2/21/73		JL	
		B		2) 5.393 ± .005 O.D. WAS 5.355 ± .005 O.D.		3/1/73		JL	
		C		22.10 WAS 22.40		4/14/73		JL	
				1) ADDED 12 HOLES, 6 IN TWO PLACES					
				2) ADDED INSTALLATION OF E3866 ⑧ BUSHINGS & ⑩ WASHERS					

QTY REQD PER DASH NO.		ITEM NO.	CODE IDENT	PART OR IDENTIFYING NO.	NOMENCLATURE OR DESCRIPTION	MATERIAL	SPECIFICATION
LIST OF MATERIAL OR PARTS LIST							
UNLESS OTHERWISE SPECIFIED		DRAWN BY		1-4-13	TITLE		
DIMENSIONS ARE IN INCHES		CHECKER		1-5-73	ARDE, INC. PARANUS, N. J.		
TOLERANCES		STRESS ENGR			TUBE - ADAPTER SPECIMEN		
XX = ± .010, XXX = ± .005		AERO THERMO			C 104678		
BREAK SHARP EDGES .005-.015		DES. ENGR		D.B. 1/4/73	05980 C		
ALL SMALL FILLETS .005-.010		PROJ. ENGR			SCALE		
THREADS PER FED. HNOBK H-38 AND					SHEET		
DIMENSIONS PER MIL-STD-8							
WELD SYMBOLS PER JAN-STD-19							
SURFACE ROUGHNESS SYMBOLS PER							
MIL-STD-10							
ALL FINISHED SURFACES 125							
NEXT ASSEMBLY							
E 3866							

ARDE, INC.  
 PARAMUS, N.Y.

TUBE -  
 ADAPTER SPECIMEN

CODE IDENT NO. C 104678

SHEET

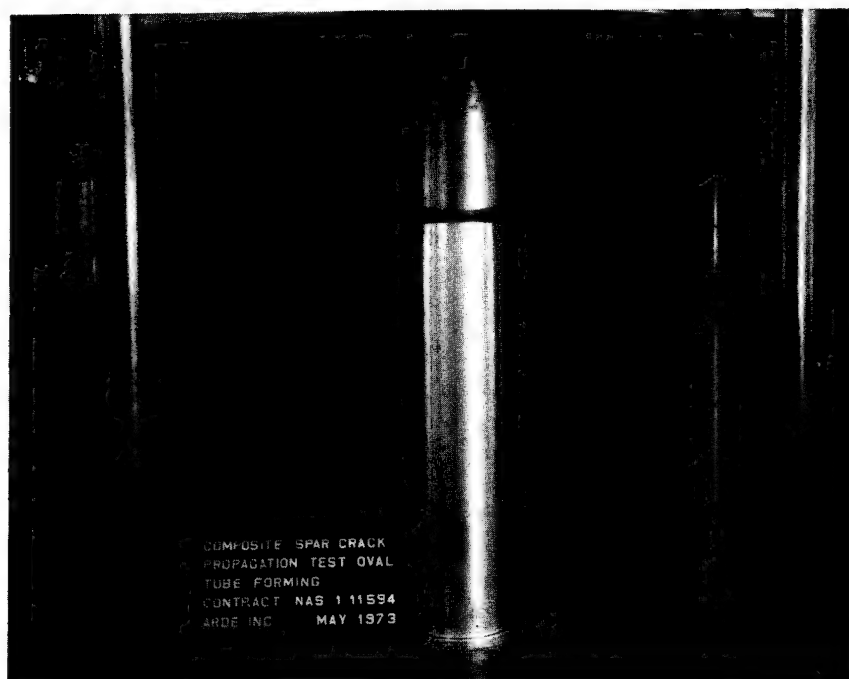


FIGURE 21

member proved simple and was quite successful. It would appear to have application to rotor connection structural components or other structures requiring circular to oval or circular to any smoothly varying rotationally symmetric cross-sectional shape.

### 3.2.3.3 E 3866D Composite Spar Crack Propagation Test Specimen Assembly

These test specimen assemblies were put together by the fiber wrap vendor (Hercules, Inc., Alleghany Ballistics Laboratory) using components provided by ARDE. The E 3866-1 and E 3866-2 adapters were bonded and bolted together as indicated on the drawing. The bi-axial glass cloth doubler was bonded to the D 3819 Spar, Composite Assembly. One (1) each of the attached -1 and -2 aluminum adapters were then bonded to each end of the D 3819 composite spar assembly and overwrapped with hoop fiberglass as required to complete the assembly. All bonding was done with room temperature curing epoxy base adhesives. Photographs of completed composite spar crack propagation test specimen assemblies are shown on figures 22 and 23.

After room temperature curing, the test specimens were subjected to an axial load proof test as a check on the bonded joints. A test load of 15,000 # (215% of operating load) was applied and held for 5 minutes. After test load removal, the specimens were visually inspected for damage and/or dimensional changes. No specimen damage or dimensional changes were observed after the axial load proof tests. The axial load proof test set up is shown on figure 24.

The completed and proof tested composite spar crack propagation test specimens were shipped to ARDE for final machining and inspection. A 3/8" diameter hole was machined completely through the fiberglass (and bi-axial cloth doubler) in the spar specimen center, thus exposing the metal for subsequent application of a brittle arc burn and initiation of a starting fatigue crack.

### 3.2.4 Description of Test Set-Up & Procedures

#### 3.2.4.1 Crack Propagation Tests

An arc burn was put in the metal liner of each of the E 3866D test specimen assemblies at the fiberglass cutout station. This arc burn embrittled the metal and served as a stress riser for subsequent initiation of a "starting" fatigue crack. Each specimen was appropriately strain gaged and statically

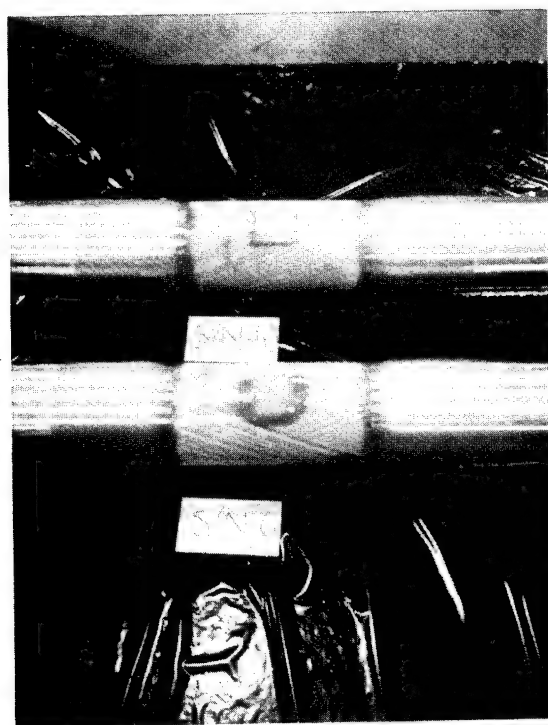
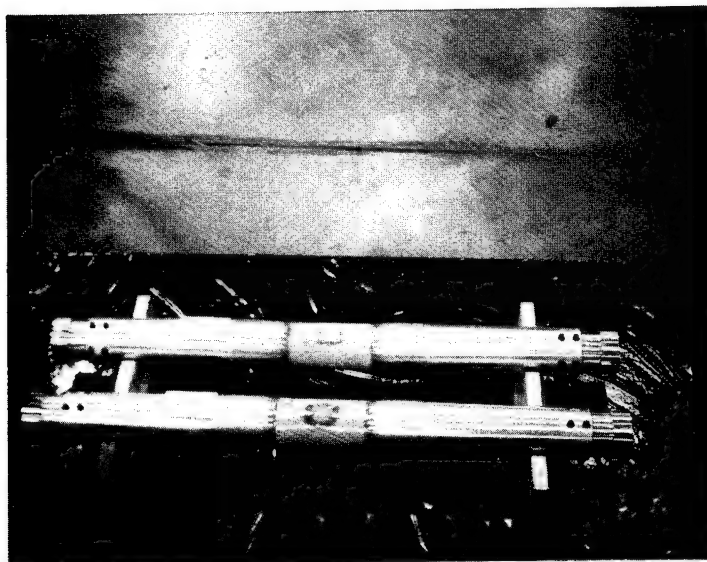


FIGURE 22

COMPOSITE SPAR CRACK PROPAGATION TEST ASSEMBLY  
P/N E3866D S/N 6 & 10



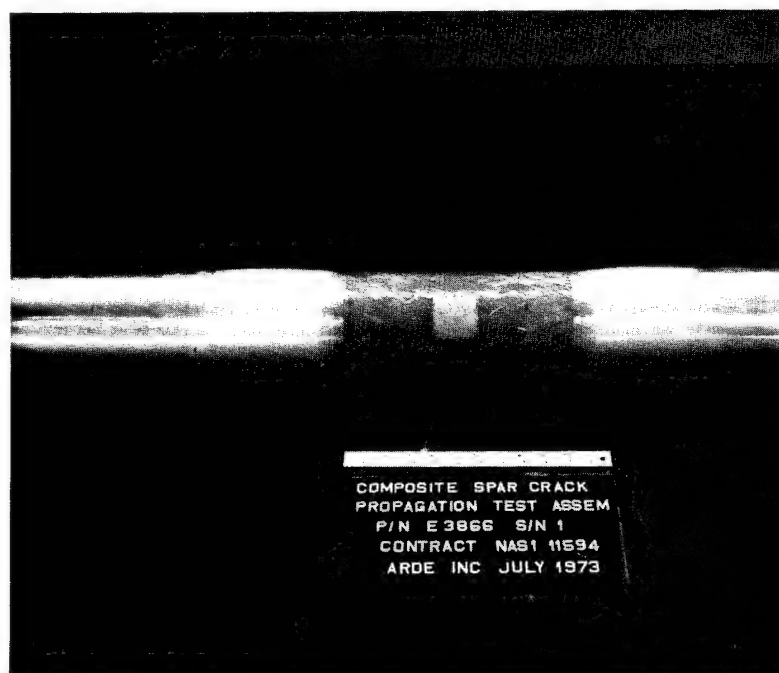
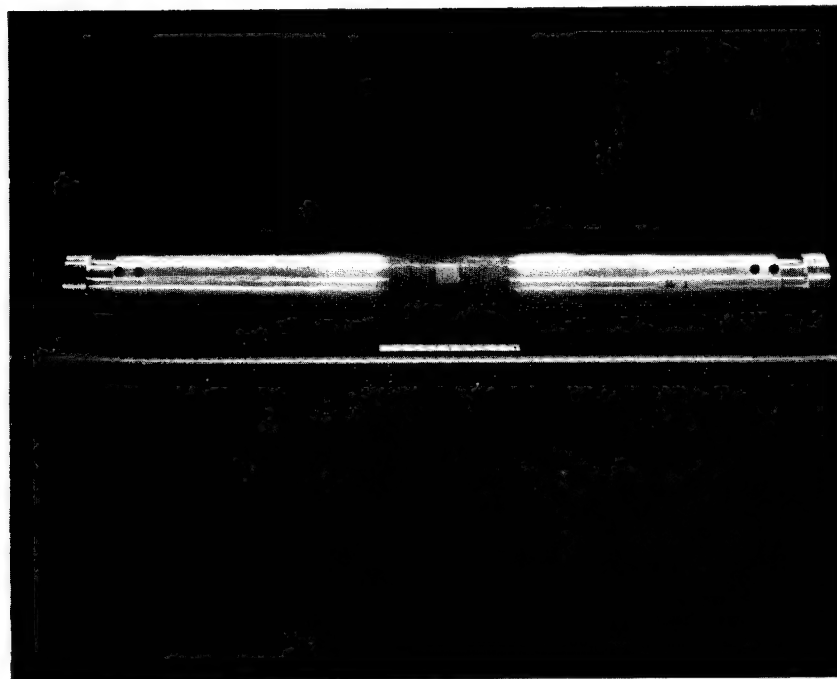


FIGURE 23

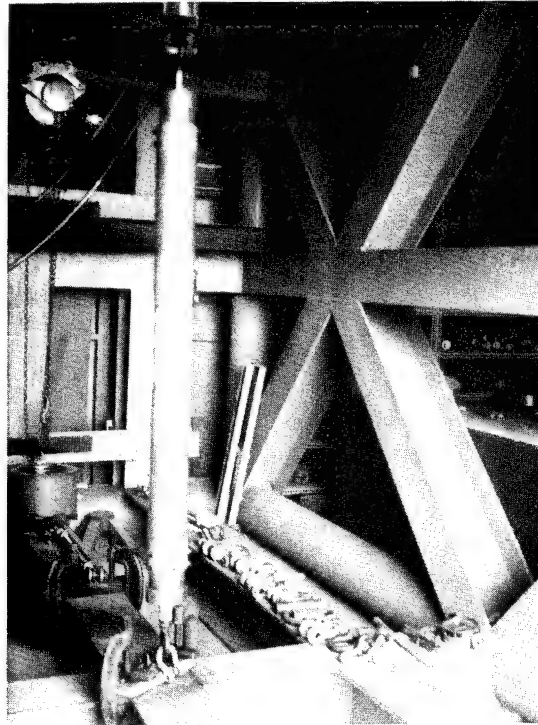


FIGURE 24  
COMPOSITE SPAR CRACK PROPAGATION TEST ASSEMBLY  
P/N E3866D S/N 1  
AXIAL LOAD PROOF TEST SET-UP

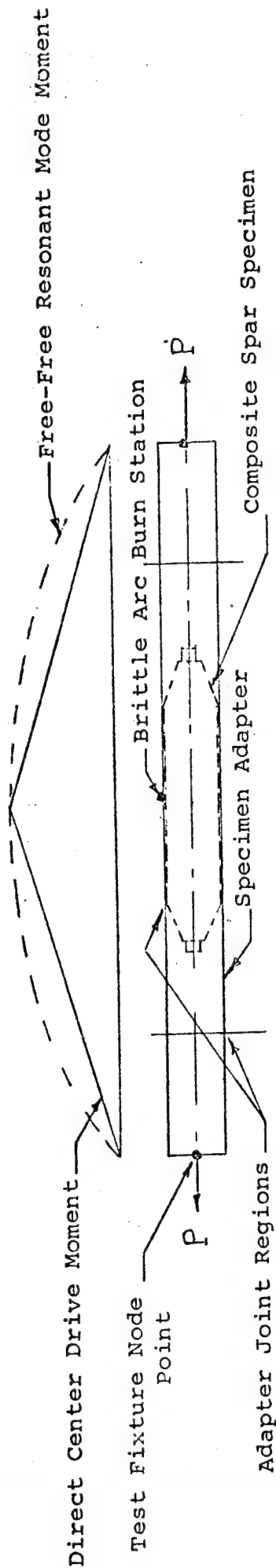
calibrated as a simply supported beam on knife edges. The "beam-column" correction to the bending strain was small (less than 2%) and accordingly was ignored. The statically derived relation between moment and bending strain was used subsequently to define the dynamic bending moment from the measured strain gage output.

The specimens were installed in an existing resonant blade fatigue testing machine capable of applying steady axial tension and alternating bending moment about the "weaker axis" of the specimen. The arc burn (crack station) was located at the spar mid-section at the maximum distance from the neutral axis on the tension side of the "beam-column" specimen. A constant axial tensile load of 7000 pounds (simulating centrifugal force) was applied and maintained for the duration of the tests. The initial stress state of the prestressed composite spar specimen metal liners prior to crack propagation testing was -50 ksi axial compression due to the fiber wrap applied prestress and + 11 ksi axial tension due to the constant 7000 pound axial load applied.

The prestressed composite spar specimen assemblies were excited in bending through a frequency range of 0 - 100 Hz and the natural resonant frequency of the system established. The spar test units were then resonated at their natural frequencies under high bending stresses until a fatigue crack was observed at the arc burn stations. Crack propagation testing then continued at a force driven rather than a resonant mode. Various levels of alternating bending stresses,  $\sigma_i$ , were applied in increments for numbers of cycles,  $N_i$ , until crack growth (of the initial fatigue crack) was noted. Then crack growth versus numbers of cycles was monitored. The bending stress level,  $\sigma_i$ , which initiated crack growth, was held constant for this portion of the test.

Crack start and growth was directly monitored (measured) when the crack was visible within the 3/8" diameter cut out region in the fiberglass. X-ray techniques were used to obtain crack progression data when the crack extended under the fiberglass wrap. Metal liner compressive prestress held the crack tightly together making X-ray monitoring difficult. This problem was solved by opening the crack up again on the tension side of the spar beam by static application of bending moment.

A schematic of the crack propagation test set up and a summary of some key data for the three (3) crack propagation test specimens are given on figure 25. Columns 3 and 4 give the number of bending stress cycles and applied alternating bending stress levels required to initiate the reference fatigue crack at the arc burn station. The alternating bending stress values for start of the reference fatigue crack growth are listed in column 5.



# (1) Metal Liner Stress State (Prior to Crack Propagation Testing)

(+11/33 ksi tension) due to constant axial load.  
 (-50 ksi compression) due to fiberwrap prestress.

Brittle arc burn defect applied at composite spar center through machined hole in fiberglass wrap.  
 Composite spar cycled in bending to initiate fatigue crack in arc burn region.

① Specimen No.	② S/N	③ Cycles of bending stress to start crack in arc burn	④ Bending stress applied	⑤ Bending stress for start of crack growth*
02	06	$8 \times 10^4$	$\pm 33$ ksi	$\pm 30$ ksi
03	01	$3 \times 10^4$	$\pm 33.5$ ksi	$\pm 25$ ksi ( $\pm 10$ without prestress)
01	10	$7 \times 10^4$	$\pm 29$ ksi	$\pm 10$ ksi (Invalid failure specimen) Test equipment failure

## (2) Crack Propagation Testing

Various alternating bending stress levels applied for number of cycles, Ni, until crack growth start noted (\*see column 5 above). Then crack growth versus number of cycles monitored.

Figure 25  
 Crack Propagation Test Set-Up Schematic

### 3.2.4.2 Ballistic Tests

Three (3) target points were marked with crosses at center and end regions on the exterior fiber wrap of a prestressed composite spar specimen. The specimen under zero external load was then placed in a ballistic test range and impacted with three (3) 30 caliber high velocity projectiles at (or near) the target points. The specimen was then inspected for damage.

### 3.2.5 Test Results

#### 3.2.5.1 Crack Propagation Tests

##### 3.2.5.1.1 S/N 10 Prestressed Composite Spar (Specimen No. 1)

##### a) Specimen Calibration and Initial Loading

The specimen was strain gaged on the fiber wrap as shown in figure 26 and statically calibrated as a simply supported beam in bending. Figure 27 gives a typical static moment diagram derived from a measured transverse (shear) applied approximately at mid span. Strain gage outputs were recorded for each applied shear load increment to provide the required relation between axial fiber strain and bending moment.

The prestressed composite spar test specimen was then installed into the resonant blade fatigue test fixture. An axial tensile load of 7000 pounds was applied to the specimen by means of a springbank arrangement. The axial load was monitored by calibrated load links between the springbank and the specimen and checked by the spring rate of the springbank.

The test specimen was left overnight under axial load. The following morning it was observed that a failure had occurred at the bonded joint between the aluminum tube adapter and the prestressed composite spar specimen. A photograph of the failed bonded joint region of the S/N 10 test specimen assembly is shown on figure 28.

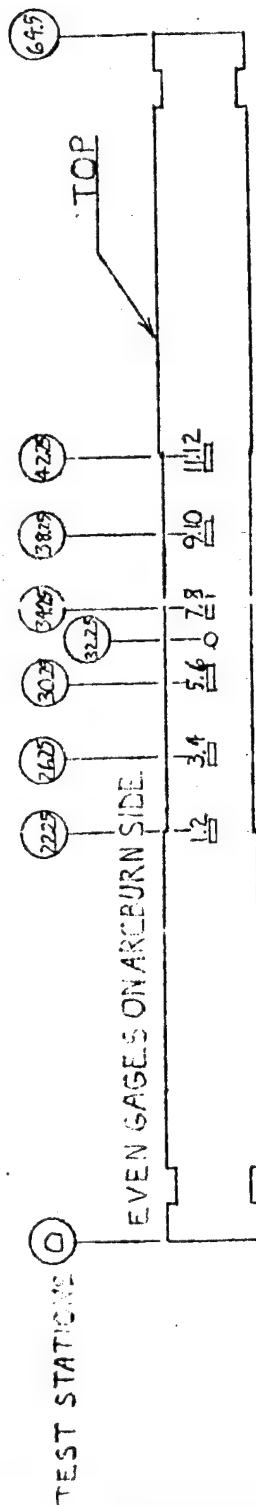
##### b) Test Fixture and Test Specimen Modification

Reconfigurations of the prestressed composite spar crack propagation test specimen assembly (figure 19) as well as modifications to the existing blade fatigue test fixture were made to solve the test fixture to test specimen

# Composite Metallic-Fiberglass Prestressed Spar Structural Model Tests

EW 7000-52060-11C01-000000

SPECIMEN No. 1 S/H 10



CRACK INITIATION FREQUENCY = 40 Hz  
CYCLES - CRACK INITIATION = .071 X 10<sup>6</sup>  
CONTROL ON GAGES 7/8

CRACK PROGRESSION FREQUENCY = 15 Hz  
CYCLES - CRACK PROGRESSION = 1.65 X 10<sup>6</sup>  
CONTROL ON GAGE 8

STRAIN GAGES	7/8	5	7	8	11
CRACK INITIATION ± MOMENT IN LBS.	21,000	21,000	21,000	31,700	130,200
CRACK INITIATION ± STRESS PSI	27,700	24,000	23,400	31,100	
CRACK PROGRESSION ± STRESS PSI	9,900	8,065	11,000	8,500	
CRACK INITIATION ± STRAIN (in/in)	1065	922	11050	1196	
ON FIBERGLASS					
CRACK PROGRESSION ± STRAIN (in/in)	367	321	421	344	
ON FIBERGLASS					

STRESS VALUES CALCULATED ASSUMING STRAIN IN STEEL EQUALS STRAIN IN FIBERGLASS.

FIGURE 26 J.D.F. 10/11/73  
S.P.M. 4-22-73

# STATIC CALIBRATION OF SPECIMEN STATIC BENDING MOMENT VS. TEST STATIONS S/NIO

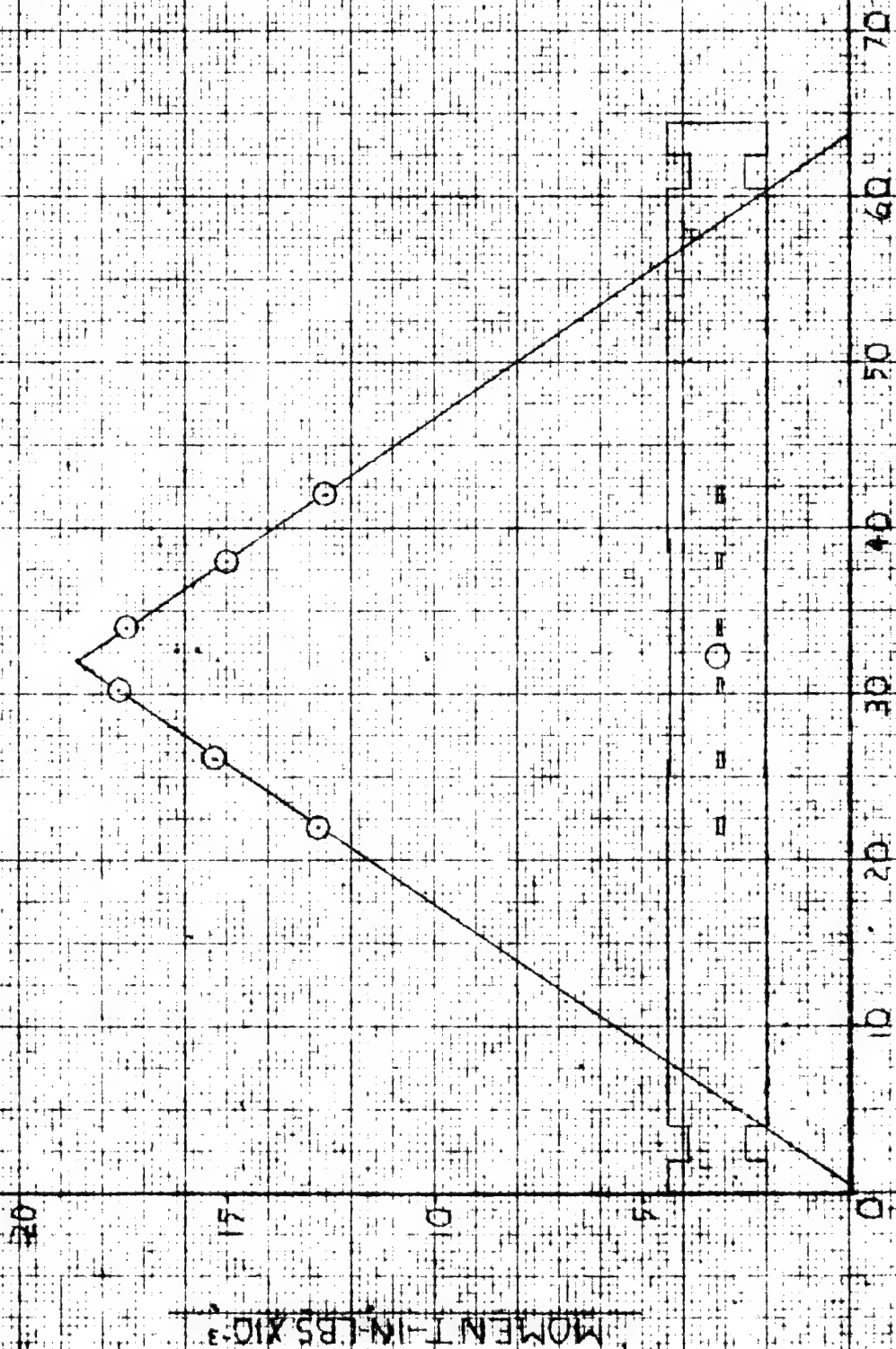


Figure 27



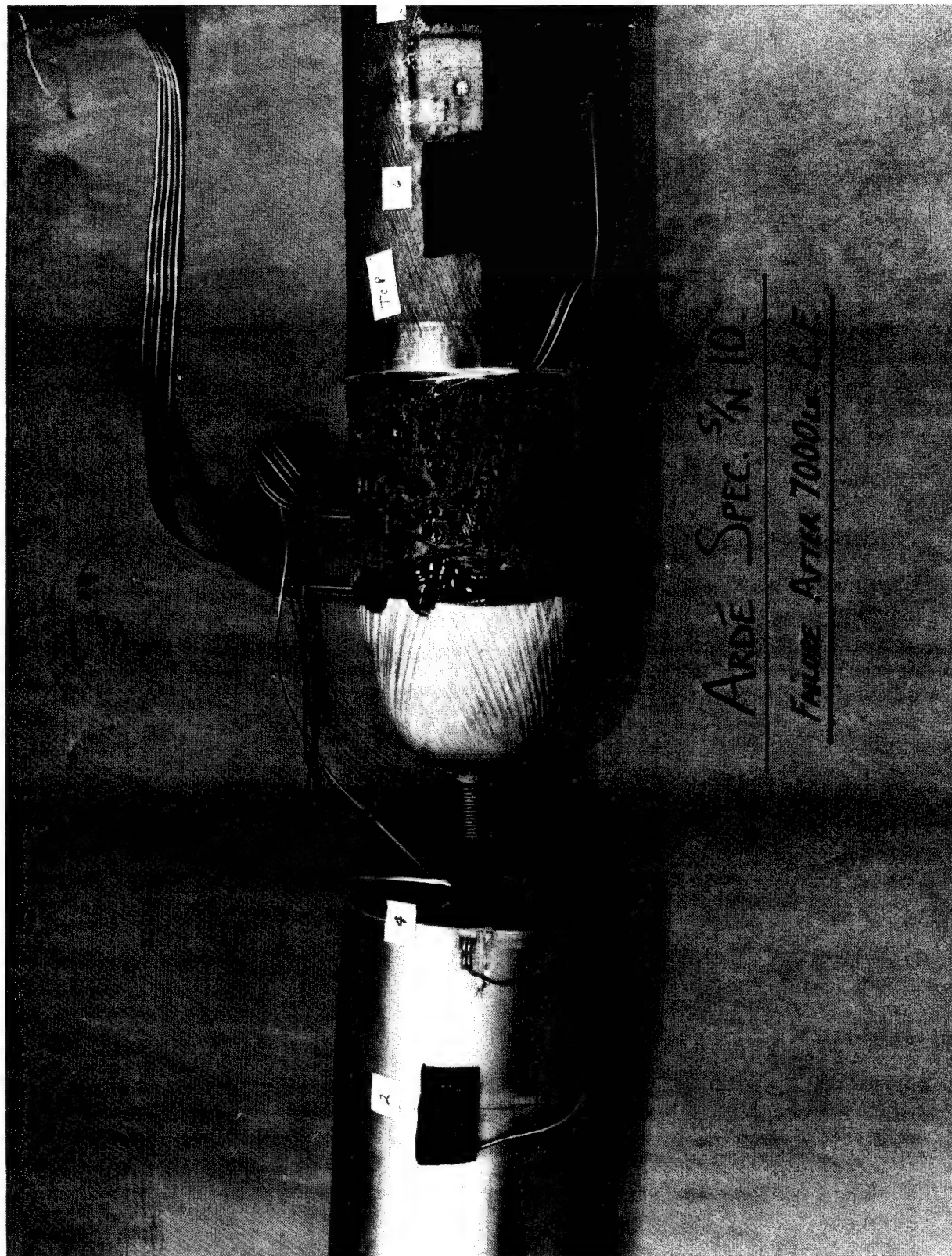


Figure 28 -

BOND FAILURE AFTER 7000 LB. AXIAL  
TENSION LOAD APPLICATION



load transfer problem. These modifications provided for direct axial load transfer as well as moment transfer to the test specimen by transverse bearing forces (rather than by the high risk load transfer through adhesive shear).

The fatigue test fixture was modified to permit direct axial load application to the prestressed composite spar through the central threaded metal bosses in each metal liner head. Threaded rod ends were then attached between the threaded bosses on each end of the composite spar specimen and the aluminum pillow blocks at the test specimen assembly ends. The rod end bearings prevented bending moment transfer to the threaded bosses of the heads. The joints between the aluminum tube adapter and the composite spar specimen heads were potted with epoxy to facilitate bending moment transfer from the tube-adapters to the heads of the prestressed composite spar specimen. Aluminum clamps were also used in this region to help in the bending moment transfer from the tube adapters to the spar specimen heads and to add rigidity to the structure. The screw attachment between the aluminum pillow block and the aluminum tube adapter was removed (see figure 19) and replaced by aluminum clamps to eliminate axial load transfer and to provide for the bending moment transfer from the test fixture to the test specimen assembly. A sketch of the modified crack propagation test specimen assembly is given on figure 29. A photograph of a reconfigured crack propagation test specimen assembly installed in the blade test fixture is shown on figure 30.

#### c) Crack Initiation and Growth

A natural resonant frequency of 40 Hz was established and the spar test specimen excited at  $\pm 29$  ksi in the metal liner at the arc burn station. After  $.071 \times 10^6$  cycles, a fatigue crack .13 inches long was initiated in the arc burn. Crack propagation testing was then continued at 15 Hz at  $\pm 10$  ksi in the liner at the crack station in a force driven rather than a resonant mode. A hydraulic actuator was used to apply the alternating shear force at specimen station 29.0 (close to crack station 32.25) as detailed on figure 29 and shown in the photograph of figure 30.

After  $1.65 \times 10^6$  cycles a malfunction of the test rig and hydraulic actuator caused a severe overload condition on the specimen which precluded further testing. A bending stress of approximately  $\pm 100$  ksi (about three times the maximum anticipated value) was inadvertently applied to the liner at the crack station. This high bending stress, together with the -39 ksi net liner axial compression, caused liner buckling as detailed in the Appendix, section 6.2.3. Total crack length at this stage was .44 inches. Crack length versus cycles data for S/N 10 prestressed composite spar specimen is given on figure 31.

# ROD END ASSEMBLIES

STAINLESS STEEL SPECIMEN  
1/2 IN THICK 4340 STEEL PLATES

1/4 IN 11-THREAD ROD

ROD ENDS

93% EPOXY

CLAMP ASSEMBLY

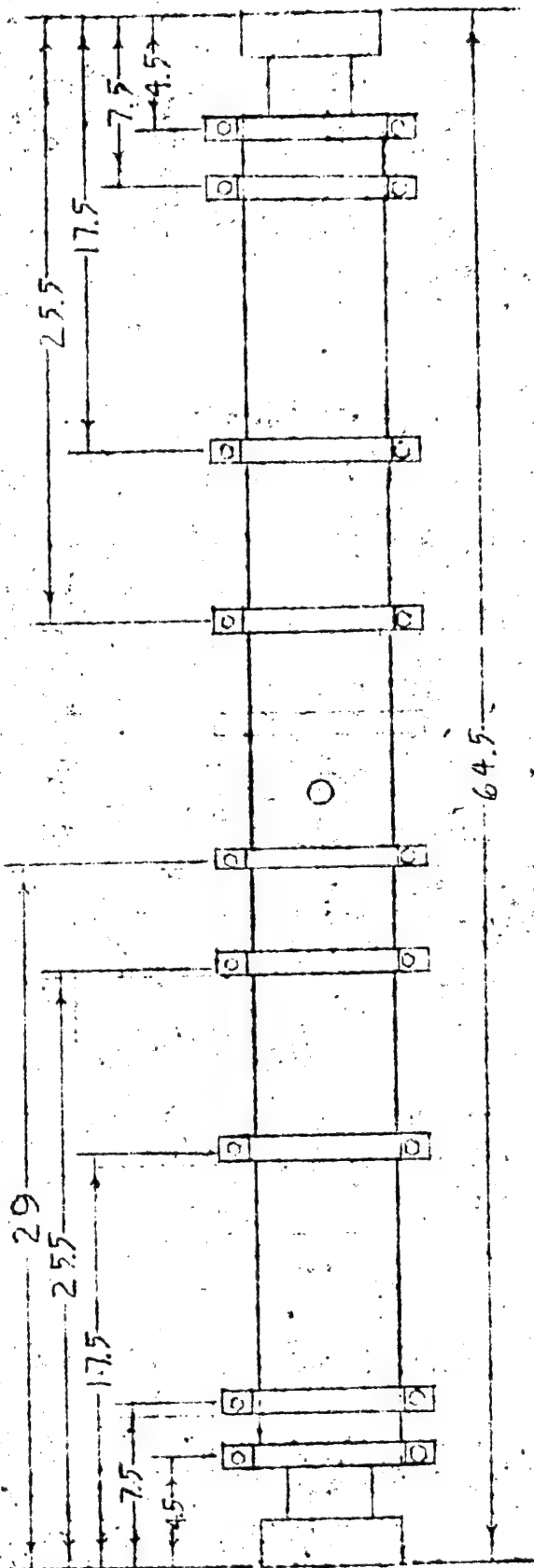
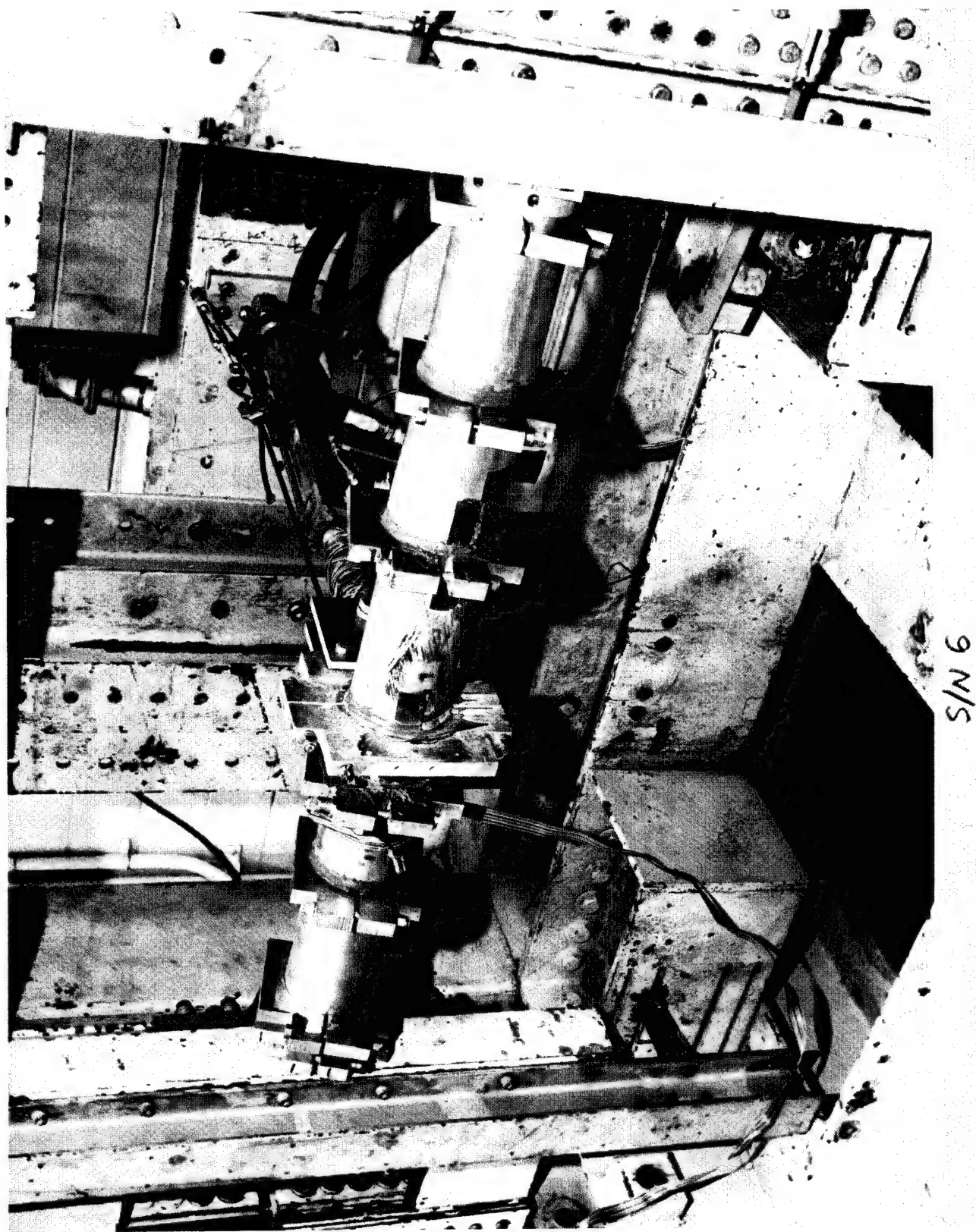
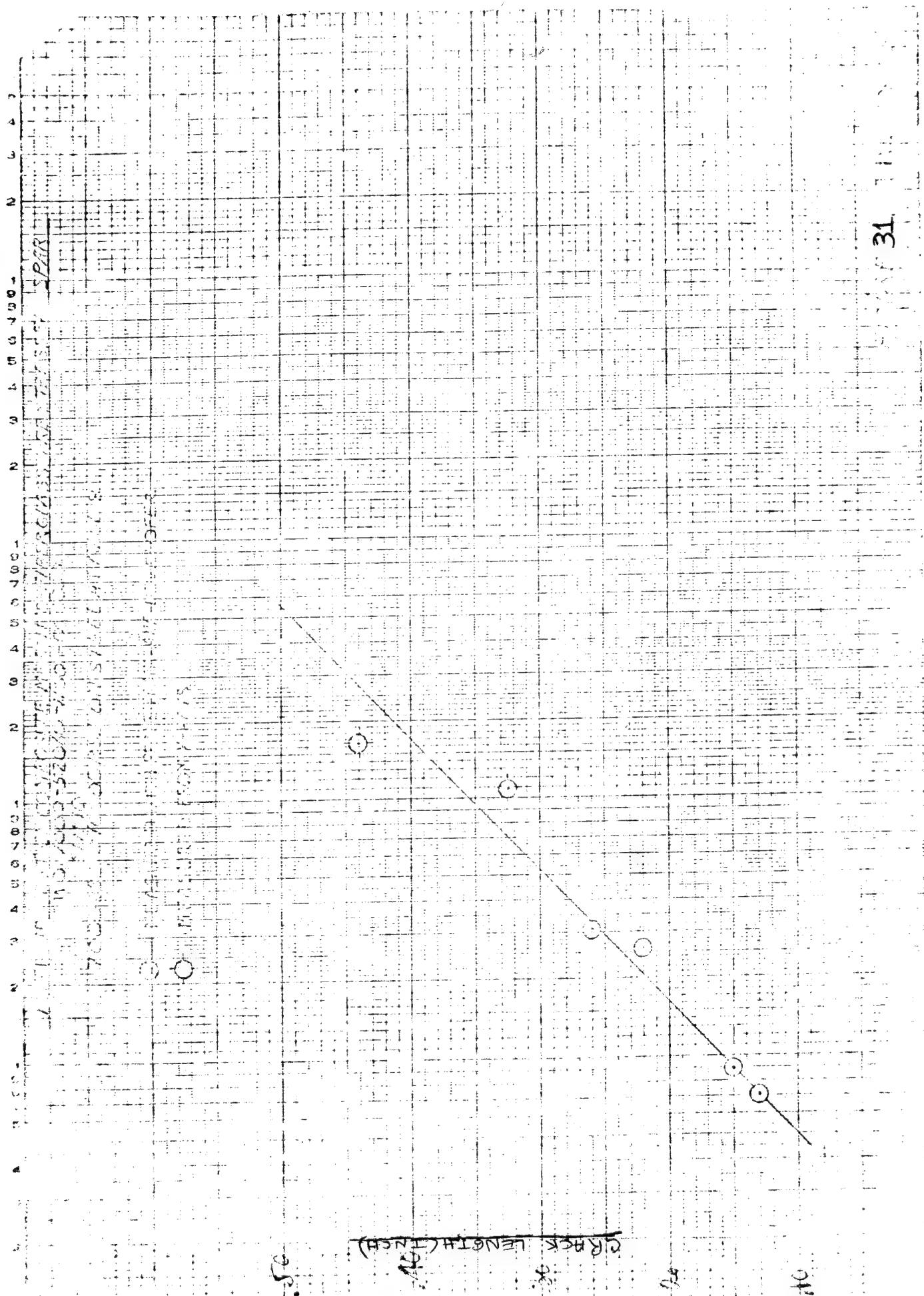


Figure 29



SPECIMEN #2 IN TEST FIXTURE

Figure 30 -



31

100000  
1000000

### 3.2.5.1.2 S/N 6 Prestressed Composite Spar (Specimen No. 2)

#### a) Specimen Calibration

The S/N 6 crack propagation test specimen assembly was put together using the modified configuration (figure 29). The specimen was strain gaged and statically calibrated in bending in a manner similar to that described for S/N 10 specimen. A typical static moment versus test station calibration curve is given on figure 32.

The S/N 6 test unit was then installed in the blade fatigue test fixture. An arc burn was made in the metal liner at the fiberglass cut out location (station 32.25) and an axial tensile load of 7000 pounds was applied. The specimen was excited at a natural frequency of 38.4 Hz for  $.081 \times 10^6$  cycles at an alternating bending stress of  $\pm 33$  ksi applied to the liner at the arc burn station. This cyclic loading initiated a fatigue crack .14 inches total length in the liner. The S/N 6 spar test specimen was then force driven at 20 Hz with the alternating input force (and accompanying variable bending stress) applied by the hydraulic actuator.

The alternating bending stress level at the crack station was applied in increments (starting with  $\pm 8.5$  ksi) for  $2 \times 10^6$  cycles each increment. Crack growth (if any) from the .14 inch long artificially induced fatigue crack was monitored. Table I lists the applied bending stress levels at the crack station versus cycles. No crack growth was noted at stress levels from  $\pm 8.5$  ksi to  $\pm 26.5$  ksi after  $16 \times 10^6$  cycles. Crack growth was finally observed at  $\pm 30$  ksi bending stress level at the arc burn station after about an additional  $10^5$  cycles. Testing was then continued at  $\pm 30$  ksi bending stress level for another  $7 \times 10^6$  cycles (for a total of more than  $23 \times 10^6$  cycles) before appreciable crack growth (12.4 inches) was noted. Crack propagation testing of S/N 6 specimen was terminated at this point although the prestressed composite spar was still intact and could still resist load. The crack growth curve at  $\pm 30$  ksi bending stress level is plotted on figure 33. Photographs of figures 34 and 35 show views of S/N 6 specimen during and after the crack propagation test at  $\pm 30$  ksi bending stress.

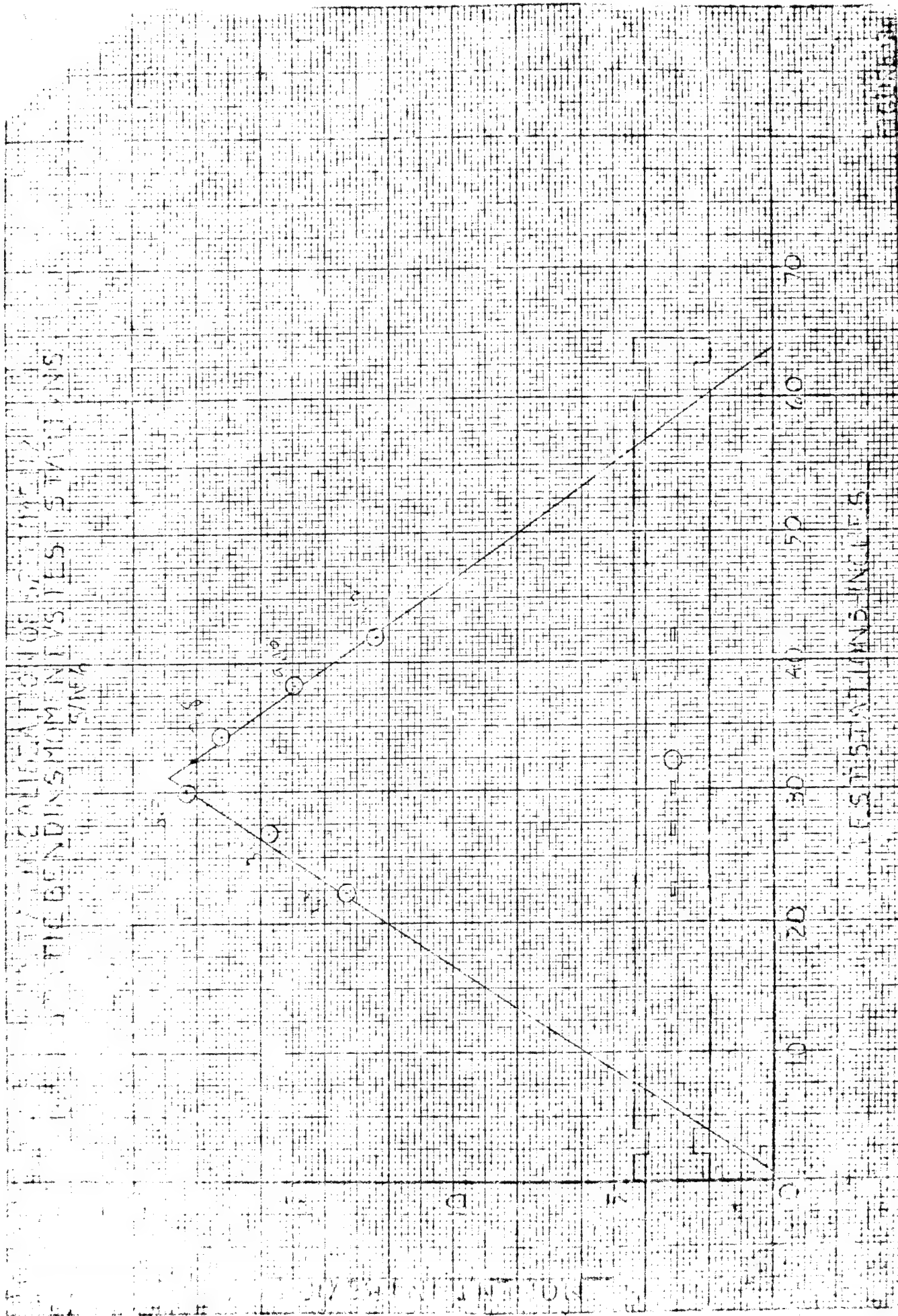




Figure 32

TABLE 1

Specimen No. 2 (S/N 6)

Alternating Stress Level VS. No. of Cycles

Alternating Bending Stress at Crack Station (ksi)	Number of Cycles	Crack Growth
8.5	$2 \times 10^6$	none
12.5		
15.0		
17.5		
20.0		
22.5		
25.0		
26.5		
30.0	$2 \times 10^6$ approx. $10^5$	none start of crack growth
$\Sigma$	$>16 \times 10^6$	



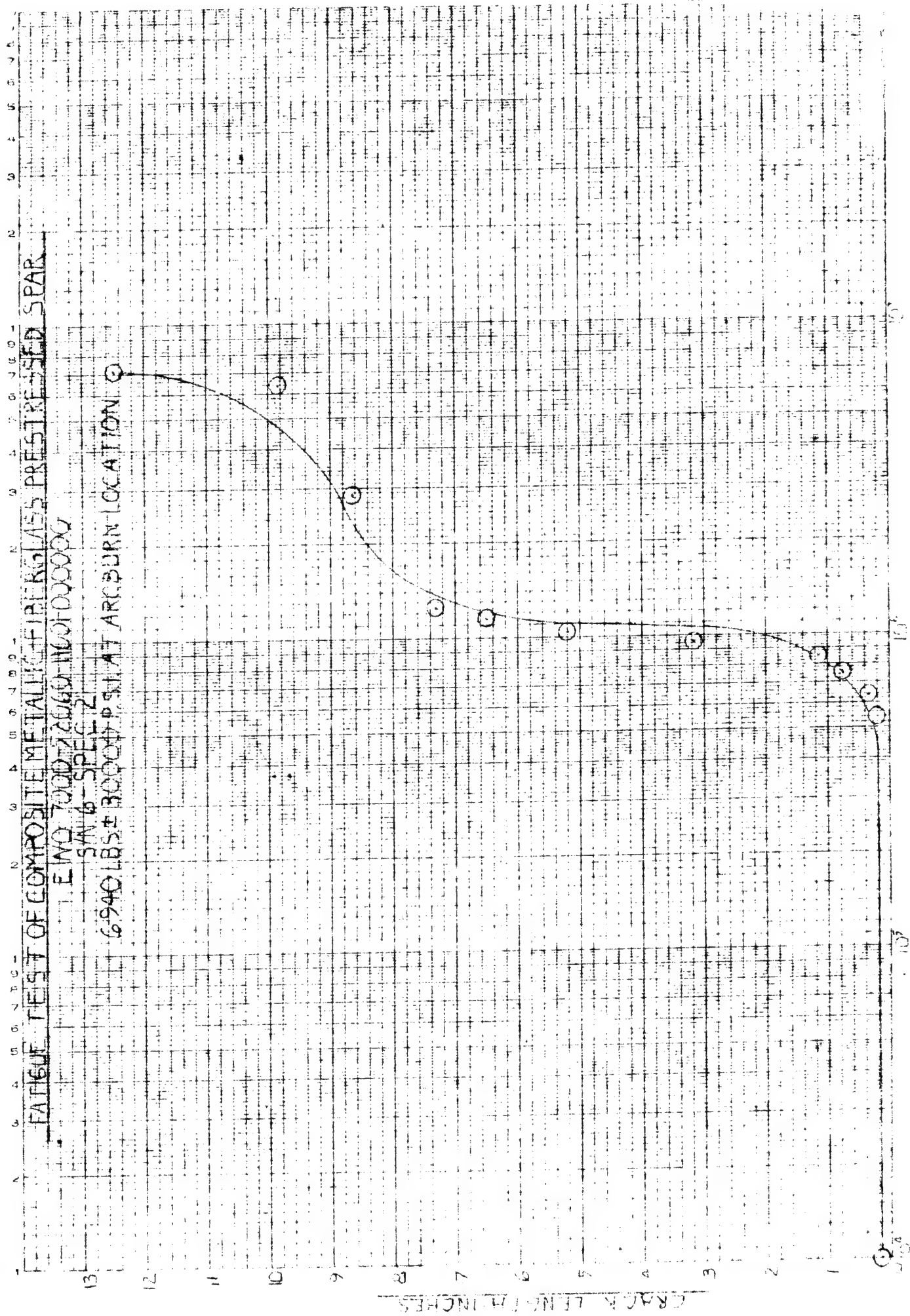


Figure 33





Figure 34 - SPECIMEN #2 IN CRACK PROGRESSION TEST

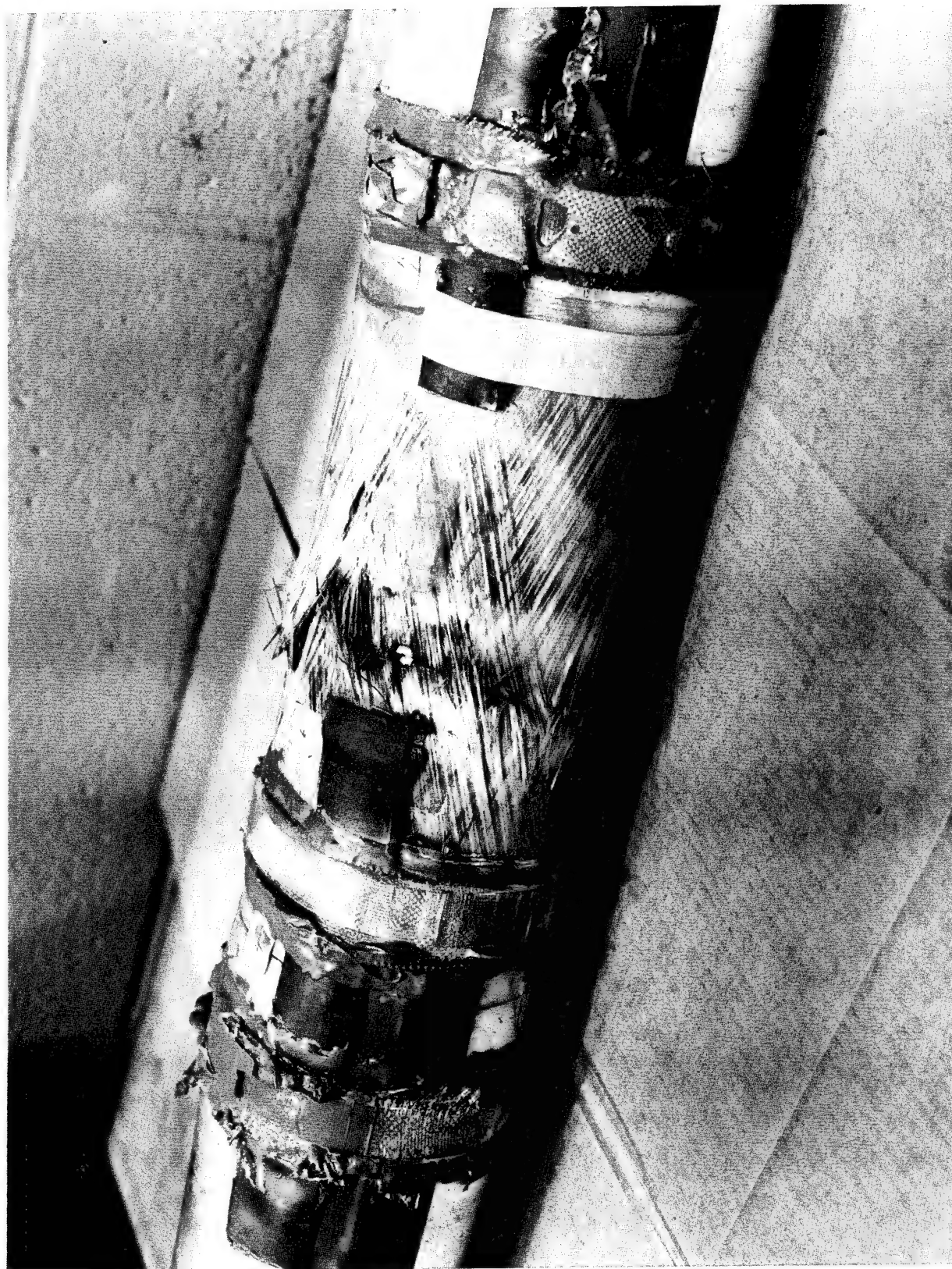


Figure 35

SPECIMEN #2 AFTER CRACK PROGRESSION TEST

### 3.2.5.1.3 S/N 1 Prestressed Composite Spar/Specimen No. 3

The S/N 1 crack propagation test specimen assembly was put together (figure 29) and strain gaged, statically calibrated in bending, installed in the blade fatigue test fixture, arc burned at stations 32.25 and an axial tensile load of 7000 pounds applied in a manner similar to that use for S/N 6 and 10 units. The static moment versus test station calibration curve for S/N 1 spar specimen is shown on figure 36.

The S/N 1 specimen was then cycled at its natural frequency (43 Hz) at an alternating stress of  $\pm 33$  ksi on the arc burn. At  $.03 \times 10^6$  cycles a crack of .25" was initiated. The S/N 1 test unit, with the 7000 pound axial tension still applied, was then force driven by the hydraulic actuator at 20 Hz to obtain crack progression data. No crack progression was noted with alternating stresses of  $\pm 10$  ksi,  $\pm 15$  ksi and  $\pm 20$  ksi applied at the arc burn station for  $.072 \times 10^6$  cycles each stress condition. At  $\pm 25$  ksi applied on the arc burn station, crack growth was noted after  $.072 \times 10^6$  cycles. This data substantiated previous results with S/N 6 prestressed spar specimen (no crack growth occurring until  $\pm 30$  ksi alternating stress).

To obtain data comparing compressively prestressed and unprestressed liner crack growth, S/N 1 test specimen liner was then relieved of prestress by cutting the fiberglass away completely around the specimen as shown on figure 37. The "unprestressed" S/N 1 specimen was then again cycled at 20 Hz with the alternating stress at the arc burn station reduced to  $\pm 10$  ksi. At  $.068 \times 10^6$  cycles, the crack extended the complete length of the circumference. The crack growth data (unprestressed) is plotted on figure 38. A view of S/N 1 unprestressed specimen after crack propagation testing is shown on figure 39.

### 3.2.5.2 Ballistic Test

A prestressed composite spar specimen (S/N 3) with no external loads applied was impacted with three (3) 30 caliber projectiles. The projectile types and their velocities are given below in table 2.

Table 2 - Ballistic Test Projectile Type and Velocity

<u>Round No.</u>	<u>Type Projectile</u>	<u>Velocity (Ft/Sec.)</u>
1	30 cal., AP, M2	2762
2	30 cal., AP, M2	2777
3	30 cal., Ball, M2	2724

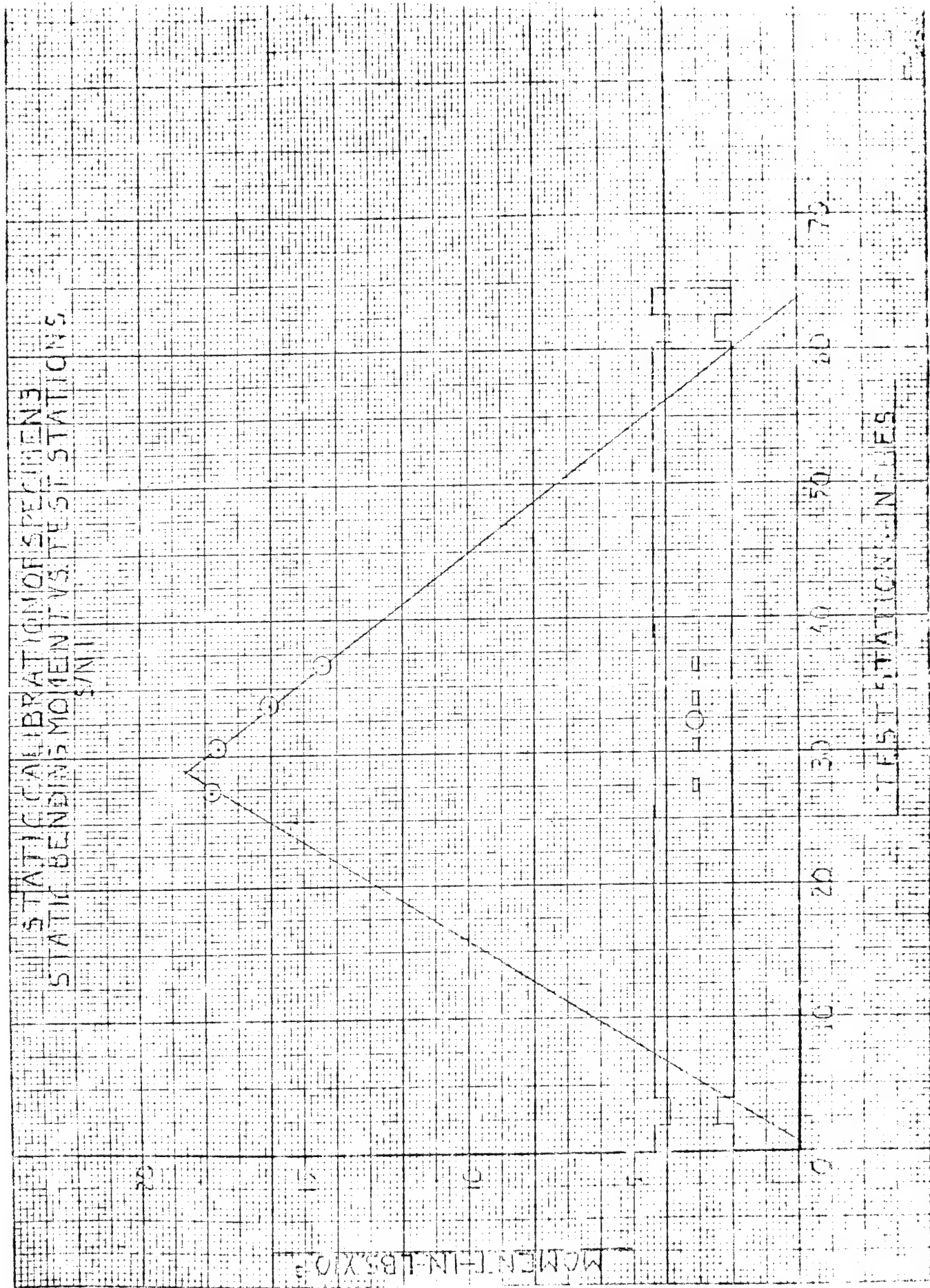
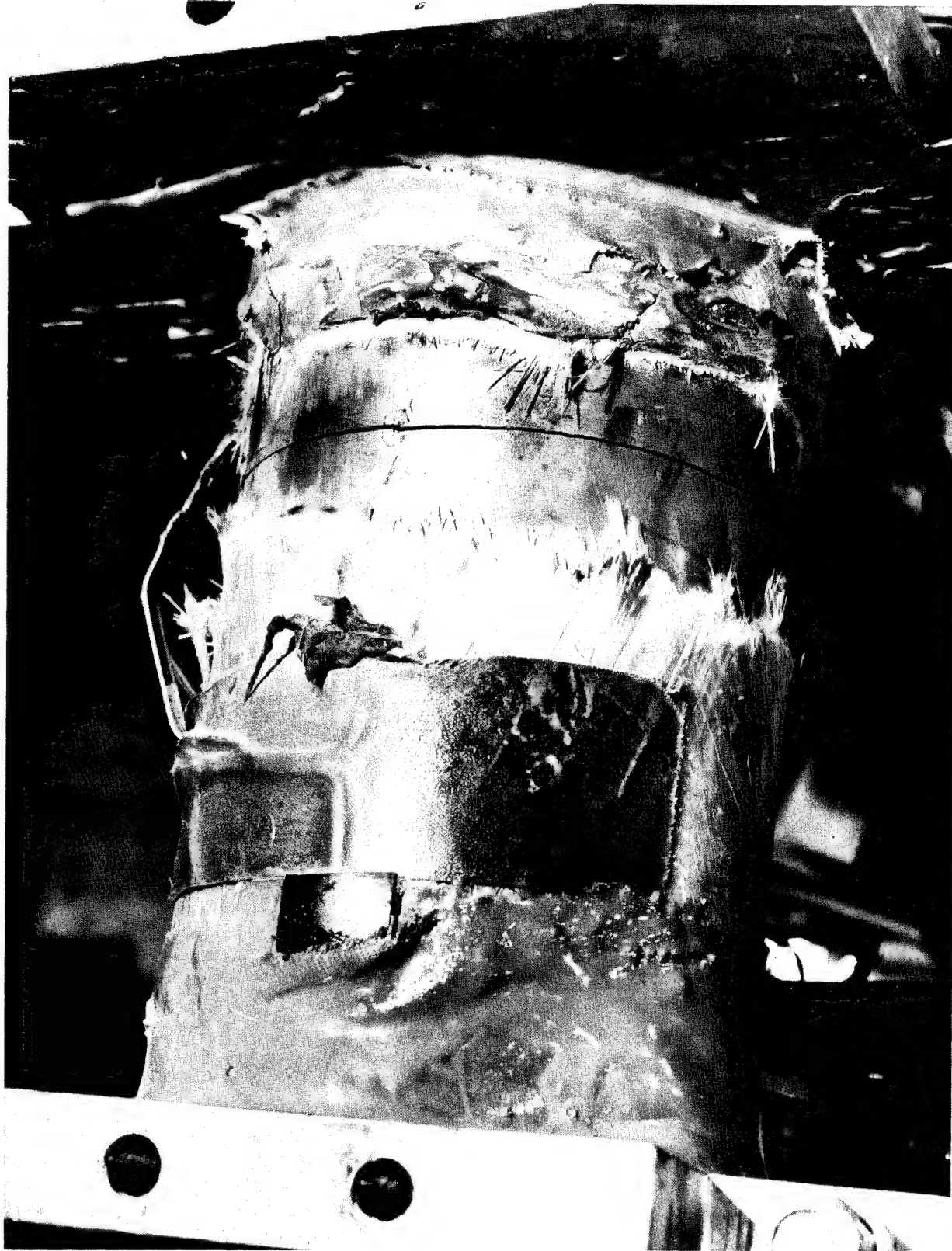


Figure 36





S/N 1

Figure 37

SPECIMEN #3 DURING CRACK PROGRESSION TEST

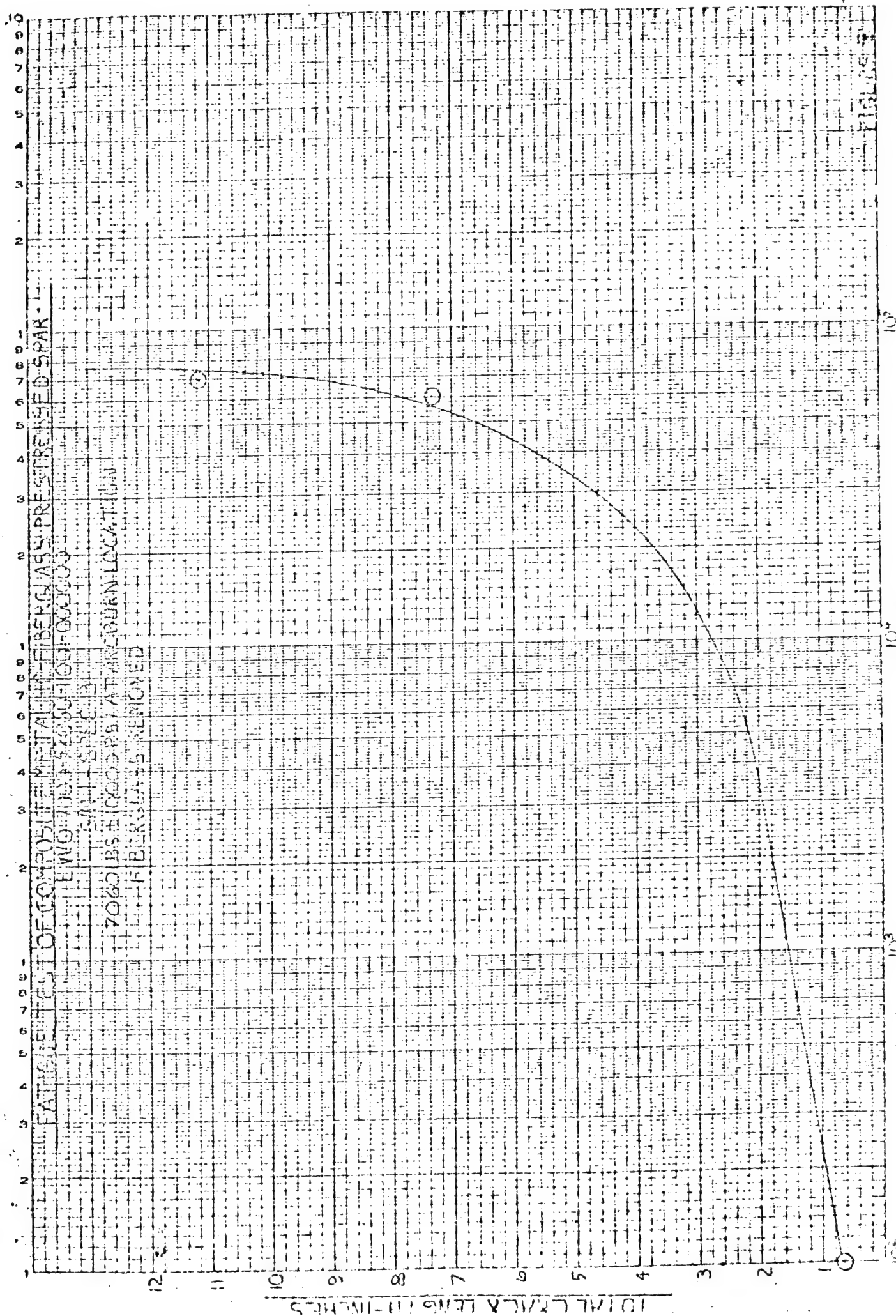


Figure 38

CYCLES

$10^3$

$10^4$

$10^5$

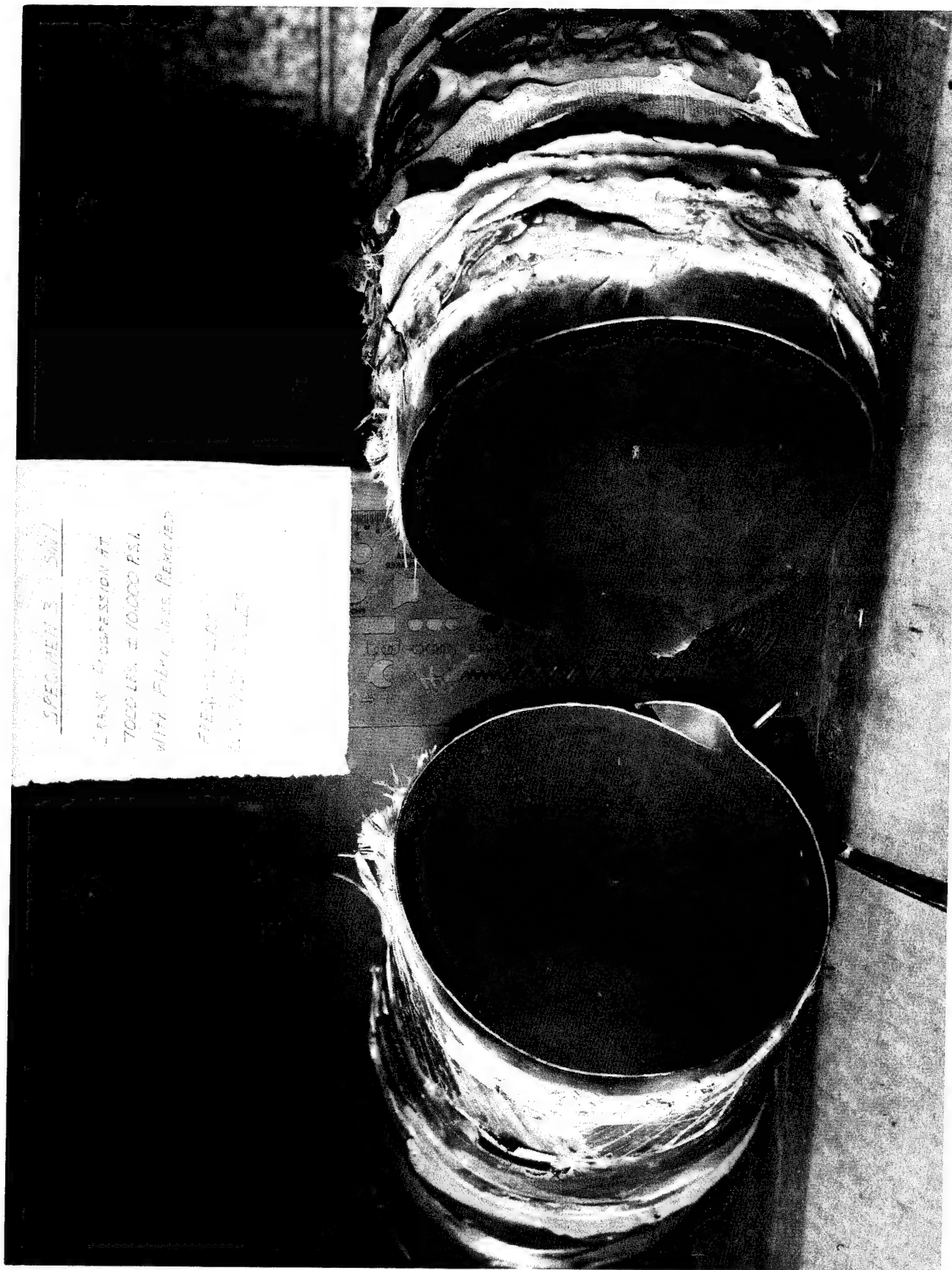


Figure 39 SPECIMEN #3 AFTER CRACK PROGRESSION TEST

The ballistic damage resulting from the projectiles entering and leaving the specimen can be seen in the photographs of figures 40 and 41.

### 3.2.5.3 Discussion of Test Results

#### 3.2.5.3.1 Crack Propagation Tests

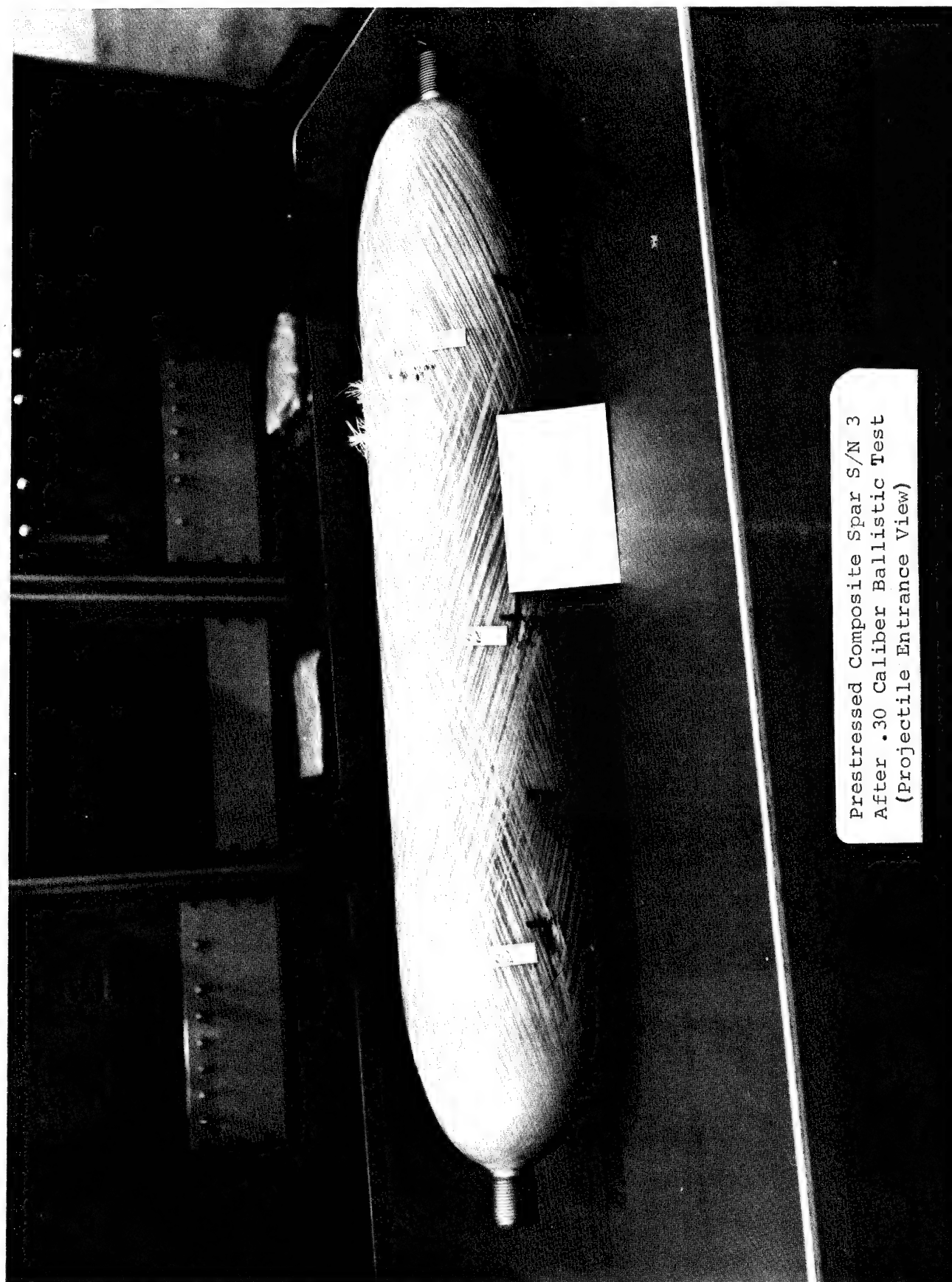
The crack propagation test data previously described in section 3.2.5.1 are summarized on figure 42 for comparison of prestressed versus unstressed specimens. Alternating bending stress at the crack station or total crack length (growth from initial artificially induced flaw length) are plotted versus number of cycles for test specimens 1, 2, and 3. The circled data points with horizontal arrows indicate no crack growth at the alternating bending stress magnitude and number of cycles shown. Circled data points (without horizontal arrows) denote crack growth start after the number of cycles at the bending stress magnitude indicated. The curves plotted show crack propagation at the alternating bending stress indicated versus number of cycles. Specimens 1 and 2 (S/N 10 and 6, respectively) were prestressed. The S/N 1 unit (specimen 3) was prestressed up until crack growth was noted and then the prestress was removed by cutting away the fiberglass.

The crack propagation test data and supporting information indicate the following:

a) Crack growth in the flawed prestressed specimens 2 and 3 did not occur until 25 ksi to 30 ksi alternating bending stress. These values compare very favorably to conventional spar results where substantial crack growth is observed at  $\pm 10$  ksi alternating bending stress. Essentially "infinite" cycle life compared to conventional spars was thus demonstrated. Considerable operational safety margin and high "damage resistance" of the prestressed composite spar construction was proven by the total of more than 23 million cycles (about 1500 operational hours) at high bending stresses accumulated by specimen 2. Particularly significant test results were 16 million cycles at bending stresses up to  $\pm 26.5$  ksi with no crack growth, followed by 7 million more cycles at  $\pm 30$  ksi bending stress before any substantial crack growth was noted.

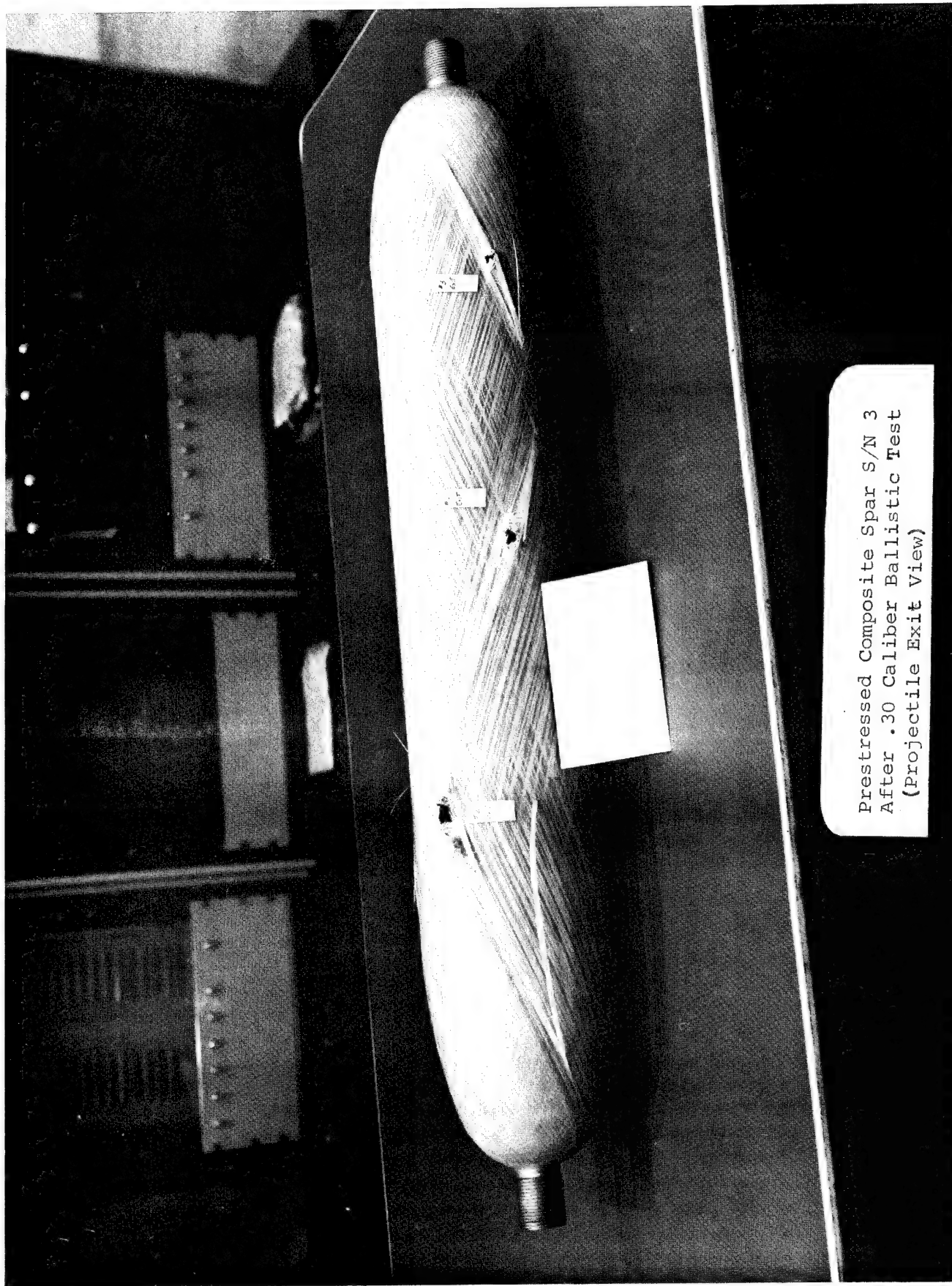
b) Crack growth initiation bending stress levels for the composite prestressed spar specimens correspond essentially to the brittle arc burn fatigue crack initiation bending stress levels (approx.  $\pm 30$  ksi as detailed in figure 25).





Prestressed Composite Spar S/N 3  
After .30 Caliber Ballistic Test  
(Projectile Entrance View)

Figure 40



Prestressed Composite Spar S/N 3  
After .30 Caliber Ballistic Test  
(Projectile Exit View)

Figure 41

# FATIGUE TEST OF PRESTRESSED COMPOSITE METALLIC-FIBERGLASS SPARS

AXIAL TENSION LOAD = 7000 LBS

STRESS AT ARCBURN LOCATION, TOTAL CRACK LENGTH VS. CYCLES

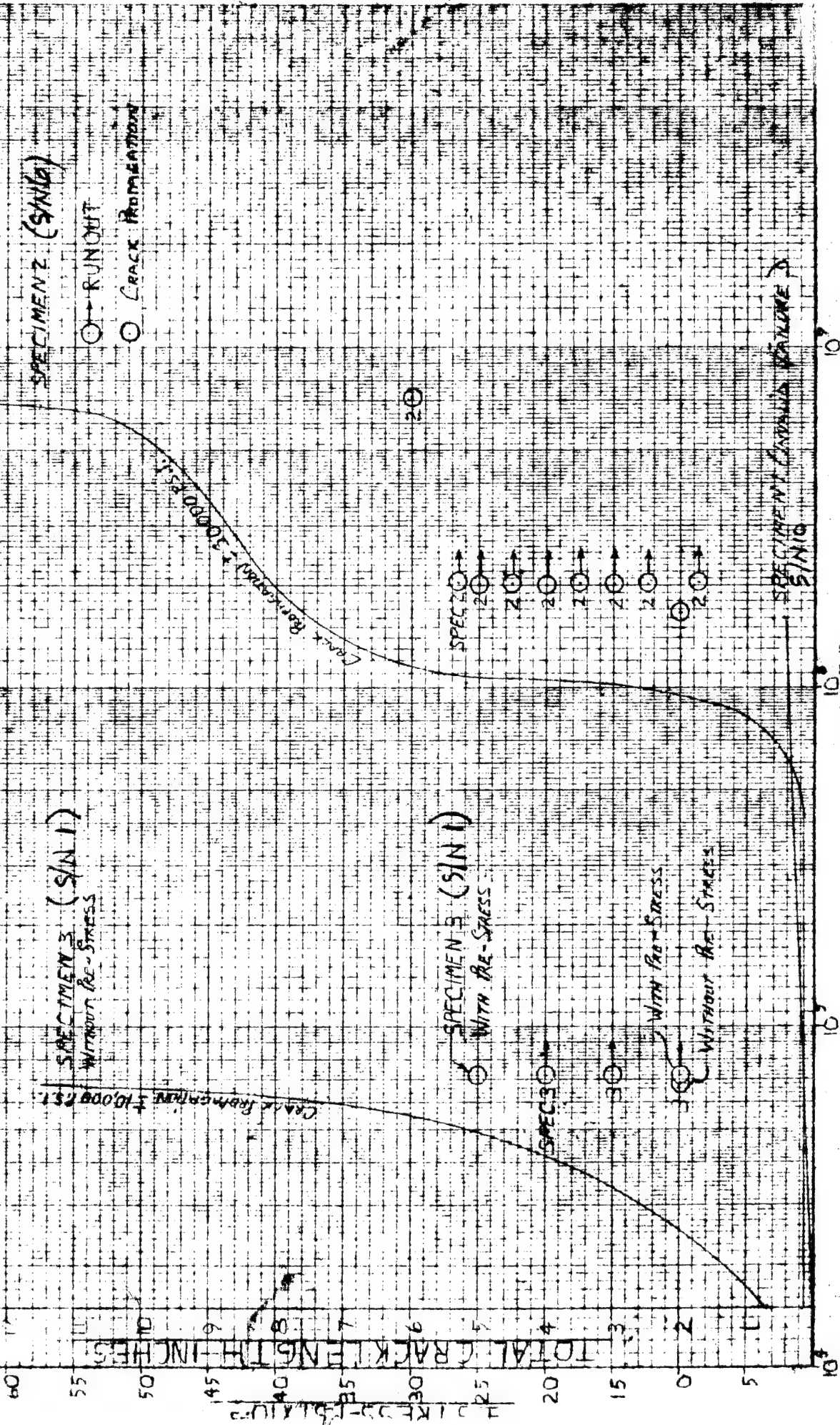


Figure 42

c) Compressive prestress significantly retards crack growth in the liner. Crack propagation at  $\pm 30$  ksi alternating bending stress on specimen 2 (with prestress) was about one hundred times slower than on specimen 3 (without prestress) at only  $\pm 10$  ksi and the same steady axial load as evidenced by the crack growth curves of figure 42. Specimen 1 (with prestress) did however show crack growth at  $\pm 10$  ksi, but this data is not considered valid since the specimen was probably damaged during resolution of loading adapter/test specimen configuration problems (see section 3.2.5.1.1). Another indication of crack growth retardation is the observed "crack tightening" due to liner compressive prestress as described in section 3.2.4.1.

The prestressed metal liner in the fiberglass cut out region (arc burn area) is under a complex shear, tensile and compressive stress state. A short distance away from the cut out in the "undisturbed region" (the order of 2 to 3 hole diameters away) the liner is under pure compression. It is postulated that zero crack growth would have occurred if the liner were subjected to a completely compressive stress field. This postulate is supported by Boeing Aerospace crack propagation data (8) obtained for prestressed composite pressure vessel applications. The propagation therefore of a defect, in addition to being significantly attenuated, would be restricted only to the small local region required for the liner stress field nonuniformities to decay to pure compression. This retardation (and confinement) of crack growth due to liner compressive prestress significantly increases blade life and would appear to be particularly important in arresting ballistically induced defects.

#### 3.2.5.3.2 Ballistic Test

This test demonstrated that no significant damage to the prestressed composite spar specimen resulted from hits from high velocity 30 caliber projectiles. There was no fragment action of the specimen or defect (crack) propagation noted. The damage was confined to the small local region of the ballistic hits, approximately 2 to 3 projectile diameters in extent, as discussed in the preceding section.

#### 3.2.6 Improved Structural Performance Options

Rather small fiber wrap helix angles ( $15^\circ$  -  $20^\circ$  range) are required to produce the prescribed longitudinal compressive prestress in the metal liner as heretofore discussed in section 3.1.1. These shallow angle fibers are effective in resisting longitudinal bending and centrifugal loads but very inefficient in torsion. Conversely, larger helix angle fibers (e.g.  $45^\circ$ ) are efficient in torsion but ineffective in bending and axial load resistance. The option exists for wrapping auxiliary fibers at various helix angles subsequent to the cryogenic prestressing operation. This permits one to "tailor the rigidities



per unit mass of the spar (i.e., "tune" the spar) to obtain desired frequencies at excellent weight trade-offs. Further improvement in rigidity per unit mass is obtained by use of high Young's modulus and low density materials for the auxiliary wrap fibers.

Figure 43 gives a tabulation of typical properties of some fiber materials of interest and projects improved structural performance hardware configuration. The numbers in parenthesis are relative values. PRD-49 III (Kevlar-49), an organic fiber developed by Dupont, appears particularly well suited for use as the basic shallow angle fiber wrap material by virtue of its relatively high stiffness and strength per unit mass as well as its relatively low cost. High modulus graphite should offer considerable advantage for auxiliary (45° torsion) fibers because of its exceedingly high stiffness per unit mass and good strength per unit mass as shown on figure 43.

Illustrative data on relative weight and stiffness of prestressed composite spar configurations compared to a reference homogeneous steel spar are given in Table 3. The data presented include the effect of 23% non-structural mass. The results were obtained by use of prestressed composite spar structural theory and calculation procedures<sup>(7)</sup> together with the fiber materials property values set forth in figure 43. Metal properties employed were Young's modulus and density values of  $E_m = 25 \times 10^3$  ksi and  $\rho_m = .285$  #/in<sup>3</sup>, respectively.

The basic 17½° fiber helix angle design point fiberglass prestressed composite spar configuration (used for the test hardware fabricated on this program exhibits bending and torsional stiffness per unit mass of 89 and 96% respectively compared to the reference homogeneous spar at only 56% of total reference blade mass, as shown under configuration (1) of Table 3. This illustrates typical advantageous weight/stiffness options available with the prestressed composite spar construction.

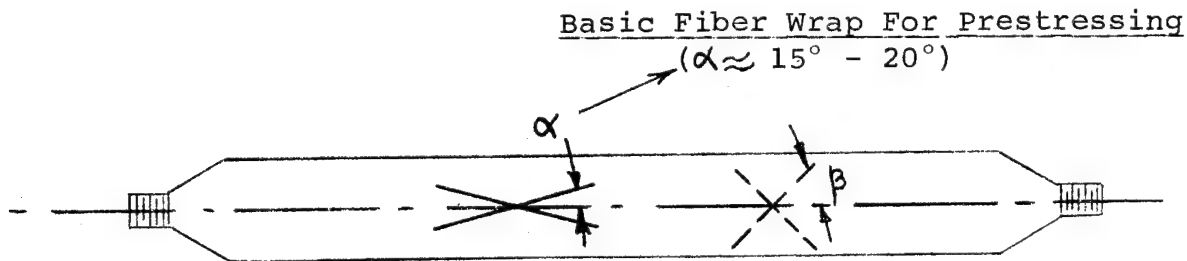
Substitution of PRD-49 III fibers (configuration 2) of the same stiffness as the glass fibers of the basic 17½° wrap design point leads to further improvements. Bending and torsional stiffness per unit mass have increased to 100 and 109%, respectively at only 50% of total reference blade mass. Finally, adding auxiliary HM graphite fibers to the PRD-49 III basic fiber configuration yields further significant increases in structural performance as shown for configuration (3) of Table 3. Addition of 100% 15° bending fibers plus 30% added 45° torsion fibers increased composite spar relative bending and torsional stiffness per unit mass to 170 and 293% respectively for only 54% of the total reference blade mass.

By proper combination of basic and auxiliary fiber wraps (material, helix angles and thickness of fibers) one can thus

PRESTRESSED COMPOSITE SPAR  
 "TUNED RIGIDITY"  
 (PRESCRIBED STIFFNESS INCREASE AT MINIMUM WEIGHT)

FIBER MATERIALS - TYPICAL PROPERTIES						
	$E \times 10^{-6}$ (psi)	$\rho_c$ (#/in <sup>3</sup> )	$\sigma_u$ (ksi)	$(E/\rho_c) \times 10^{-8}$	$(\sigma_u/\rho_c) \times 10^{-3}$	Approx. Cost (\$/#)
S-Glass	12	.072	330	1.7 (1.0)	4.6 (1.0)	8*
PRD-49 III	20	.052	350	4 (2.4)	7.0 (1.5)	5-25*
Graphite (HM)	50	.063	275	7.9 (4.6)	4.4 (.95)	50-75
Boron	50	.076	225	6.6 (3.9)	3.0 (.65)	105 large buy

\*Aerospace Grade



Auxiliary Fiber Wraps For "Tuned Rigidity"  
 Wound subsequent to prestressing (cryostretching)

$\beta = 45^\circ$  (Torsion Fibers)

$\beta$  small ( $5^\circ - 15^\circ$  Bending Fibers)

Item	Basic Fibers	Auxiliary Fibers
Current Test Hardware	S-Glass	—
Improved Structural Performance Hardware	PRD-49 III	Graphite

Figure 43

TABLE 3  
WEIGHT & STIFFNESS COMPARISONS  
PRESTRESSED COMPOSITE VERSUS  
HOMOGENEOUS MATERIAL SPARS

	CONFIGURATION		
	(1)	(2)	(3)
Parameter Ratio: <u>Composite Spar</u> Homogeneous Spar	Basic 17 1/2° wrap angle design point	Basic (But same stiffness PRD fibers instead of glass fibers)	Same as (2) except add HM Graphite fibers (100% added 15° bend- ing fibers + 30% added 45° torsion fibers Graphite fibers added
Bending Stiffness	.50	.50	.92
Torsional Stiffness	.54	.54	1.58
Structural Mass	.49	.40	.46
Total Blade Mass*	.56	.50	.54
Bending Stiffness/Unit Mass*	.89	1.00	1.70
Torsional Stiffness/Unit Mass*	.96	1.09	2.93

\*Includes effect of 23% added non-structural blade mass.

{Can "Tailor" stiffnesses (tune rigidities) to desired optimum values.}

obviously obtain optimum stiffness spars at advantageous weight values. In addition, the "tuned" rigidity options keep natural frequencies far away from critical values and thus lead to significantly increased blade operational life. It might be advantageous to trade-off some (or all) of the theoretical weight gain for significantly increased stiffness compared to an all metal spar. This would imply low metal and fiber operating stress levels for the prestressed composite spar leading to increased operational life and improved ballistic resistance. Trade-offs in the direction of increased mass also increase the mass moment of inertia and stabilizing centrifugal loads. This would aid autorotation and improve blade dynamic stability. The prestressed composite spar construction (with combinations of fiber wraps) thus offers a wide range of trade-off options to the designer.



## 4.0 Conclusions and Recommendations

### 4.1 Conclusions

a) The crack propagation test data shows that prestressed composite spar construction significantly retards crack growth and provides options of "essentially infinite" safe operational cycle life at better structural efficiency values compared to conventional metal spar configurations.

b) High ballistic resistance of prestressed composite spar structures has been proven for 30 caliber projectiles. The retardation and confinement of defects (cracks) that has been demonstrated holds promise for good ballistic resistance to other types of projectiles.

c) Agreement between measured and predicted strains and natural frequencies verifies prestressed composite spar structural design theory.

d) Some promising rotor attachment approaches were identified by structural attachment techniques successfully evolved during prestressed composite spar specimen assembly crack propagation testing.

e) Improved structural performance prestressed composite spar constructions utilizing auxillary fiber wraps and higher stiffness and less dense fibers have been defined. This provides options for "tuning" natural frequencies and "tailoring" stiffnesses to optimum values while retaining structural efficiency.

### 4.2 Recommendations

a) Apply prestressed composite spar construction to current and projected rotor blade configurations to further evaluate its apparent advantages.

b) Design, build and test appropriate prestressed composite spar hardware to evaluate and verify potential critical design items such as rotor attachment, buckling, fiber wraps, stiffness enhancement and multi-cell configurations.

## 5.0 REFERENCES

- 1) Meredith, Seiferth and Rummel, "A Graphite/Epoxy Compression Panel for the Space Shuttle", p. 99, Society of Aerospace Material and Process Engineers, Space Shuttle Materials, Volume 3, National SAMPE Technical Conference, October 5-7, 1971, Huntsville, Alabama.
- 2) Lager, J. R., "Composite Space Shuttle Engine Support Structure", p. 149, Society of Aerospace Material and Process Engineers, Space Shuttle Materials, Volume 3, National SAMPE Technical Conference, October 5-7, 1971, Huntsville, Alabama.
- 3) Gleich, D., "Cryogenically Formed Prestressed Fiber-Metal Structures for O<sub>2</sub>/H<sub>2</sub> High Pressure Gas Tanks", p. 527, Society of Aerospace Material and Process Engineers, Space Shuttle Materials, Volume 3, National SAMPE Technical Conference, October 5-7, 1971, Huntsville, Alabama.
- 4) Gleich, D., Development of a Filament Overwrapped Cryoformed Pressure Vessel, NASA CR-72753, ARDE, INC. under Contract NAS 3-11194, January 1971.
- 5) Morris, E. E., Glass-Fiber Reinforced Metallic Tanks for Cryogenic Service, NASA CR-72224, Aerojet-General Corporation under Contract NAS 3-6292, June 1967.
- 6) U. S. Patent Number 3,197,851.
- 7) Gleich, D., Final Report, Feasibility Study of Applying an Advanced Composite Structure Technique to the Fabrication of Helicopter Rotor Blades, NASA CR-112191, December 1972.
- 8) Bixler, W. D., Composite Tanks With Load Sharing Liners (Add-On), Quarterly Technical Progress Narrative No. 2, Contract NAS 3-14380 Boeing Aerospace Company, January 15, 1974.
- 9) Johns & Kaufmann, Filament Overwrapped Metallic Cylindrical Pressure Vessels, NASA TMX-52171, Lewis Research Center, 1966.
- 10) Pruhn, Analysis and Design of Flight Vehicle Structures, Tri-State Offset Company, January 1965.

## 6.0 APPENDICES

### 6.1 Appendix 1 - Test Vendor Report

Crack propagation and ballistic testing of prestressed composite spar specimens was performed under ARDE subcontract by Boeing Vertol Company. Their test report covering this work is contained in this appendix.

**BOEING VERTEL COMPANY**

A DIVISION OF THE BOEING COMPANY

P.O. BOX 16858  
PHILADELPHIA, PENNSYLVANIA 19142

CODE IDENT. NO. 77272

NUMBER T301-10272-1TITLE FATIGUE TEST OF COMPOSITE METALLIC -  
FIBERGLASS PRESTRESSED SPAR - ARDEORIGINAL RELEASE DATE \_\_\_\_\_ . FOR THE RELEASE DATE OF  
SUBSEQUENT REVISIONS, SEE THE REVISION SHEET. FOR LIMITATIONS  
IMPOSED ON THE DISTRIBUTION AND USE OF INFORMATION CONTAINED  
IN THIS DOCUMENT, SEE THE LIMITATIONS SHEET.MODEL \_\_\_\_\_ R&D \_\_\_\_\_ CONTRACT P.O. 15298

ISSUE NO. \_\_\_\_\_ ISSUED TO: \_\_\_\_\_

PREPARED BY

J. Morris

DATE

7-26-74

APPROVED BY

E. L. Riegner

DATE

4/1/74

APPROVED BY

E. Kunz

DATE

4/2/74

APPROVED BY

DATE

LIMITATIONS

This document is controlled by Engr'g. Labs. - Dept. 7524

All revisions to this document shall be approved by the  
above noted organization prior to release.

REVISIONS			
LTR	DESCRIPTION	DATE	APPROVAL

ACTIVE SHEET RECORD

SHEET NUMBER	REV LTR	ADDED SHEETS				SHEET NUMBER	REV LTR	ADDED SHEETS			
		SHEET NUMBER	REV LTR	SHEET NUMBER	REV LTR			SHEET NUMBER	REV LTR	SHEET NUMBER	REV LTR
1											
2											
3											
4											
5											
6											
7											
8											
9											
10											
11											
12											
13											
14											
15											
16											
17											
18											
19											
20											
21											
22											
23											
24											
25											
26											
27											

ABSTRACT

This report is submitted in fulfillment of contract number P.O. 15298. It contains crack propagation data for composite prestressed simulated spars and a simulated spar without prestress. It also includes the effect of ballistic impact on a prestressed spar.

KEY WORDS

Prestressed

Cutout

Arc Burn Defect



TABLE OF CONTENTS

	<u>PAGE</u>
1.0 INTRODUCTION	7
2.0 PURPOSE	7
3.0 DESCRIPTION OF TEST SPECIMENS	7
3.1 Crack Propagation Specimens	7
3.2 Ballistic Impact Specimen	7
4.0 TEST PROCEDURE	7
4.1 Crack Propagation Tests	7
4.2 Ballistic Impact Specimen	9
5.0 DISCUSSION OF RESULTS	9
5.1 Crack Propagation Tests	9
5.2 Ballistic Impact Test	10

LIST OF FIGURES

<u>Figure No.</u>		<u>PAGE</u>
1	Specimen Revisions Using Clamps and Rod End Assemblies	11
2	Typical Static Moment Curve Used for Specimen Calibration	12
3	Summary of Specimen #1	13
4	Crack Progression Curve of Specimen #1	14
5	Summary of Specimen #2	15
6	Crack Progression of Specimen #2	16
7	Summary of Specimen #3	17
8	Crack Progression of Specimen #3	18
9	Crack Progression Rates and Loads for Three Specimens	19
10	Bond Failure After 7000 Lb. Axial Tension Load Application	20
11	Specimen #2 in Crack Progression Test	21
12	Specimen #2 in Test Fixture	22
13	Specimen #2 After Crack Progression Test	23
14	Specimen #3 During Crack Progression Test	24
15	Specimen #3 After Crack Progression Test	25
16	Ballistically Damaged Spar (Entrance Damage)	26
17	Ballistically Damaged Spar (Exit Damage)	27

## 1.0 INTRODUCTION

This report contains the results of the testing performed on four specimens manufactured by ARDE Inc. in accordance with ARDE drawing D-3866. Three of the specimens were fatigue tested in the pre-stressed condition and crack propagation rates, from an induced defect, established. One specimen was tested without prestress for comparison purposes. One specimen was subjected to ballistic impact. The testing was conducted in accordance with document D210-10297-1 Rev. A, April 1972, P/S VIII which was used as a pretest report.

## 2.0 PURPOSE

The purpose of the tests were to determine and compare crack propagation rates of composite prestressed spars and a spar without prestress.

To determine the effect of ballistic impact on a prestressed spar.

## 3.0 DESCRIPTION OF TEST SPECIMENS

### 3.1 Crack Propagation Specimens

The test specimens were manufactured generally in accordance with ARDE drawing number D-3866. This configuration proved to be unsuitable for test because bond failures occurred between the aluminum extension tube and the test section. After some experimentation the configuration was modified by installing rod ends to transmit the axial tension and aluminum clamps to transmit the bending moment. A schematic of the modified assembly is shown in figure #1.

### 3.2 Ballistic Impact Specimen

This test specimen was in accordance with ARDE drawing number D-3819.

## 4.0 TEST PROCEDURE

### 4.1 Crack Propagation Tests

#### 4.1.1 Static Calibration

Each specimen was statically calibrated as a simply supported beam on knife edges. This calibration consisted of applying a shear load normal to the weaker axis at approximately midspan.

This shear load was applied in three equal increments to a maximum value of 1200 lbs. producing a maximum moment of 18,800 in-lbs. The strain gage outputs were recorded at each load increment. A relationship was thus obtained between known applied moment and strain gage output. This relationship was later used to define the dynamic bending moment from the measured gage output. A typical calibration moment diagram is shown in figure #2.

4.1.2 The specimens were installed in a resonant blade fatigue fixture capable of applying steady axial tension and alternating bending moment about the weaker axis of the specimen.

A steady axial tension of 7000 lbs. was applied and maintained for the duration of the tests.

4.1.3 The specimens were excited thru a frequency range 0-100 Hz and the natural resonant frequency of the system established.

4.1.4 Specimen No. 1 - S/N 10

An arc burn was put in the liner at the fiberglass cutout. The specimen was excited at the natural resonant frequency for  $0.071 \times 10^6$  cycles at  $\pm 28,900$  PSI at midspan. Upon inspection a crack was observed at the arc burn. Crack propagation was continued in a force driven rather than a resonant mode at 15 Hz. The stress was controlled at gage 8  $\pm 8900$  PSI calculated in the steel. The moment strain and stress distribution for the specimen is shown in figure #3. After  $1.65 \times 10^6$  cycles a malfunction of the test rig caused an overload condition on the specimen which precluded further testing. The total crack length at this stage was .44 inches. A crack propagation curve for the specimen is shown in figure #4.

4.1.5 Specimen No. 2 - S/N 6

The specimen was arc burned at the fiberglass cutout and excited at the natural resonant frequency for  $0.081 \times 10^6$  cycles at  $\pm 32,500$  PSI at the arc burn location. A crack .14 inches total length was initiated at this time. Crack propagation was continued in the force driven mode. The specimen was initially cycled at  $\pm 8,900$  PSI at the arc burn without crack propagation. The stress was incrementally increased after approximately  $2.0 \times 10^6$  cycles at each increment until crack propagation occurred at 30,000 PSI. The moment and strain distribution for the specimen is shown in figure #5. The crack propagation curve for the specimen at  $\pm 30,000$  PSI is shown in figure #6.

4.1.6 Specimen No. 3 - S/N 1

The specimen was arc burned at the fiberglass cutout. It was then excited at the natural resonant frequency for  $0.03 \times 10^6$  cycles at 33,500 PSI at the arc burn when a .25 inch crack was observed. The specimen was then force driven at various stress levels until crack propagation occurred. The initial stress was  $\pm 10,000$  PSI. This

was maintained for  $.072 \times 10^6$  cycles without crack growth. The stress was increased in  $\pm 5000$  PSI increments and  $.072 \times 10^6$  cycle runouts obtained until progression was observed at the end of the  $\pm 25,000$  PSI run.

This data substantiated previous data with the prestressed specimens. The liner was then relieved of prestress by cutting the fiberglass all the way around the specimen. The specimen was then again cycled at  $\pm 10,000$  PSI and the crack progression recorded. Figure #7 shows the stress, strain and moments for crack progression in the prestressed and unstressed conditions. Figure #8 shows the crack progression curve without prestress.

4.1.7 A summary of the crack propagation data is shown in figure #9. This curve shows the loads and cycles that each specimen was tested. It also shows the crack propagation of the specimens.

#### 4.2 Ballistic Impact Specimen

A prestressed specimen was impacted with three (3) 30 caliber projectiles. The type projectile and its velocity are described as follows:

<u>Round No.</u>	<u>Type Projectile</u>	<u>Velocity (Ft/Sec)</u>
1	30 cal., AP, M2	2762
2	30 cal., AP, M2	2777
3	30 cal., Ball., M2	2724

The ballistic damage resulting from the projectiles entering and leaving the specimen can be seen in figures #10 and #11.

### 5.0 DISCUSSION OF RESULTS

#### 5.1 Crack Propagation Tests

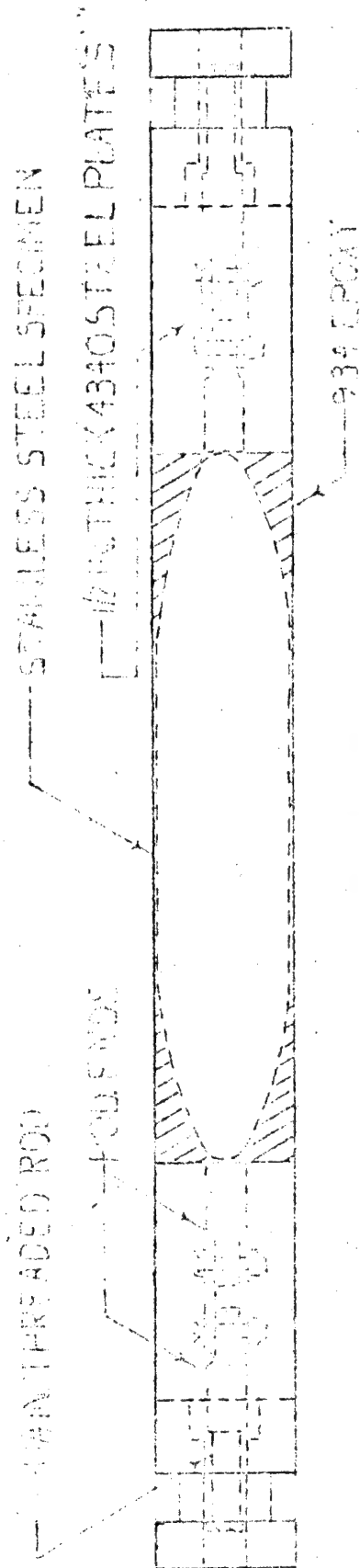
The crack propagation data is summarized in figure #9 which compares an unstressed specimen with the prestressed concept, specimens 2 and 3 with prestress versus specimen 3 without prestress. Crack propagation did not occur until 25,000 to 30,000 PSI from the precracked specimens.

On specimen 2 with prestress the crack propagation at  $\pm 30,000$  PSI was much slower than on specimen 3 without prestress at  $\pm 10,000$  PSI. Specimen 1 with prestress did however show crack propagation at  $\pm 10,000$  PSI but it is believed this data was not valid as the specimen could have been damaged in the early stages during optimization of the test configuration.

## 5.2 Ballistic Impact Test

The ballistic impact damage was no more or less than would be expected for a normal 30 cal. hit.

# ROD END ASSEMBLIES



# CLAMP ASSEMBLY

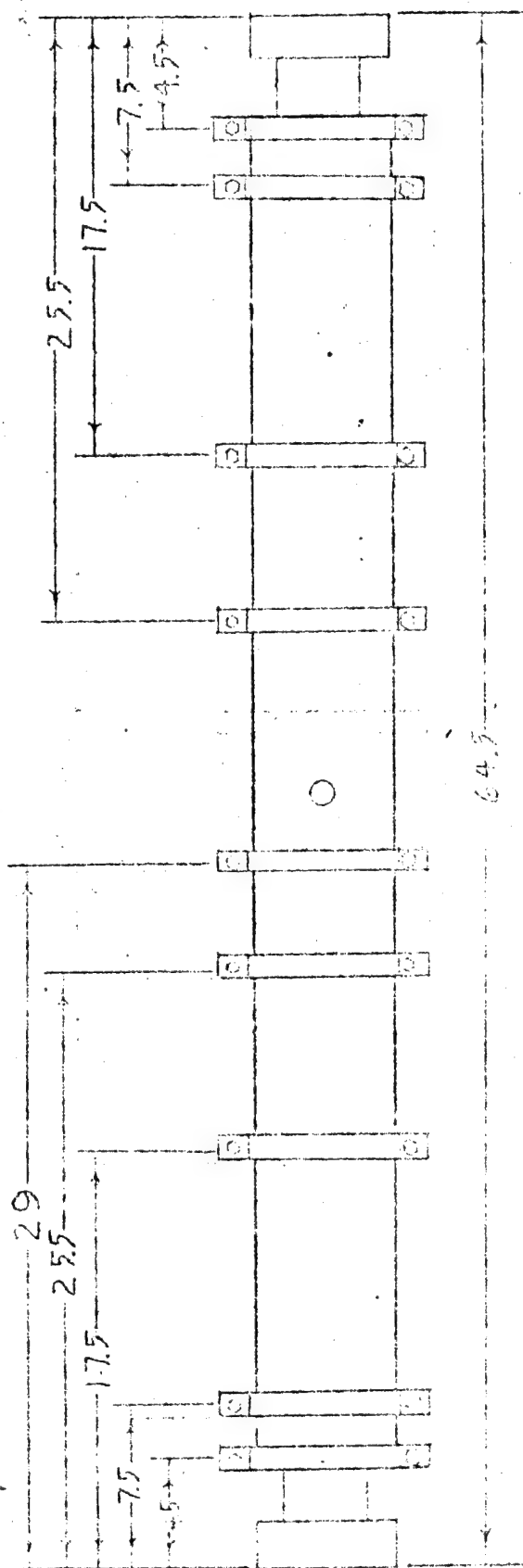
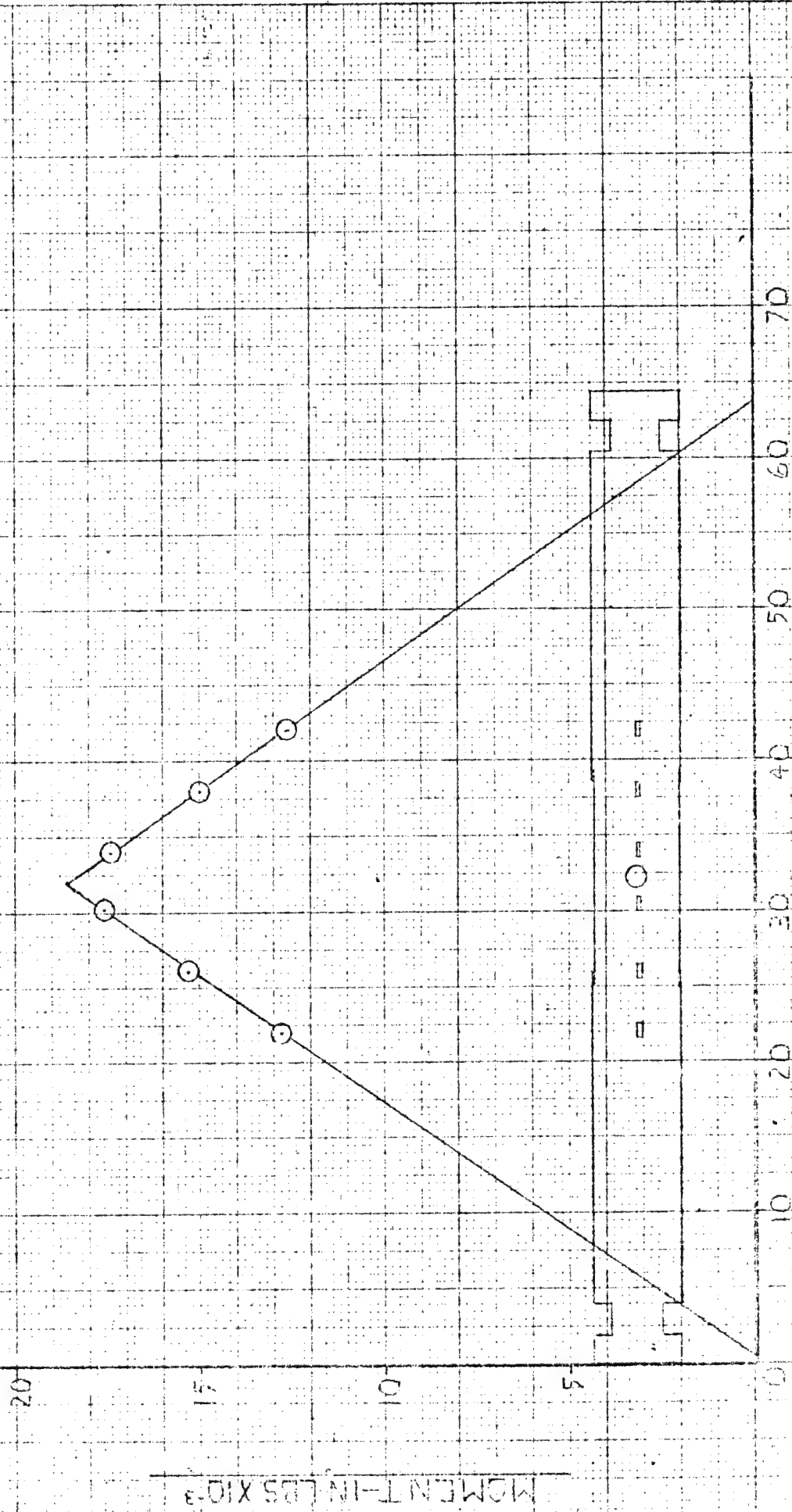


FIGURE 1

STATIC CALIBRATION OF SPECIMEN  
STATIC BENDING MOMENT VS. TEST STATIONS  
S/N 10



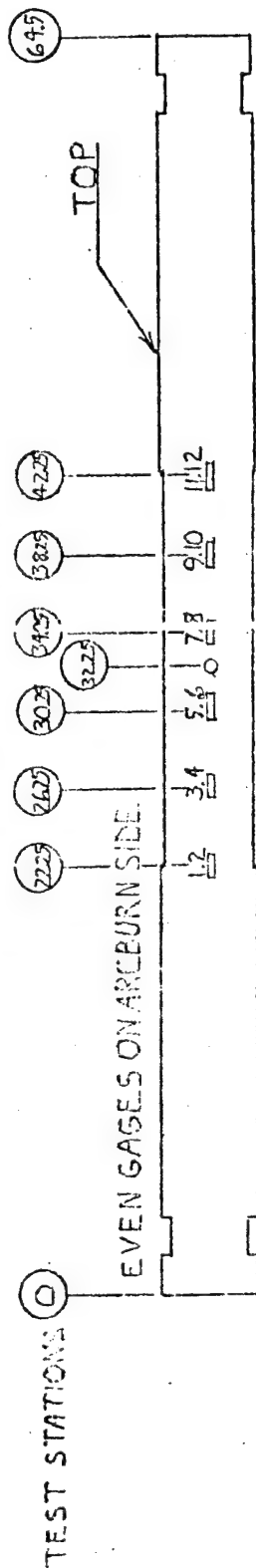
TEST STATIONS-INCHES

FIGURE 2

# Composite Metallic-Fiberglass Prestressed Spar Structural Model Tests

EWO 7000-52060-11C01-000000

SPECIMEN No. 1 S/H 10



CRACK INITIATION FREQUENCY = 40 HZ  
CYCLES - CRACK INITIATION = .071 X 10<sup>6</sup>  
CONTROL ON GAGES 7/8

CRACK PROGRESSION FREQUENCY = 15 Hz  
CYCLES - CRACK PROGRESSION = 1.65 X 10<sup>6</sup>  
CONTROL ON GAGE 8

STRAIN GAGE 5	7/8	5	7	8	11
CRACK INITIATION ± MOMENT IN LBS.	2072	2100	2100	3170	1200/12100
CRACK INITIATION ± STRESS PSI	7107	7400	7340	3100	
CRACK PROGRESSION ± STRESS PSI	1950	2072	1100	870	
CRACK INITIATION ± STRAIN (mm/m)	1065	922	1090	1196	
ON FIBERGLASS					
CRACK PROGRESSION ± STRAIN (mm/m)	367	321	421	344	
ON FIBERGLASS					

STRESS VALUES CALCULATED ASSUMING STRAIN IN STEEL EQUALS STRAIN IN FIBERGLASS.

FIGURE 3  
J.D.P. 10/11/73  
J.P.M. 11-22-73



348 100 L TEN 1000  
 SEMI-LOGARITHMIC  
 4 CYCLES X 10 DIVISIONS PER INCH

FUC DFLT  
 MADE IN U.S.A.

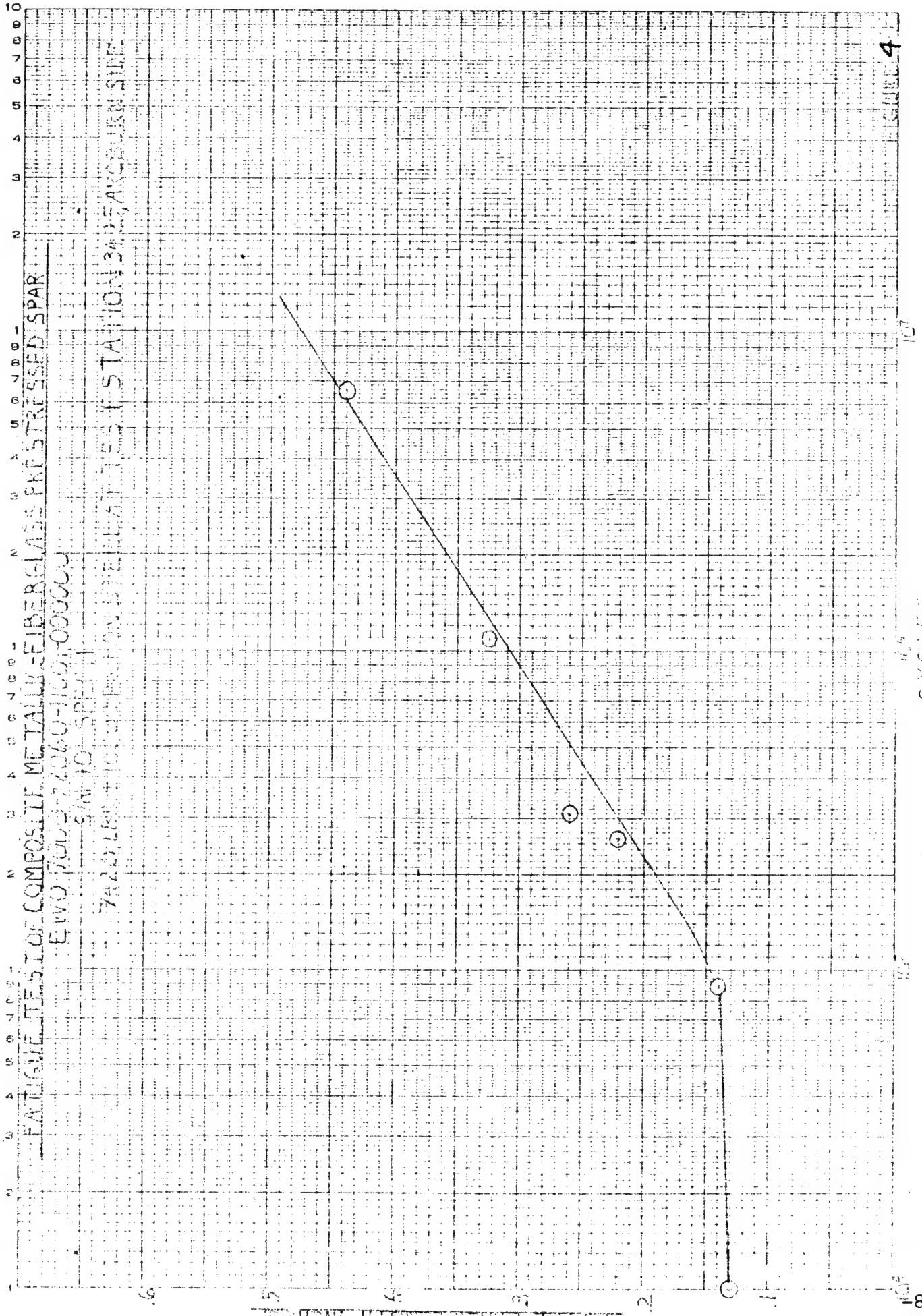


FIGURE 4

CYCLES

PREPARED BY:  
CHECKED BY:  
DATE:

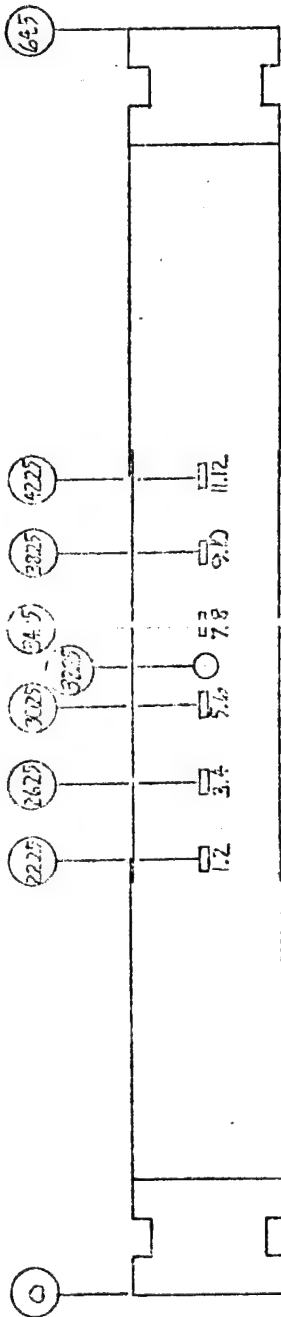
NUMBER  
REV LTR  
MODEL NO.

FIGURE 5

# FATIGUE TESTS OF PRESTRESSED COMPOSITE METALLIC-FIBERGLASS SPARS

EWO 7000 52060 11001 100000

SPECIMEN 2 5/11/16



EVEN GAGES ON ARCBURN SIDE, ODD GAGES ON OPPOSITE SIDE.

AXIAL TENSION LOAD = 70,000 LBS.

## CRACK INITIATION

CRACK PROGRESSION

+28700 P.S.I. ON STEEL AT GAGE 8.

± 30000 P.S.I. AT ARCBURN

FREQUENCY = 38.4

FREQUENCY = 20 C.P.S.

$$\text{CYCLES} = .081 \times 10^6$$
$$\text{CYLES} = 7.100 \times 10^5$$

STRESS AT ARCBURN ( $\pm$ P.S.I.)	STRAIN ON FIBER GLASS ( $\pm$ IN./IN.)					BENDING MOMENT ( $\pm$ IN. LBS.)				CYCLES X 10 <sup>6</sup>
	5	6	7	8		1/2	5/16	7/8	1 1/2	
8900	361	388	283	306		3070	6620	5570	3400	2.032
12500	516	539	415	435		4010	9500	8000	4930	2.016
15000	590	660	470	512		4660	11100	9260	5940	2.016
17500	675	738	535	585		5130	14400	10600	6530	2.022
20000	784	858	613	664		5830	14400	12000	7640	2.016
22500	885	955	691	722		6410	16200	13300	8140	2.016
25000	1020	1080	783	824		6640	18400	15100	9000	2.004
26400	1090	1150	835	877		6930	19900	16100	9680	2.070
(30000)	—	1790	955	1000		7670	(22000)	18400	11700	7.100

301-10272-1  
 SEMI-LOGARITHMIC  
 4 CYCLES X 10 DIVISIONS PER INCH  
 EUC JET. CO.  
 MADE IN U.S.A.

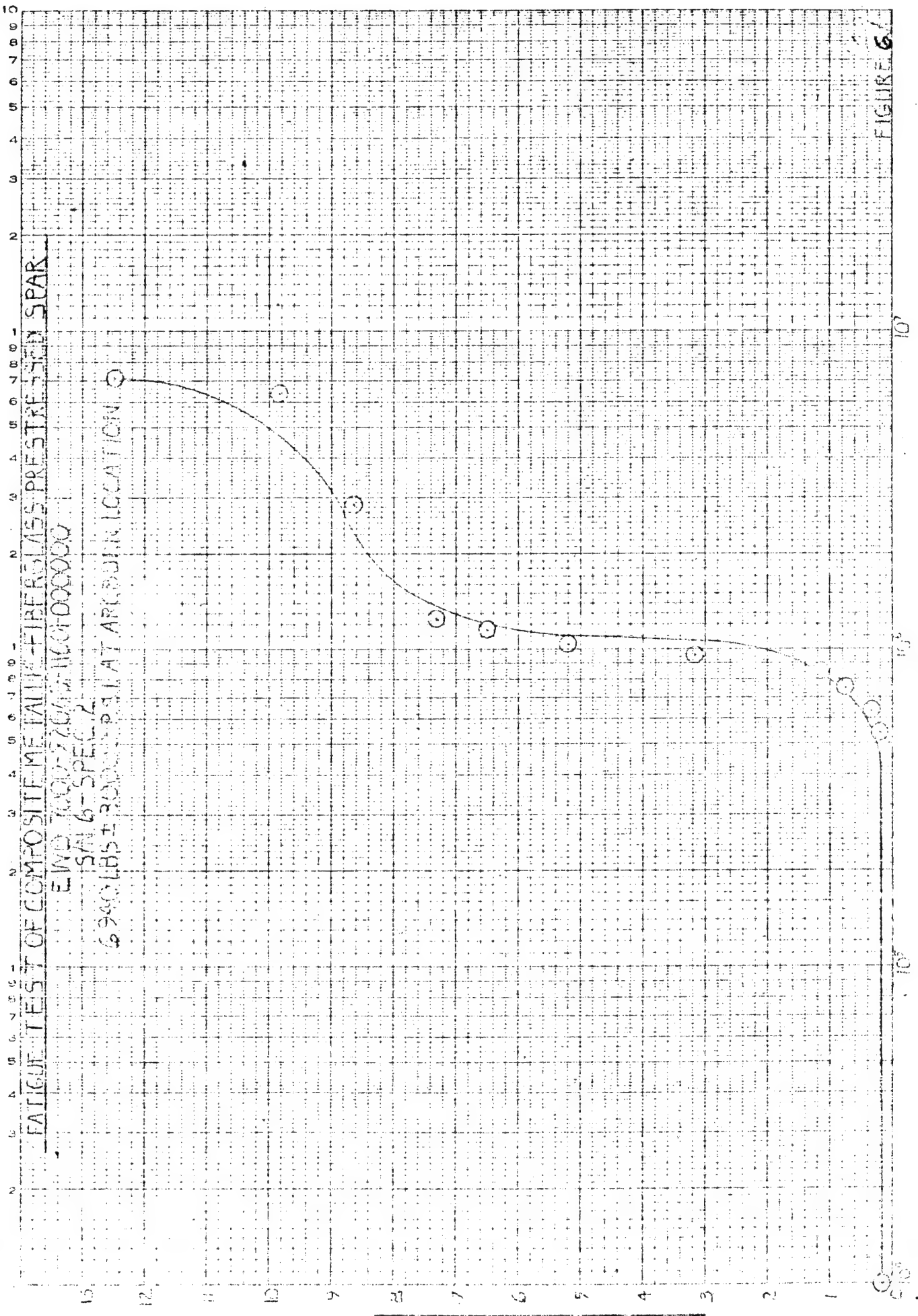


FIGURE 6

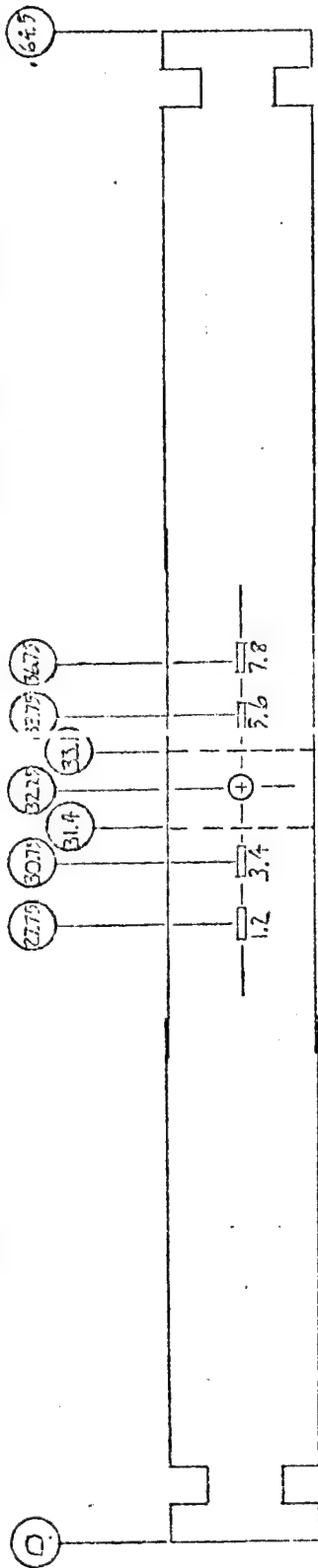
CYCLES

THE **BOEING** COMPANYPREPARED BY:  
CHECKED BY:  
DATE:NUMBER  
REV LTR  
MODEL NO.

## FATIGUE TEST OF PRESTRESSED COMPOSITE METALLIC-FIBERGLASS SPARS

FIND 7000-52060-11001-020000

SPECIMEN B-SIN1 CRACK PROGRESSION WITHOUT FIBERGLASS WRAP



ODD GAGES ON ARCBURN SIDE, EVEN GAGES ON OPPOSITE SIDE.  
CRACK PROGRESSION AT 7000 LBS.  $\pm$  10000 P.S.I. - FIBERGLASS CUT BETWEEN STATIONS  
31.4 AND 33.1 COMPLETELY AROUND SPECIMEN.

## CRACK INITIATION

7000 LBS.  $\pm$  33500 P.S.I. (ARCBURN)

FREQ. = 430 P.S.

CRACK LENGTH = 0.25 INCHES

CYCLES =  $0.30 \times 10^5$ 

## CRACK PROGRESSION

WITH FIBERGLASS

7000 LBS.  $\pm$  25000 P.S.I.

FREQ. = 200 P.S.

CYCLES =  $0.72 \times 10^6$ 

## CRACK PROGRESSION

WITHOUT FIBERGLASS

7000 LBS.  $\pm$  10000 P.S.I.

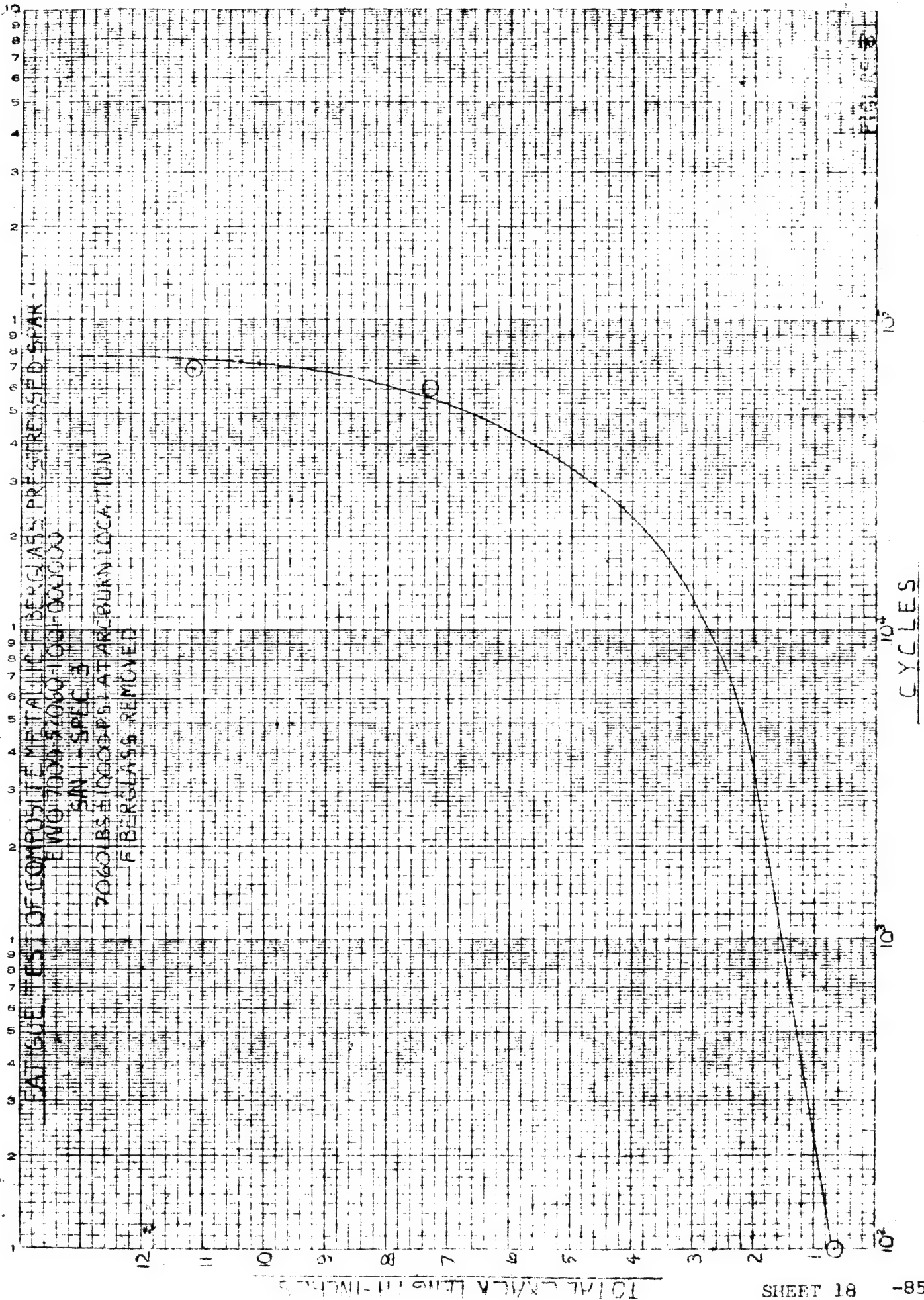
FREQ. = 200 P.S.

CYCLES =  $0.068 \times 10^6$ 

TEST CONDITION — GAGES		1	2	3	4	5	6	7	8	1/2	3/4	5/6	7/8
CRACK INITIATION		± STRESS ON FIBERGLASS - PSI											
CRACK PROGRESSION WITH FIBERGLASS		1400	1070	1450	1280	1190	988	1400	1040	1980	2190	2100	1800
CRACK PROGRESSION WITHOUT FIBERGLASS		990	910	1260	1150	800	890	896	820	1540	1810	1680	1530
CRACK PROGRESSION WITH FIBERGLASS		342	332	170	244	—	198	335	312	5980	7000	6720	5470
CRACK PROGRESSION WITHOUT FIBERGLASS		± STRESS ON STEEL - P.S.I.											
CRACK INITIATION		36300	27200	36000	33300	30900	25700	36200	27100				
CRACK PROGRESSION WITH FIBERGLASS		2570	2260	2780	3060	2080	2780	2300	2180				
CRACK PROGRESSION WITHOUT FIBERGLASS		9780	9100	11200	11400	8700	8200	9880	8700				

FIGURE 7

NO. 2400-4111 PARTS OF PRESTRESSED SPAN  
 SL 10000  
 1 CYCLES X 10 DIV 5 IN PER INCH



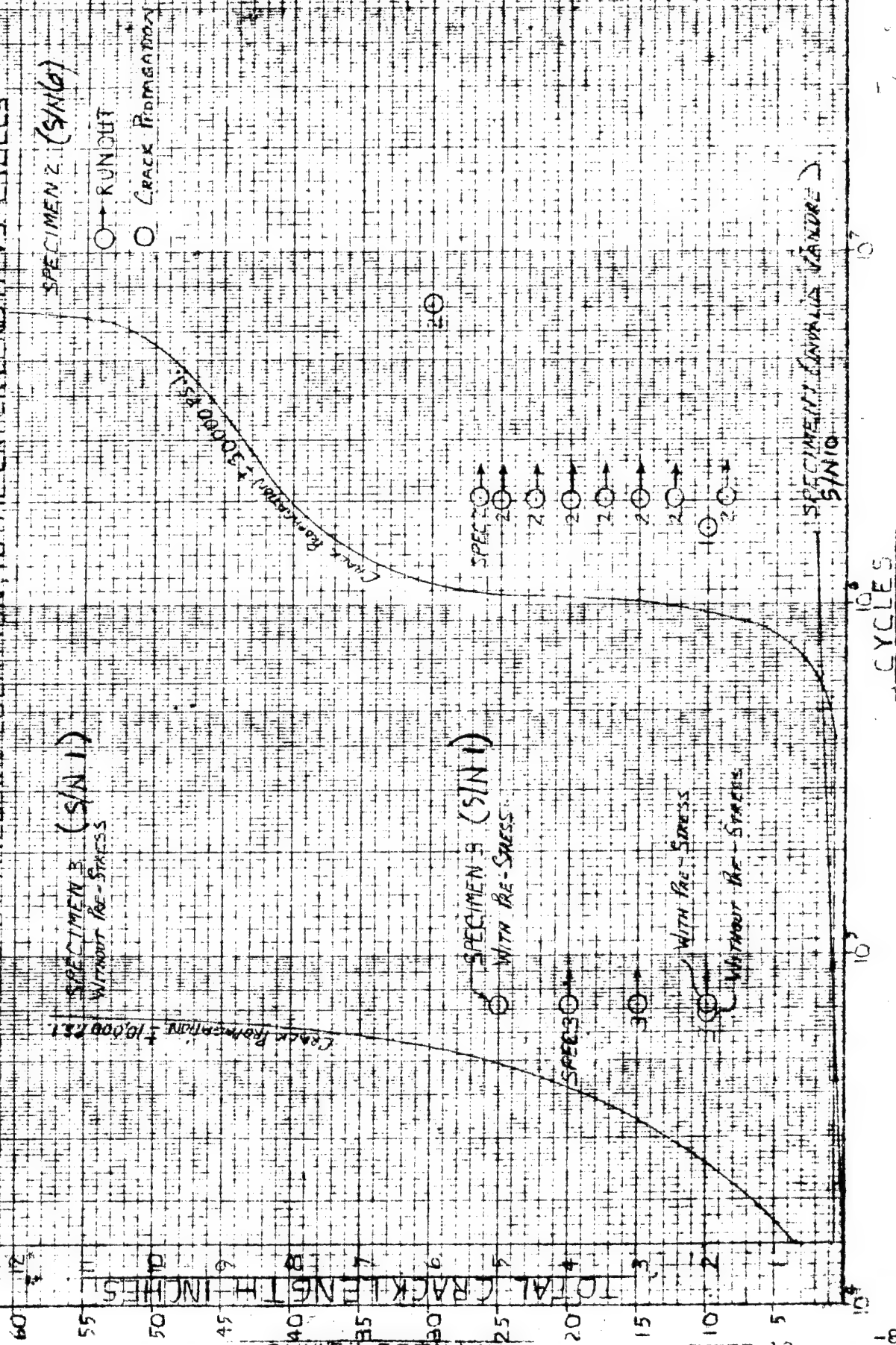


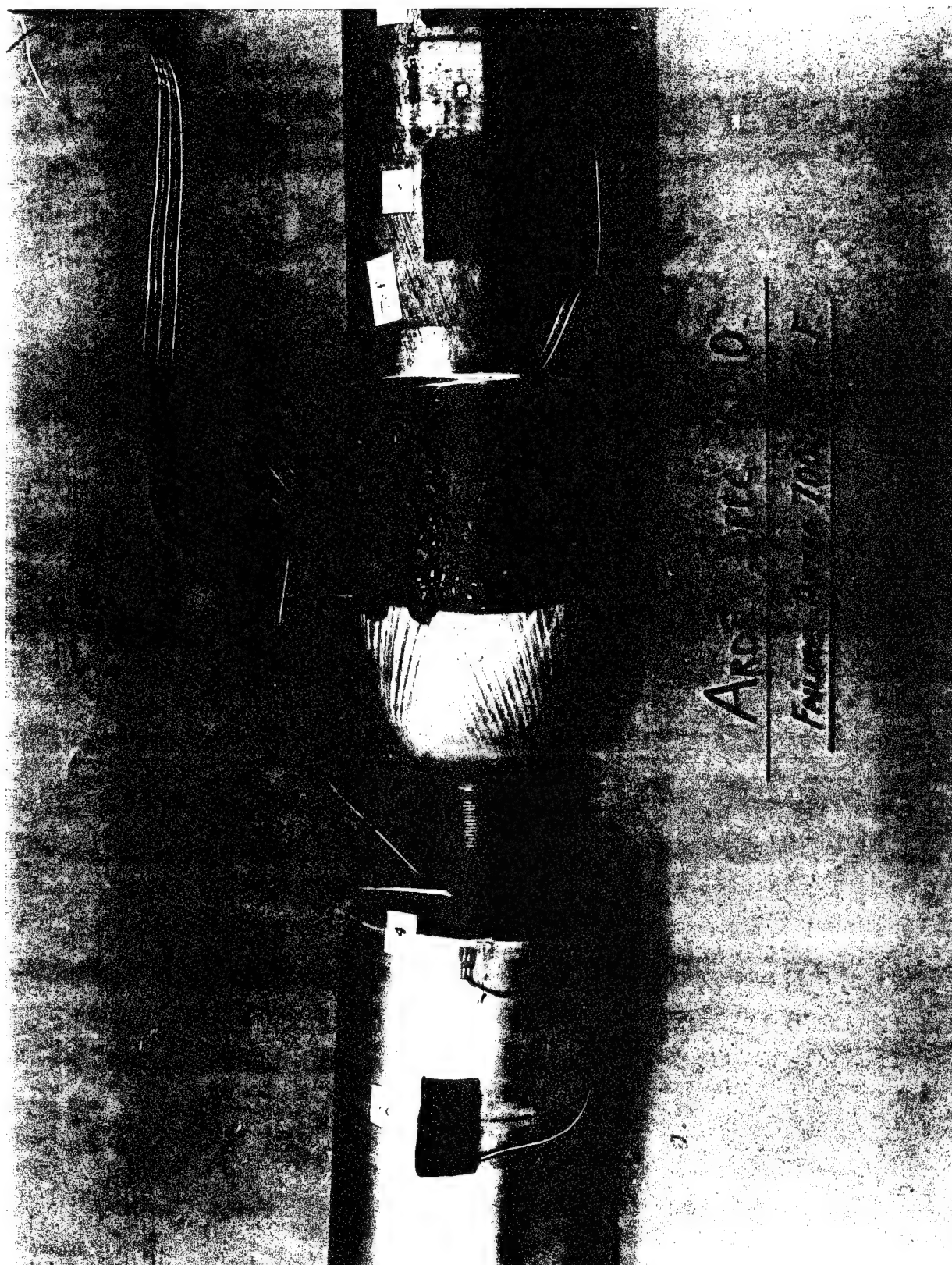
# FATIGUE TEST OF PRESTRESSED COMPOSITE METALLIC-FIBERGLASS SPARS

EWD 7000 52060 1001 000000

AXIAL TENSION LOAD = 7000 LBS

STRESS AT ARCBURN LOCATION, TOTAL CRACK LENGTH VS. CYCLES





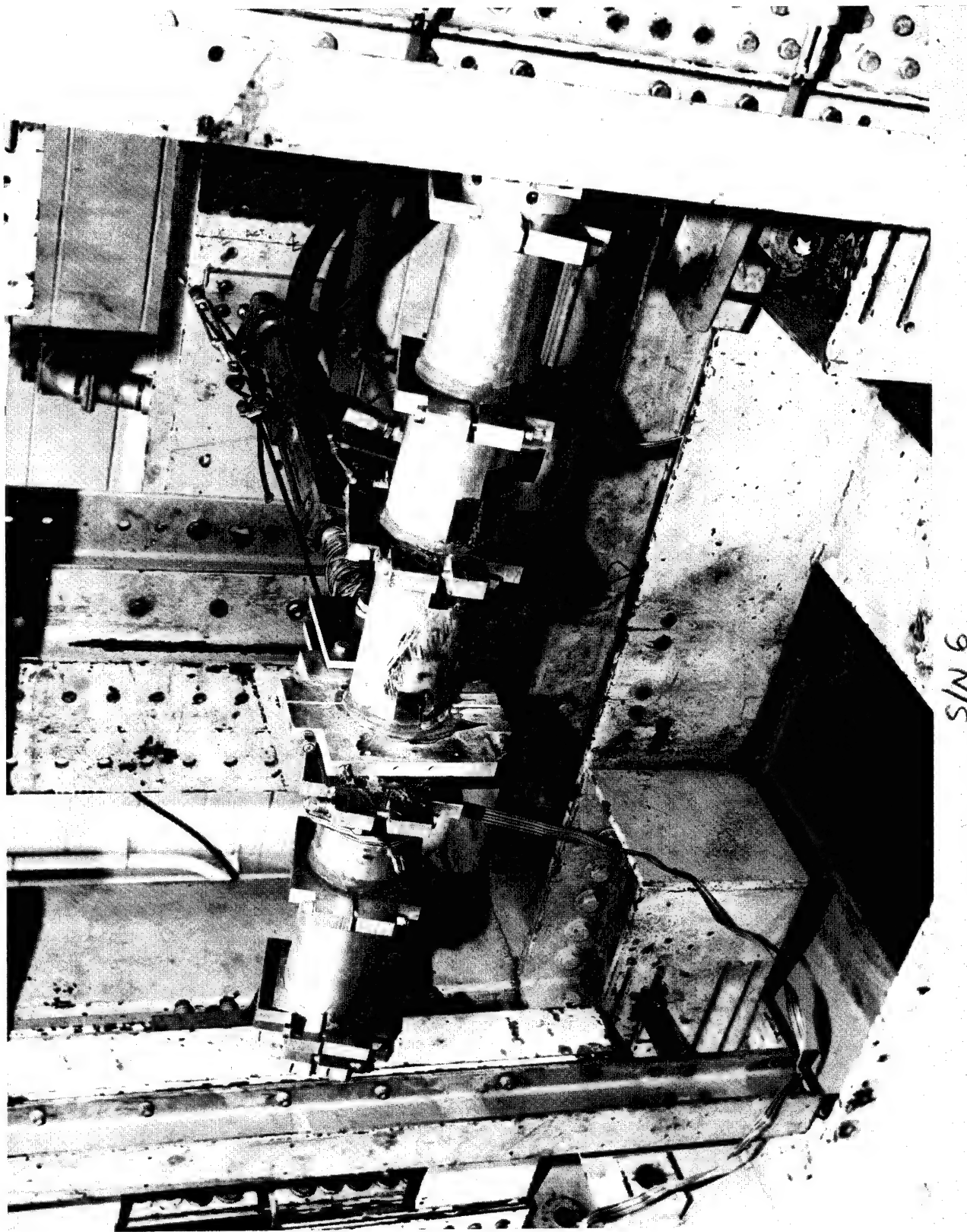
BOND FAILURE AFTER 7000 LB. AXIAL  
TENSION LOAD APPLICATION



SPECIMEN #2 IN CRACK PROGRESSION TEST

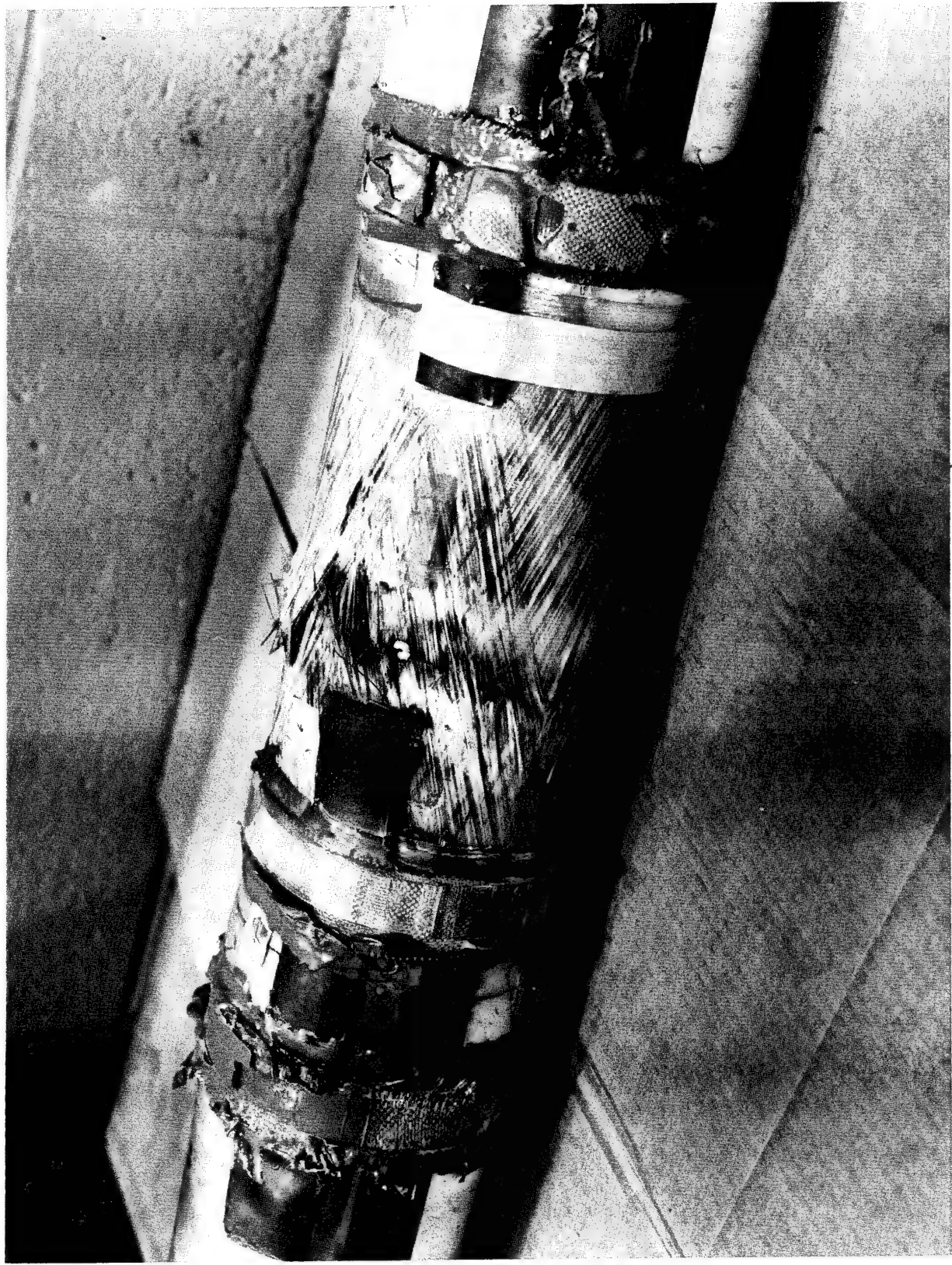


T301-10272-1  
Figure #12



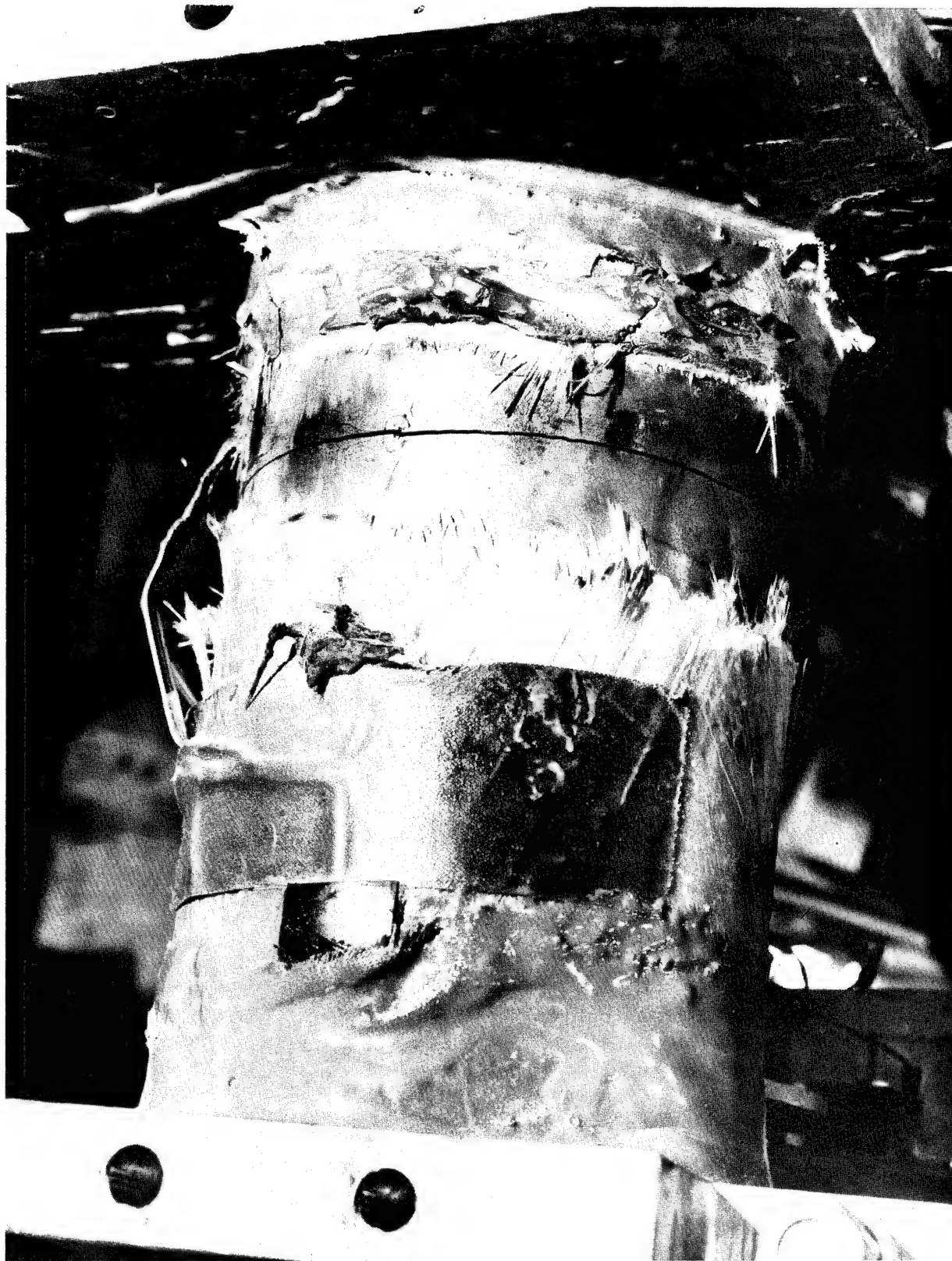
S/N 6

SPECIMEN #2 IN TEST FIXTURE



T301-10272-1  
Figure #13

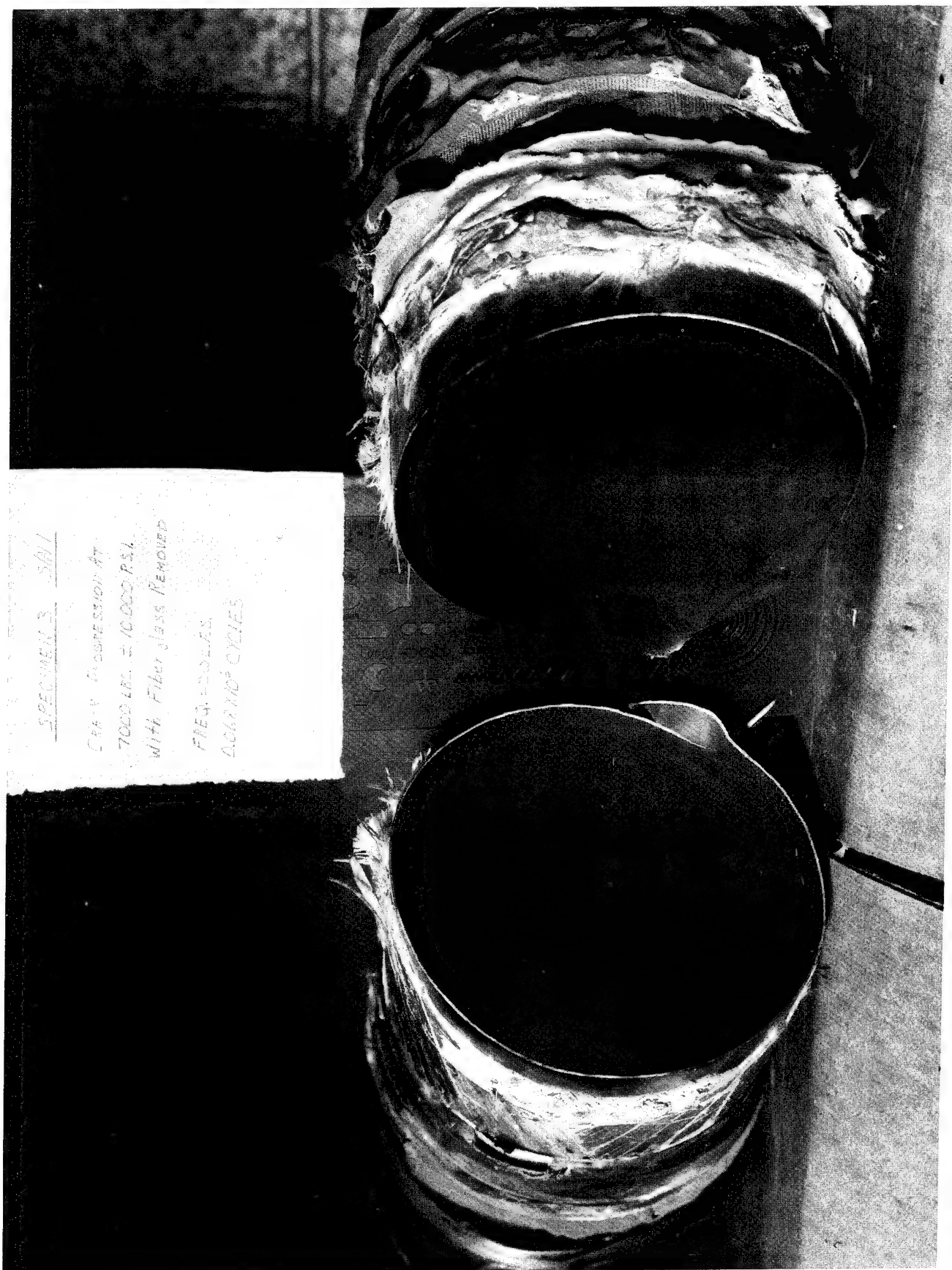
SPECIMEN #2 AFTER CRACK PROGRESSION TEST



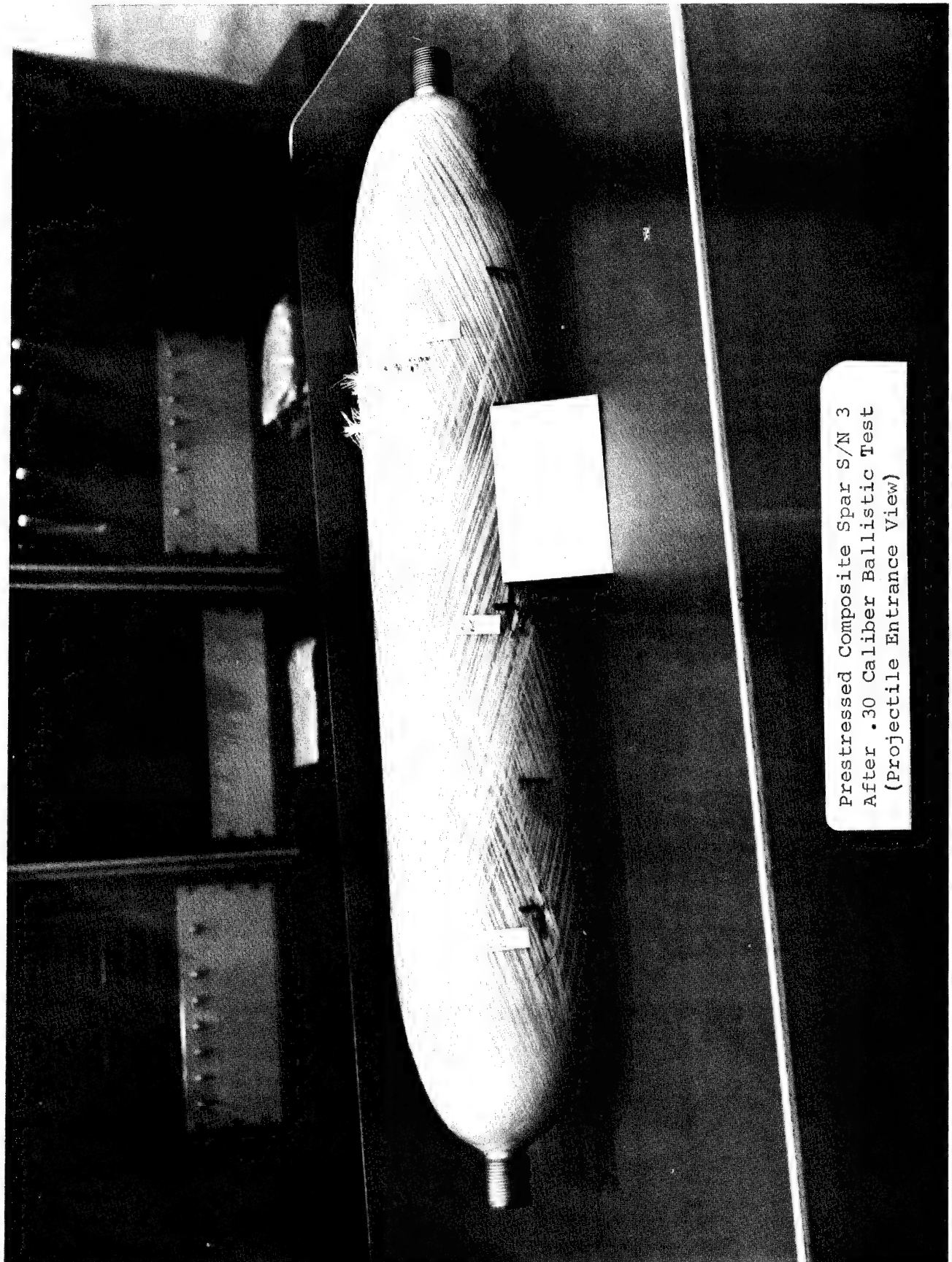
1 M/S



T301-10272-1  
Figure #15

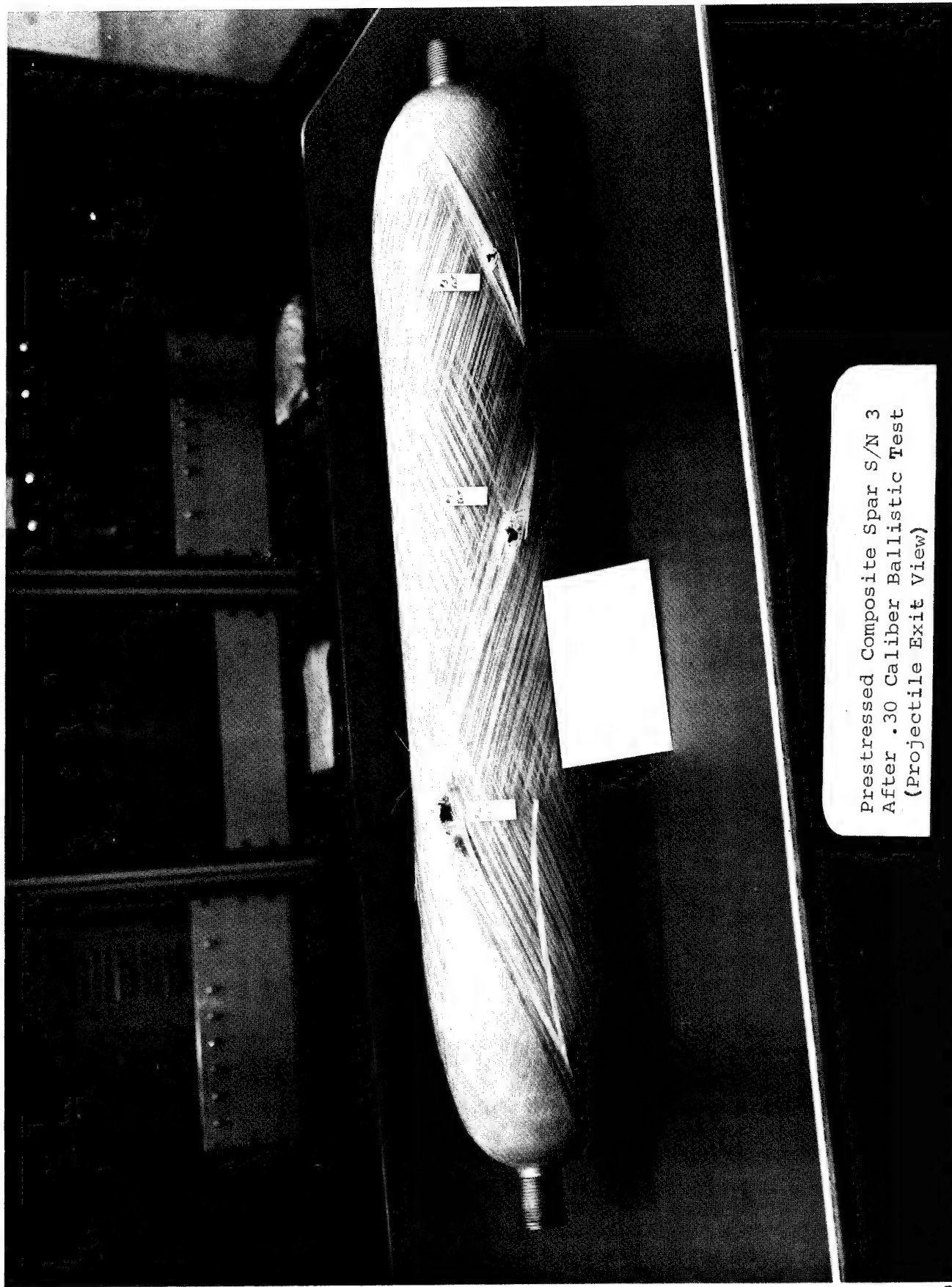


#3



Prestressed Composite Spar S/N 3  
After .30 Caliber Ballistic Test  
(Projectile Entrance View)

BALLISTICALLY DAMAGED SPAR (ENTRANCE DAMAGE)



T301-10272-1  
Figure #17

Prestressed Composite Spar S/N 3  
After .30 Caliber Ballistic Test  
(Projectile Exit View)

BALLISTICALLY DAMAGED SPAR (EXIT DAMAGE)

## 6.2 Appendix 2 - Calculations and Analysis

Calculations and analysis, supporting the discussions in the main body of the text, are given herein. Unless otherwise noted, formulae, materials properties and other data used have been derived or otherwise given in the final report of the prior prestressed composite spar program<sup>(7)</sup>.

### 6.2.1 Determination of Test Loads

The prestressed composite spar test specimen cross-section shape and dimensions are given on the sketch of figure A-1. The measured prestresses in the metal liner and fibers were,

$$(A-1) \quad - - - \quad \left\{ \begin{array}{l} \sigma_{MX}' = -50 \text{ ksi (metal longitudinal Compressive prestress)} \\ \sigma_{MB}' = -7 \text{ ksi (metal hoop compressive prestress)} \\ \sigma_f' = 40 \text{ ksi (fiber tensile prestress)} \end{array} \right.$$

From prestressed composite spar structural theory,<sup>(7)</sup> the metal and fiber bending and direct longitudinal (axial) stresses are defined by,

$$\sigma_{Mb} = E_M \left\{ \frac{M}{E_M I_M + E_f \cos^4 \alpha' I_f} \right\} = \left( \frac{M}{I_M} \right) \left\{ \frac{1}{1 + \frac{I_f}{I_M} \frac{E_f \cos^4 \alpha'}{E_M}} \right\} \quad - - - (A-2)$$

$$\sigma_{Mx} = \sigma_{Mb} / \sigma_{fb} = \frac{E_M}{E_f \cos^4 \alpha'} \quad - - - (A-3)$$

with,

$$\left( \frac{M}{M_f} \right) = 1 + \frac{M_M}{M_f} = 1 + \frac{E_M t_M}{E_f \cos^4 \alpha' t_f} \quad - - - (A-4)$$

and

$$\left( \frac{I}{I_M} \right) = \frac{I_M + I_f}{I_M} = 1 + \frac{I_f}{I_M} = 1 + \frac{t_f}{t_M} \quad - - - (A-5)$$

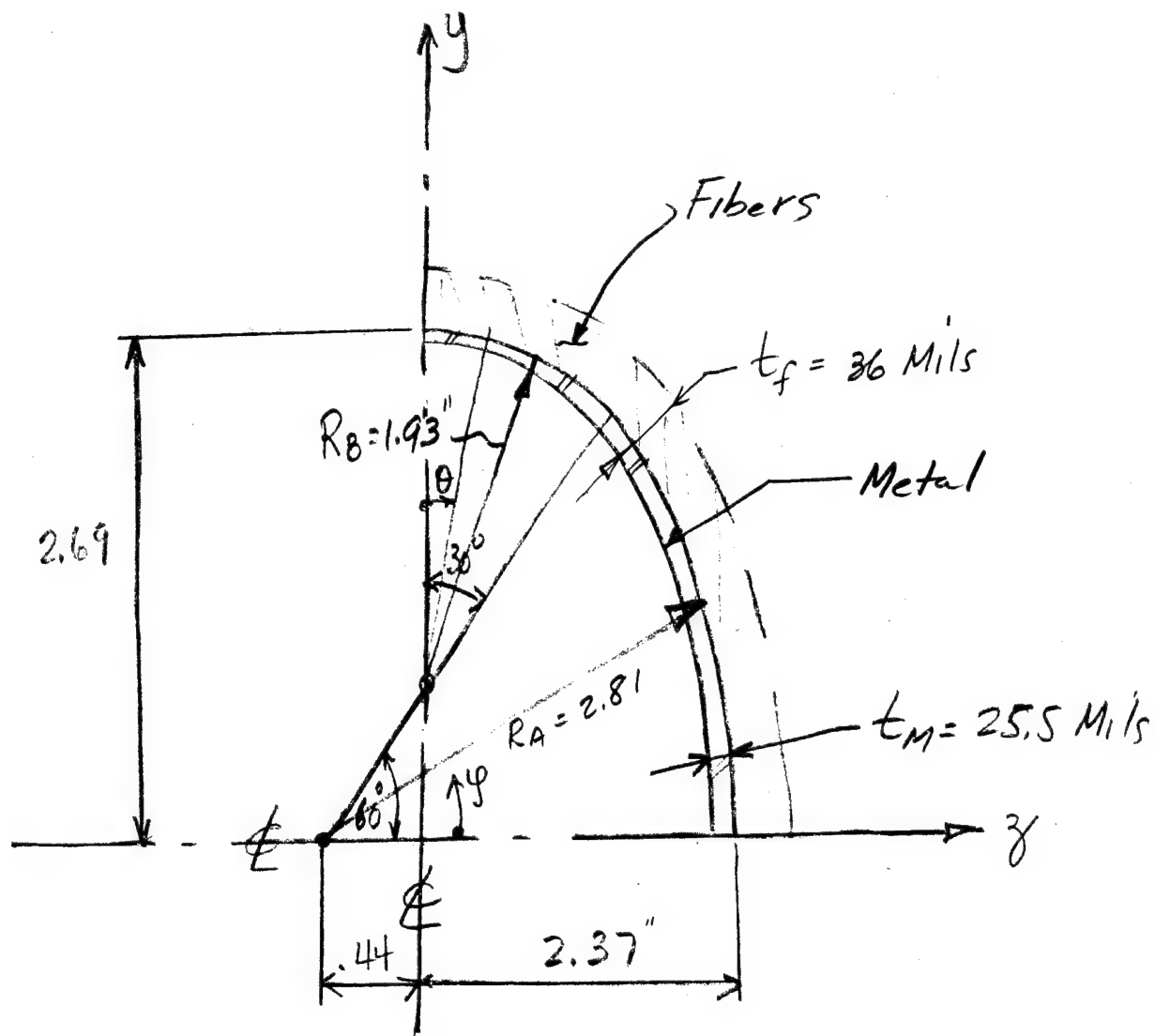


Figure A-1

Sketch of Prestressed Composite Spar Specimen Cross-Section



where,

$E_M$  = Metal Young's modulus

$E_f$  = Fiber Young's modulus

$I$  = Moment of inertia

$I_M$  = Metal moment of inertia

$I_f$  = Fiber moment of inertia

$M$  = Applied bending moment

$M_M$  = Bending moment resisted by metal

$M_f$  = Bending moment resisted by fiber

$y$  = Distance from neutral axis

$\alpha'$  = Fiber helix angle after cryostretching

$\sigma_{Mb}$  = Metal longitudinal bending stress

$\sigma_{MX}$  = Metal longitudinal direct stress

$\sigma_{fb}$  = Fiber stress due to bending

$\sigma_{fx}$  = Longitudinal component of fiber direct stress

$t$  = Total wall thickness

$t_m$  = Metal thickness

$t_f$  = Fiber thickness

Using the data of figure A-1 we compute the metal and fiber moment of inertias about the weak axis as indicated below,

$$I_{My} = 4 \times .036 \left\{ \int_0^{\pi/3} (2.80 \cos \varphi - .44)^2 (2.80) d\varphi + \int_0^{\pi/3} (1.92)^3 \sin^2 \theta d\theta \right\} = 1.14 \text{ in}^4$$

$$I_{fy} = 4 \times .0255 \left\{ \int_0^{\pi/3} (2.83 \cos \varphi - .44)^2 (2.83) d\varphi + \int_0^{\pi/3} (1.95)^3 \sin^2 \theta d\theta \right\} = 1.67 \text{ in}^4$$

$$I_y = I_{fy} + I_{My} = 2.81 \text{ in}^4$$

With  $\alpha' = 20^\circ$  ( $\cos^4 \alpha' = .78$ ),  $E_f = 12.4 \times 10^3$  ksi, and  $E_M = 25 \times 10^3$  ksi, the fiber to metal bending stiffness ratio is,

$$\frac{E_f \cos^4 \alpha' I_f}{E_M I_M} = \frac{(12.4)(.78)}{(25)} \times \frac{1.67}{1.14} = .567$$

Designing, for a maximum metal bending stress of  $\pm 34$  ksi, we have from A-2 with  $\beta = 2.37$ ,

$$\sigma_{Mb} = 34 = \frac{M(2.37)}{1.14} \times \frac{1}{1.567} \quad \text{or,}$$

$$M = 25.5 \text{ (in. Kips)}$$

as the theoretical maximum applied test bending moment.

The metal and fiber cross-sectional areas are (see figure A-1)

$$A_M = 4 t_M \left\{ \int_0^{\pi/3} R_A d\varphi + \int_0^{\pi/6} R_B d\varphi \right\} = 4 \times .0255 \times \frac{\pi}{6} (2R_A + R_B)$$

$$A_M = \frac{2\pi}{3} (.0255) \{ 2 \times 2.80 + 1.92 \} = .402 \text{ in}^2$$

similarly,

$$A_f = \frac{2\pi}{3} (.036) \{ 2 \times 2.83 + 1.95 \} = .572 \text{ in}^2$$

$$A = A_M + A_f = .974 \text{ in}^2$$

The prestressed composite spar objective is to provide a residual compression in the metal under operating conditions. Selecting -5 ksi as the design minimum residual metal compression at maximum metal bending stress of  $\pm 34$  ksi we have then (noting that the metal compressive prestress is -50 ksi),

$$\sigma_{MX} = -50 + 34 + \sigma_{MX}^0 = -5 \quad \text{or,}$$

$$\sigma_{MX}^0 = 11 \text{ (ksi)}$$

as the applied constant axial metal tensile stress simulating centrifugal effects.

From A-3, using the appropriate numerical values, we find,

$$P = \sigma_{mx} A_m + \sigma_{fx} A_f = \sigma_{mx} \left\{ A_m + A_f \frac{E_f \cos^4 \alpha'}{E_m} \right\}$$

$$P = 11 \left\{ .402 + .572 \left( \frac{12.4 \times .78}{25} \right) \right\} = 6.85 \text{ say } \underline{7 \text{ Kips}}$$

as the constant axial tensile load to be applied during spar testing.

### 6.2.2 Comparison of Theory & Test Stiffnesses and Strains

Using the test data for S/N 6 prestressed composite spar specimen (figure 32) we compute the metal bending stress at strain gage station 6 from the moment calibration data for 30 ksi bending stress as,

$$\sigma_{mb}(\text{sta } 6) = \pm 30 \times \frac{M_6}{M_{\text{crack sta } 30.25}} = \pm 30 \times \frac{18.3}{18.1} = \pm 30.4 (\text{ksi})$$

Since as previously derived,  $M_{\text{crack}} = 25.5$  in kips for a metal bending stress of  $\pm 34$  ksi, we have as the predicted bending moment at strain gage station 6,

$$M_6 = 25.5 \times \frac{30.4}{34} = 22.7 (\text{in. Kips})$$

This theoretical value agrees very closely with the test result of 22 (in kips) given for strain gage station 6 on figure 5 of the Boeing test report contained in section 6.1 herein.

From prestressed composite spar structural theory<sup>(7)</sup>, fiber strain  $\epsilon_f$  is given by,

$$\epsilon_f = \sigma_f / E_f = \frac{\sigma_{fx}}{E_f} = \frac{\sigma_{mx} E_f \cos^4 \alpha'}{E_f E_m \cos^2 \alpha'} = \frac{\sigma_{mx} \cos^2 \alpha'}{E_m} = \epsilon_{fx} \cos^2 \alpha'$$

or,

$$\epsilon_{fx} = \sigma_{mx} / E_m \quad \text{--- (A-6)}$$

This defines the axial fiber strain  $\epsilon_{fx}$  in terms of metal axial stress and Young's modulus.

For S/N 6 unit, at  $\sigma_{MX} = \pm 30$  ksi metal axial bending stress at the crack station we have,

$$\epsilon_{fx} = \frac{30}{25 \times 10^3} = 1200 \text{ micro-inch/inch}$$

Since  $M_{crack}/M_6 = 18.1/18.3$  we obtain,

$$\epsilon_{fx}(\text{sta. 6}) = 1200 \times \frac{18.3}{18.1} = 1215 \text{ micro-inch/inch}$$

as the theoretically predicted fiber bending strain at strain gage station 6 for a  $\pm 30$  ksi metal bending stress at the crack station. This predicted fiber strain is very close to the measured fiber strain of 1290 micro-inch/inch at strain gage station 6. Again agreement between theory and test results is very good.

Additional verification was obtained by good agreement between measured bending natural frequency (38.4 Hz) and estimated value (39 Hz) based on use of computed bending stiffnesses and appropriate mass terms for the prestressed composite spar crack propagation test assembly (figure 29). Prestressed composite spar structural design theory has thus been proven by the test results.

### 6.2.3 Preliminary Buckling Data Evaluation

A very limited amount of data regarding compressive instability of prestressed composite spars has been generated on the program. This section gives a simplified preliminary treatment of this data. Additional tests, oriented specifically towards determination of the buckling resistance of prestressed composite spar metal liners, are obviously needed.

For purposes of preliminary analysis, the metal liner is treated as a "circular" cylinder of radius  $R$  equal to the larger radius of the oval cross-section liner. Thickness and length ( $t_m, L$ ) are taken as actual values. The cross-sectional geometry has been previously defined by figure A-1. Critical buckling stresses are estimated using "classical theory" since no theoretical basis has yet been established for buckling of composite prestressed structures subjected to axial compression and bending. Tentative conclusions are then drawn.

#### 6.2.3.1 Prestress Mode

Take  $\pi/t_m = \frac{2.81}{25.5 \times 10^{-3}} = 110$  and  $L \approx 36''$ . Then curvature parameter<sup>(10)</sup>,  $Z \approx \frac{L^2}{\pi t_m} = \frac{(36)^2}{2.81 \times 25.5 \times 10^{-3}} = 18.1 \times 10^3$  (long cylinder range) so that the critical compressive stress for axial compression becomes,

$$\sigma_{crc} = C_c E_M \frac{t_m}{\pi} \quad \text{--- (A-7)}$$

The lower bound test data value of  $C_c$  is about 20% of the theoretical value of .605 or,

$$C_c \approx .12 \quad \text{--- (A-8)}$$

as indicated by the data presented in section C.8.2 of Bruhn<sup>(10)</sup>.

From (A-7) and (A-8) with metal Young's modulus  $E_M = 25 \times 10^3$  ksi we have,

$$\sigma_{crc} \approx \frac{.12 \times 25 \times 10^3}{110} = 27.3 \text{ (ksi)}$$

as the lower bound buckling stress estimate for axial compression.

The actual axial compressive prestress applied was -50 ksi and the liners did not buckle. This would indicate the beneficial effect of the fiber wrap in raising the critical buckling stress level as discussed in section 3.1.1.

#### 6.2.3.2 Test Mode

##### a) Normal Operation Condition (S/N 6 and S/N 1)

The critical compressive stress in bending is<sup>(10)</sup>,

$$\sigma_{crb} = C_b E_M \frac{t_m}{\pi} \quad \text{--- (A-9)}$$

with

$$C_b \approx C_c \approx .12 \quad \text{--- (A-10)}$$

as the lower bound buckling stress coefficient.

We then have as before,

$$\sigma_{crb} = \sigma_{crc} = 27.3 \text{ (ksi)} \quad \text{--- (A-11)}$$

Defining now the ratios of applied stresses to buckling stresses,

$$R_c = 39/27.3 = 1.43, \quad R_b = 34/27.3 = 1.25$$

and computing the margin of safety for combined axial compression and bending we obtain<sup>(10)</sup>,

$$M.S. = \frac{1}{R_b + R_c} - 1 = \frac{1}{1.43 + 1.25} - 1 = -.627$$

This large negative M.S. value indicates the metal liner should have buckled based on "classical" theory. Since the S/N 1 and 6 spar metal liners did not buckle under the test loads, the benefit of the fiber wrap in providing additional buckling resistance can again be presumed.

b) Actuator Overload Condition (S/N 10)

The S/N 10 specimen was buckled due to inadvertent actuator overloading as discussed in section 3.2.5.1.1. The overload bending moment at the crack station was about three times the maximum anticipated value. Applied maximum bending stress was then (see section 6.2.1),

$$\sigma_{Mb} = \pm 3 \times 34 = \pm 102 \text{ (ksi)}$$

and the direct axial compression was the constant value of -39 ksi. Then,

$$R_b = \frac{102}{27.3} = 3.74, \quad R_c = \frac{39}{27.3} = 1.43$$

and,

$$M.S. = \frac{1}{3.74 + 1.43} - 1 = -.807$$

Buckling is again indicated by the large negative value of the margin of safety.

The maximum total stress,  $\sigma_M = -102 - 39 = -141$  ksi (compression). Test data<sup>(4)</sup> shows that the metal liner .2% offset compressive yield point is about 2/3 of the .2% offset tensile yield point, or approximately  $2/3 (220) = 147$  ksi. Since the maximum applied compressive yield

stress is very close to the compressive yield point, "plastic buckling" is indicated due to the marked reduction of tangent modulus compared to the  $25 \times 10^3$  ksi elastic value. Inspection of the buckled liner revealed that the deflected liner shape was a very local cusp-like buckle at the maximum compressive stress region similar to that sketched on figure 4, instead of the classical diamond-shaped buckle pattern running over extensive areas of the shell(10).

It is concluded that the S/N 10 metal liner failed by plastic buckling. However, the difference in buckling behavior (mode shape) indicates the influence of the tensioned fibers of the prestressed composite spar specimen. It is speculated that the fibers could have suppressed liner buckling had the maximum compressive liner stress been further away from the compressive yield point, thus avoiding the very significant reduction in liner tangent modulus, i. e., stiffness.

7.0 DISTRIBUTION LIST FOR FINAL REPORT - NASA CR-132611  
 CONTRACT NAS1-11594  
 ARDE, INC.

	<u>No. Of Copies</u>
NASA Langley Research Center	
Hampton, Va. 23665	
Attn: Report & Manuscript Control Office, Mail Stop 180A	1
Raymond L. Zavasky, Mail Stop 115	1
Carl E. Swindlehurst, Jr., Mail Stop 266	5
Technology Utilization Office, Mail Stop 139A	1
NASA Ames Research Center	
Moffett Field, Ca. 94035	
Attn: Library, Mail Stop 202-3	1
Frederick H. Immen, Mail Stop 207-5	1
NASA Flight Research Center	
P. O. Box 273	
Edwards, Ca. 93523	
Attn: Library	1
NASA Goddard Space Flight Center	
Greenbelt, Md. 20771	
Attn: Library	1
NASA Johnson Space Center	
2101 Webster Seabrook Road	
Houston, Tx. 77058	
Attn: JM6/Library	1
Jet Propulsion Laboratory	
4800 Oak Grove Drive	
Pasadena, Ca. 91103	
Attn: Library, Mail 111-113	1
NASA Lewis Research Center	
21000 Brookpark Road	
Cleveland, Oh 44135	
Attn: Library, Mail Stop 60-3	1
Raymond F. Lark, Mail Stop 49-1	1
NASA John F. Kennedy Space Center	
Kennedy Space Center, Fl. 32899	
Attn: Library, IS-DOC-IL	1
NASA Marshall Space Flight Center	
Huntsville, Al. 35812	
Attn: Library	1



	No. Of <u>Copies</u>
National Aeronautics & Space Administration Washington, DC 20546	
Attn: KSS-10/Library	1
RA/NASA Headquarters	1
RH/John F. Ward	1
 Fairchild-Hiller Corporation Helicopter Development Center Farmingdale, NY 11735	  1
 Gyrodyne Company of America, Inc. Flowerfield, St. James, NY 11780	 1
 Hughes Tool Company Aircraft Division Culver City, Ca. 90230	  1
 Kaman Aircraft Division Kaman Corporation Old Windsor Road Bloomfield, Ct. 06002 Attn: Justin J. Barzda	    1
 Kellett Aircraft Corporation Central Airport Camden, NJ 08109	
 Lockheed Aircraft Corporation Lockheed-California Company Burbank, Ca. 91503	  1
 United Aircraft Corporation Research Laboratories East Hartford, Ct. 06108	  1
 United Aircraft Corporation Sikorsky Aircraft Division Stratford, Ct. 06497	  1
 Union Carbide Corporation Carbon Products Division P. O. Box 6116 Cleveland, Oh 44101 Attn: Director, Research & Advanced Technology	    1
 HITCO P. O. Box 1097 Gardena, Ca. 90249 Attn: Librarian, Materials Science Center	   1

	No. Of <u>Copies</u>
Director U. S. Army Air Mobility Research & Development Laboratory Eustis Directorate Fort Eustis, Va. 23604 Attn: SAVDL-EV-TAS/C. H. Carper	1
Bell Helicopter Company P. O. Box 482 Fort Worth, Tx. 76101	1
The Boeing Company Vertol Division P. O. Box 16858 Philadelphia, Pa. 19142 Attn: Librarian	1
Doman Helicopters, Inc. P. O. Box 609 Danbury, Ct. 06810 Attn: Director of Research & Development	1
NASA Scientific & Technical Information Facility P. O. Box 33 College Park, Md. 20740	30 plus reproducible